**CZECH UNIVERSITY OF LIFE SCIENCES PRAGUE**
FACULTY OF ENVIRONMENTAL SCIENCES
DEPARTMENT OF ENVIRONMENTAL GEOSCIENCES

**ENVIRONMENTAL GEOSCIENCES PROGRAM**

**MASTER THESIS**

# MERCURY CHEMOSTRATIGRAPHY ACROSS THE SILURIAN–DEVONIAN BOUNDARY EVENT IN THE PRAGUE BASIN

AUTHOR: LAURA MARCELA CAICEDO FLOREZ, B.A.
SUPERVISOR: Prof. RNDr. JIŘÍ FRÝDA, Dr.

PRAGUE 2021

# CZECH UNIVERSITY OF LIFE SCIENCES PRAGUE

Faculty of Environmental Sciences

# DIPLOMA THESIS ASSIGNMENT

Laura Marcela Caicedo Florez

Geology

Environmental Geosciences

Thesis title

**Mercury chemostratigraphy across the Silurian–Devonian boundary event in the Prague Basin**

---

**Objectives of thesis**

The main aim of the present study is to analyze mercury chemostratigraphic record in continental shelf sediments of the Silurian–Devonian boundary interval from the Prague Basin as tracers of the intense volcanic activity of a large igneous province (LIP) and to test possible temporal links between extinction events and intense volcanism.

**Methodology**

Fieldwork in the Prague Basin (GSSP Klonk and Opatřilka sections)

Basic methods of carbonate petrology for microfacies analyses.

Atomic absorption spectrometry (AAS) – Hg analyses

XRF – major and trace elements

ICP-MS – trace elements

The normality of variables was tested by using the Shapiro-Wilk test. Standard parametric, and non-parametric statistical methods, are used for the evaluation of relationships between geochemical variables. Two software were used for data processing: software package Past 4.03 for testing normality for obtained variables, and calculation of Spearman correlation coefficient, and R-studio for construction of the scatter plots illustrating the correlation between chemical variables.

**The proposed extent of the thesis**

40 pages

**Keywords**

Silurian–Devonian boundary, GSSP, Prague Basin, Mercury chemostratigraphy, volcanism, extinctions

---

**Recommended information sources**


Buggisch, W., & Mann, U. 2004. Carbon isotope stratigraphy of Lochkovian to Eifelian limestones from the Devonian of central and southern Europe. International Journal of Earth Sciences, 93(4), 521–541. https://doi.org/10.1007/s00531-004-0407-6

Frýda, J., Hladil, J., & Vokurka, K. 2002. Seawater strontium isotope curve at the Silurian–Devonian boundary: A study of the global Silurian–Devonian boundary stratotype. Geobios, 35(1), 21–28. https://doi.org/10.1016/S0016-6995(02)00006-2

Hladil, J., 1991. Evaluation of the sedimentary record in the Silurian–Devonian boundary stratotype at Klonk (Barrandian area, Czechoslovakia). Newsl. Stratigr. 115–125.

Hladil, J. (1992). Are there turbidites in the Silurian–Devonian boundary stratotype? (Klonk near Suchomasty, Barrandian, Czechoslovakia). Facies, 26(1), 35–54. https://doi.org/10.1007/BF02539792

Chlupáč, I., & Hladil, J. 2000. The global stratotype section and point of the Silurian Devonian boundary. (pp. 1–7).

Kalvoda, J., Kumpan, T., Qie, W., Frýda, J., & Bábek, O. 2019. Mercury spikes at the Devonian-Carboniferous boundary in the eastern part of the Rhenohercynian Zone (central Europe) and in the South China Block. Palaeogeography, Palaeoclimatology, Palaeoecology, 531. https://doi.org/10.1016/j.palaeo.2019.05.043

Manda, Š., & Frýda, J. 2010 Silurian–Devonian boundary events and their influence on cephalopod evolution: Evolutionary significance of cephalopod egg size during mass extinctions. Bulletin of Geosciences, 85(3), 513–540. https://doi.org/10.3140/bull.geosci.1174

Racki, G. 2019. Big 5 Mass Extinctions. In Encyclopedia of Geology (2nd ed.). Elsevier Inc. https://doi.org/10.1016/b978-0-12-409548-9.12028-7

Shen, J., Chen, J., Algeo, T. J., Feng, Q., Yu, J., Xu, Y. G., Xu, G., Lei, Y., Planavsky, N. J., & Xie, S. 2021. Mercury fluxes record regional volcanism in the South China craton prior to the end-Permian mass extinction. Geology, 49(4), 452–456. https://doi.org/10.1130/G48501.1

Wang, X., Cawood, P. A., Zhao, H., Zhao, L., Grasby, S. E., Chen, Z. Q., Wignall, P. B., Lv, Z., & Han, C. 2018. Mercury anomalies across the end Permian mass extinction in South China from shallow and deep water depositional environments. Earth and Planetary Science Letters, 496, 159–167. https://doi.org/10.1016/j.epsl.2018.05.044

**Expected date of thesis defence**
2021/22 WS – FES

**The Diploma Thesis Supervisor**
prof. Dr. RNDr. Jiří Frýda

**Supervising department**
Department of Environmental Geosciences

Electronic approval: 8. 12. 2021
**prof. RNDr. Michael Komárek, Ph.D.**
Head of department

Electronic approval: 8. 12. 2021
**prof. RNDr. Vladimír Bejček, CSc.**
Dean

Prague on 08. 12. 2021

## AUTHOR'S DECLARATION

I hereby declare that I have independently elaborated the diploma thesis with the topic of: "Mercury chemostratigraphy across the Silurian–Devonian boundary event in the Prague Basin" and that I have cited all the information sources that I used in the thesis and that are also listed at the end of the thesis in the list of used information sources.

_____ _____

Prague 2021 Laura Marcela Caicedo Florez

ACKNOWLEDGEMENTS

First and foremost, I want to deeply thank my supervisor prof. RNDr. Jiří Frýda Dr, for all the valuable time dedicated to academic, technical, and field support. Also, for always maintained a kindly space where I felt encouraged to perseverate, even in difficult times.

From the Czech Geological Survey in Barrandov, Prague: Mgr. Stanislava Vodrážková, Ph.D., for her contribution with the microfacies analysis, and for providing me with useful literature references. Mgr. Michal Kubajko, for his help with the preparation of the samples. Irena Svobodová, for the Hg analysis. RNDr. Ludmila Dempírová, CSc, for the total carbon, total sulfur, and $CO_2$ analyses, and once again prof. RNDr. Jiří Frýda Dr, for the major and trace element analyses.

To all those who gave me all kinds of support in Prague, from my home country Colombia, and other places: Marcela Ulloa, Stefany García, Melisa Ayala, Juan Navarro, Dayana Corzo, and Rafael Villamizar.

To my family for their unconditional support in all my projects and make it possible to study in my home country and abroad.

This thesis was supported by the Grant Agency of the Czech Republic (project GA17-18120S) and presents a contribution to the Strategic Research Plan of the Czech Geological Survey (DKRVO/ČGS 2018-2022).

## ABSTRACT

The evolution of global biodiversity and its relationship to environmental change over geological time is a major goal of Earth and Life Sciences research. The increase in global biodiversity during the Phanerozoic was often interrupted by global extinction events which are not fully understood. In the last decade, evidence has emerged of intense Large Igneous Province (LIP) volcanic activity having caused changes in global climate, biosphere, and global extinction events.

Extinctions near the Silurian-Devonian boundary are well documented worldwide, and they have contributed to the reduction of Paleozoic global marine biodiversity. This critical period has been characterized by many global events: climate oscillations, eustatic sea-level changes, anoxic/hypoxic events in seawater, and instability of the global carbon cycle, but the possible link between these extinctions and intense volcanic activity has never been analyzed.

Mercury enrichments in sedimentary rocks are often used as diagnostic fingerprints of major volcanic eruptions and as possible links to the Phanerozoic mass extinctions. In geological history, Hg was dominantly emitted via volcanism in the atmosphere–land-ocean cycle before sinking to the seafloor. I report (for the first time) the mercury (Hg) chemostratigraphic record across the Silurian-Devonian boundary interval focusing on the analysis of Hg, major and trace elements contents from two sections of different depositional environments of the continental shelf sediments of the Prague Basin: the Opatřilka section representing the nearshore environment, and the Klonk section, characterized by offshore deposition which was approved by the International Commission on Stratigraphy as the Global Boundary Stratotype Section and Point (GSSP). The present study is based on 83 rock samples collected from these sections and analyzed for their total sulfur, total carbon, $CO_2$, and major and trace element contents, including mercury. Main lithological types were also characterized by microfacial analysis.

Mercury content differs in both sections, ranging from 1 up to 18 ppb in the Opatřilka section (except for one sample showing 230 ppb), and from 11 up to 87 ppb in the Klonk section. Data obtained from statistical correlation analyses showed that Hg exhibits positive correlations with most of the major and trace elements, except those that are components of the carbonate fraction of the rock (Ca, Sr, and $CO_2$) which shows that the Hg content in the sections mainly depends on the detritic component of the rock as well as by total organic carbon and total sulfur contents. Significant differences were found between sections but the correlations between the detrital component and total organic carbon and total sulfur do not allow us to distinguish whether mercury is controlled by TOC and TS only or also by detritus.

A significant finding of this work is the observation of a Hg peak (ca. 230 ppb) in the lower part of the Silurian *Monograptus transgrediens* graptolite Biozone at the Opatřilka section. The Hg peak cannot be explained as of detrital or TOC origin. It is unclear if the Hg anomaly represents an indication of extensive volcanic activity or Hg accumulation resulting from diagenetic/hydrothermal mercury mobilization. Further investigations of the anomaly are needed. It should be noted this thesis is the first application of Hg chemostratigraphy in the classic Barrandian area.



KEYWORDS: *Silurian–Devonian boundary, GSSP, Prague Basin, Mercury chemostratigraphy, volcanism, extinctions.*

## ABSTRAKT

Vývoj globální biodiverzity v průběhu geologické historie a jeho vztah ke změnám životního prostředí je jedním z hlavních témat výzkumu v oblasti věd o Zemi a živé přírodě. Nárůst globální biodiverzity během fanerozoika byl často přerušován globálními událostmi, které nejsou zcela pochopeny. V posledním desetiletí se objevily důkazy o tom, že intenzivní aktivita velkých vulkanických provincií (LIP) mohla způsobit změny globálního klimatu, biosféry i globální vymírání.

Vymírání v blízkosti hranice siluru a devonu je celosvětově dobře zdokumentováno a přispělo ke snížení globální mořské biodiverzity. Toto kritické období bylo charakterizováno mnoha globálními událostmi: oscilacemi klimatu, eustatickými změnami mořské hladiny, anoxickými/hypoxickými událostmi v mořské vodě a nestabilitou globálního cyklu uhlíku. Možná souvislost mezi vymíráním a intenzivní vulkanickou činností avšak nebyla v tomto časovém intervalu nikdy analyzována.

Obohacení rtutí (Hg) sedimentárních hornin se stále častěji používá jako diagnostický znak velkých sopečných erupcí a jako možná příčina hromadných vymírání ve fanerozoiku. V geologické historii byla rtuť dominantně emitována do životního prostředí pouze vulkanismem. Následně přes koloběh v systému atmosféra-půda-oceán byla pohřbívána s organickou hmotou na mořském dně. Předložená studie poprvé analyzuje chemostratigrafický záznam rtuti (Hg) napříč hraničními sedimenty siluru a devonu, a zaměřuje se na analýzu obsahů Hg, hlavních a stopových prvků ze dvou geologických profilů, reprezentujících různá sedimentární prostředí kontinentálního šelfu pražské pánve: profilu Opatřilka s mělkovodním sedimentárním záznamem, a profilu na Klonku s hlubokovodní sedimentací. Profil na Klonku byl schválen Mezinárodní stratigrafickou komisí jako globální hraniční stratotyp (GSSP) hranice silur/devon. Předložená studie je založena na analýze obsahu celkové síry, celkového uhlíku, $CO_2$ a hlavních a stopových prvků, včetně rtuti, v 83 vzorcích hornin odebraných z těchto profilů. Hlavní litologické typy byly rovněž charakterizovány mikrofaciální analýzou.

Obsah rtuti se v obou profilech liší a pohybuje se v profilu Opatřilka (s výjimkou jednoho vzorku vykazujícího 230 ppb) od 1 do 18 ppb a od 11 do 87 ppb v profilu Klonku. Výsledky statistických analýz ukázaly, že Hg vykazuje pozitivní korelace s většinou hlavních a stopových prvků, s výjimkou těch, které jsou složkami karbonátové frakce horniny (Ca, Sr, $CO_2$). Výsledky studie ukazují, že obsah Hg v profilech souvisí s množstvím detritické složky a celkovým obsahem organického uhlíku (TOC) a celkové síry (TS). Mezi jednotlivými profily byly zjištěny významné rozdíly, ale vzájemné korelace mezi obsahem detritické složky, TOC a TS neumožňují rozlišit, zda je obsah rtuti řízen pouze obsahem TOC a TS, nebo také detritem.

Významným výsledkem předložené studie je zjištění anomální obsahu Hg (cca 230 ppb) ve spodní části silurské graptolitové biozóny *Monograptus transgrediens* v profilu Opatřilka. Tento pík Hg nelze vysvětlit zvýšeným detritickým nebo TOC obsahem. Není jasné, zda tato anomálie Hg představuje stopu po rozsáhlé vulkanické činnosti nebo je akumulace Hg důsledkem diagenetické/hydrotermální mobilizace rtuti. Další výzkum této anomálie je tedy nutný. Předložená studie je první aplikací chemostratigrafie Hg v klasické barrandienské oblasti.



KLÍČOVÁ SLOVA: *hranice siluru a devonu, GSSP, pražská pánev, chemostratigrafie Hg, vulkanismus, vymírání*

# TABLE OF CONTENTS

DIPLOMA THESIS ASSIGNMENT ..... i
AUTHOR'S DECLARATION ..... iv
ACKNOWLEDGEMENTS ..... v
ABSTRACT ..... vi
ABSTRAKT ..... vii
1. INTRODUCTION ..... 1
2. AIMS ..... 3
3. LITERATURE REVIEW ..... 4
3.1. MERCURY GEOCHEMICAL CYCLING ..... 4
3.2. MERCURY AND MASS EXTINCTIONS ..... 5
3.3. GEOLOGICAL SETTINGS ..... 7
3.3.1. THE SILURIAN–DEVONIAN BOUNDARY INTERVAL IN THE PRAGUE BASIN ..... 7
3.3.2. SILURIAN VOLCANISM IN THE PRAGUE BASIN ..... 8
3.3.3. OPATŘILKA SECTION ..... 9
3.3.3.1. LITHOLOGY AND BIOSTRATIGRAPHY ..... 9
3.3.3.2. PREVIOUS STUDIES: CARBON ISOTOPES AND EXTINCTIONS ..... 10
3.3.4. KLONK SECTION ..... 11
3.3.4.1. LITHOLOGY AND BIOSTRATIGRAPHY ..... 11
3.3.4.2. CHEMOSTRATIGRAPHY ..... 13
4. METHODOLOGY ..... 14
4.1. CHARACTERISTICS OF THE STUDY AREA ..... 14
4.2. SAMPLE PREPARATION ..... 15
4.3. MICROFACIES ANALYSES ..... 17
4.4. ELEMENTAL ANALYSIS ..... 17
4.5. TOTAL CARBON (TC) AND TOTAL SULFUR (TS) ANALYSES ..... 18
4.6. THE CARBONATE CARBON ANALYSIS ..... 18
4.7. MERCURY ANALYSIS ..... 18
4.8. DATA PROCESSING ..... 19
5. RESULTS ..... 19
5.1. MICROFACIES ANALYSES ..... 19
5.2. MERCURY CHEMOSTRATIGRAPHY ..... 24

5.2.1. OPATŘILKA SECTION ..... 24
5.2.2. KLONK SECTION ..... 35
6. DISCUSSION ..... 46
6.1. WHAT INFLUENCES THE MERCURY CONTENT OF THE SEDIMENTS STUDIED? ..... 46
6.2. MERCURY ANOMALY ..... 48
7. CONCLUSIONS. ..... 50
8. REFERENCES ..... 52
9. APPENDICES. ..... 58
APPENDIX A ..... 58
APPENDIX B ..... 59
APPENDIX C ..... 61
APPENDIX D ..... 63
APPENDIX E ..... 64
APPENDIX F ..... 66
APPENDIX G ..... 68
APPENDIX H ..... 75

# 1. INTRODUCTION

The Prague Basin (sometimes also called as Prague Synform) is well known for exhibiting sedimentary sequences of the Silurian–Devonian (S–D) boundary interval (Chlupáč et al., 1998; Kříž et al., 1986; Kříž 1991, 1992). This basin is a younger component of the Proterozoic crustal block (the Teplá-Barrandian terrane), and its sedimentary record represents the only deposition in a small part of a former Palaeozoic basin. The Prague Basin preserves evidence of intense volcanic activity during the Silurian (Tasáryová, 2014, 2018; Stampfli, 2002; Elbra, 2015; and references therein).

The S–D boundary was defined in 1972 as the first Global Stratotype Section and Point (GSSP) within the Prague Basin, in Klonk near Suchomasty. The Prague Basin has evidenced significant changes in faunal communities close to the S–D boundary (Chlupáč et al., 1972, 1998; Kříž et al., 1986). Distinct changes in faunal communities were reported from different paleoregions located in temperate as well as tropical paleolatitudes (Melchin et al., 2012, 2021, and references therein). During the last decades, three different bioevents [the Silurian–Devonian boundary Event (Walliser 1985), Transgrediens Event (Urbanek 1995; Štorch, 1995), and Klonk Event (Jeppsson 1998)] were defined within the S–D boundary interval. However, only several studies of those bioevents were analyzed based on quantitative data (e.g., Manda & Frýda, 2010; Racki et al., 2012; Spiridonov et al., 2020; and references therein).

Munnecke et al. (2003) showed that all major Silurian biotic crises were closely linked with the collapse of the global carbon cycle, manifested by positive carbon isotope anomalies (see Cramer et al., 2011, and references therein). Carbon isotope excursion at the S–D boundary was reported from many paleocontinents (see Melchin et al., 2021 for a review), and also from Prague Basin (Hladíková et al., 1997; Buggisch & Mann, 2004; Manda & Frýda, 2010).

The relationship of the extinction events close to the S–D boundary to collapse of the global carbon cycle, anoxia (Porebska & Sawlowicz, 1997), and climatic changes (Joachimski et al., 2009) is still poorly known. In contrast to other Paleozoic extinction events (Racki, 2020; Kalvoda et al., 2019; Wang et al., 2018; Shen et al., 2021) the influence of volcanic activity on the bioevents close to the S–D boundary has never been studied. Volcanic emissions were the only natural source of direct release of elemental Hg ($Hg^0$) to the atmosphere in the past (Pyle & Mather, 2003). Accordingly, Hg chemostratigraphy has been recently used as a proxy of past volcanism.

Besides the short-term direct Hg poisoning effects, studies on volcanism-related extinction events invoke anoxia, acidification, and the effects of rapid warming (Wang et al., 2018), as later consequences of excessive release of $CO_2$ (Sun et al., 2012). Other factors such as anti-greenhouse feedbacks, and short-term cooling effects seem to have operated in the Paleozoic crises, marked by rather prolonged glaciations within a greenhouse overall scenario (Racki, 2019).

The present work aims to analyze Hg chemostratigraphy in continental shelf sediments of two Silurian–Devonian boundary sections of the Prague Basin: The Opatřilka section, representing near-shore deposition setting, and the off-shore Klonk section, which was selected in 1972 as Global Boundary Stratotype Section and Point (GSSP) for the Silurian–Devonian boundary. By discriminating Hg enrichments caused by local adsorptive processes from enrichments related to the intense volcanic activity of a large igneous province (LIP), this study intends to test possible temporal links between extinction events

closed to the S–D boundary and volcanism. The present work represents the first application of the Hg-chemostratigraphy at the Silurian–Devonian boundary interval as well as within the Prague Basin.

## 2. AIMS

The main aim of the present study is to analyze mercury chemostratigraphic record in continental shelf sediments of the Silurian–Devonian boundary interval from the Prague Basin as tracers of the intense volcanic activity of a large igneous province (LIP), and to test possible temporal links between extinction events and intense volcanism.

# 3. LITERATURE REVIEW

## 3.1. MERCURY GEOCHEMICAL CYCLING

Hg exists as a metallic liquid at ambient conditions. It has a high density, is highly volatile, and bioaccumulates as a toxic metal, therefore its potentially harmful effects on the environment have been a pollution issue of global concern. Hg has a residence time in the atmosphere of about 1 year (Pyle & Mather, 2003), and it occurs in three oxidation states: $Hg^0$, $Hg^{+1}$, and $Hg^{+2}$ (WHO, 2000), being $Hg^0$ the most abundant form in the atmosphere (Selin, 2009).

Volcanic emissions are the only natural source of direct release of elemental Hg ($Hg^0$) to the atmosphere (Pyle & Mather, 2003). Part of the released Hg oxidizes to $Hg^{+2}$ and is subsequently methylated or transformed to organic mercury compounds. In the latter, the Hg atom is covalently bound to one or two carbon atoms (WHO, 2000).

Currently, anthropogenic sources such as coal-fired power plants are responsible for Hg emissions of ~2200–4000 Mg $year^{-1}$ (Selin, 2009). According to the latter author, such emissions release Hg as Hg associated with particulate matter Hg(P), and $Hg^{+2}$. These forms are more soluble in water than $Hg^0$, have a shorter lifetime (days to weeks) than $Hg^0$, and are the most common forms of Hg deposited in the terrestrial surface ecosystems by wet and dry deposition (Selin, 2009). More than 90% of it resides in soil and is associated with organic matter, binding strongly to reduced sulfur groups (Skyllberg et al., 2003). Once deposited, part of it quickly revolatilize to the atmosphere, and the rest is contained into a soil pool, where is retained and takes centuries to millennia to be released back to the atmosphere by its reduction to $Hg^0$, which is mainly considered as an abiotic process (Selin, 2009). However, Fritsche et al., (2008) demonstrated that biotic processes (microbial) may also play a role in $Hg^0$ emissions from soils.

In freshwater systems, Hg is mainly deposited as $Hg^{2+}$. A small fraction of $Hg^{2+}$ is converted to the more toxic form of methylmercury (MeHg) which occurs by a biological process facilitated by sulfate-reducing bacteria (Benoit et al., 2002) as well as iron-reducing ones (Kerin et al., 2006). According to Mason et al., (1993) and Morel et al., (1998), Hg can be found in the forms $Hg^0$, $Hg^{+2}$, methylmercury, dimethylmercury, and particulate and colloidal Hg in the ocean. As in freshwater systems, $Hg^{2+}$is deposited in the ocean by wet and dry deposition (**Figure 1**), and $Hg^0$ by dry deposition. $Hg^{2+}$ can be reduced to $Hg^0$, adsorbed onto particles, or methylated (Selin, 2009).

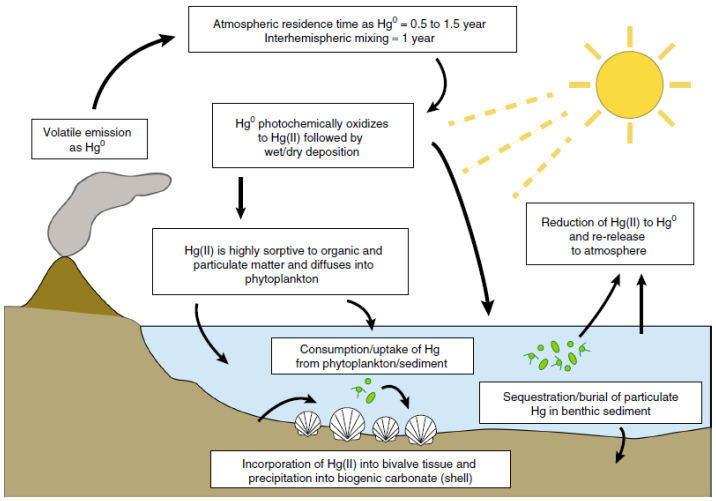


**Figure 1.** Model of Hg emission from volcanoes and later incorporation into marine biota. Modified from (Meyer et al., 2019).

## 3.2. MERCURY AND MASS EXTINCTIONS

A mass extinction was defined by Sepkoski (1986) as any significant increase in the amount of extinction suffered by more than one geographically widespread higher taxon during a geologically insignificant period of time, resulting in a temporary decline in their diversity. Raup and Sepkoski statistically identified "Big five" mass extinctions events (**Figure 2**) that occurred in the end-Ordovician (~440 Ma), end-Devonian (~360Ma), late Permian (~252 Ma), end-Triassic (~201 Ma), and end-Cretaceous (~65.5 Ma). The relation of volcanism with mass extinctions has been broadly studied and a summary is presented in the following paragraphs.

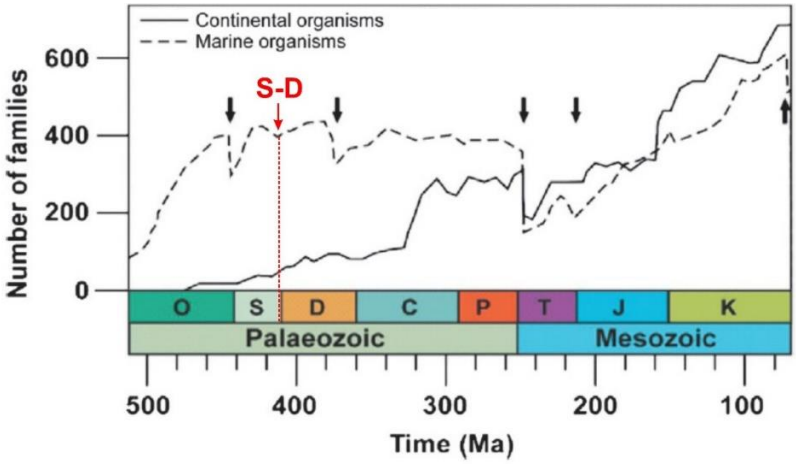


**Figure 2.** Patterns of family-level biodiversity evolution in the continent (solid line) and the ocean (dotted line). The black arrows mark the big five mass extinctions of Raup and Sepkoski, and the red arrow marks the Silurian–Devonian boundary extinction crisis of the present study. Modified from (Racki, 2019).

A volcanic trigger has been considered as an explanation for the catastrophic climate change that occurred at the end-Ordovician mass extinction (EOME). Such reasoning has

been supported by anomalous Hg contents found from marine successions from South China, and a Hg spike reported just below the first pulse of the biotic crisis. Such anomalies have been considered as consequences of a large igneous province (LIP) emplacement which has been also confirmed by Hg signatures of EOME successions from Poland (Racki, 2019, and references therein).

The end–Devonian mass extinction occurred in a stepwise manner, with several climate change episodes and periodic and sudden drops in biodiversity (Li et al., 2021, and references therein). Among several debated causes of this extinction, recent evidence of Hg enrichments worldwide connected with the emplacement of a LIP in eastern Siberia, and pulses of intrusions and eruptions have been postulated as possible causes of this extinction event (Racki, 2020). Moreover, the harmful effects of Hg on living organisms due to methylmercury poisoning, and Hg spikes in marine successions were reported by Rakociński et al. (2020) as support for the hypothesis on the causal link between intensive volcanism and the crisis at this time.

The coincidence of the end-Permian mass extinction horizon with Hg enrichments was reported by Wang et al., (2018) from deep water marine sediments of South China. The analysis of Hg contents and isotopes demonstrated that such enrichments were of atmospheric origin connected with volcanism associated with the Siberian LIP. Other studies also reported enhanced volcanic emissions, and Hg enrichments during this time although the impact of such spikes on the organisms during this time was uncertain (Li et al., 2021). However, Grasby et al., (2020) analyzed the origin of such Hg enrichments and their effects on the ecosystems, finding that pulses of Hg emissions to the atmosphere greatly exceeded the normal background concentrations. As a result, an increase in the greenhouse gas levels, and global warming occurred and were reported by Joachimski et al. (2012) in a study of apatite oxygen isotopes from two of the sections that were also analyzed by Wang et al. (2018). Additionally, extended anoxic environments reported by Brennecka et al. (2011) might have increased the MeHg production (Li et al., 2021), which likely had catastrophic impacts on the marine and terrestrial organisms explaining the extinctions that occurred in this interval (Grasby et al., 2020).

Similar findings have been reported for the end-Triassic, although such studies present limitations due to poor evidence of the process of Hg methylation at that time. In addition, the Hg toxic effects on the organisms that lived millions of years ago may not be the same as the effects on current organisms (Li et al., 2021).

The most recent study on the end-Cretaceous mass extinction, well known for the extinction of most dinosaur groups (Meyer et al., 2019), analyzed by first time biogenic carbonate clumped isotope paleothermometry and Hg concentrations in marine mollusks from wide global distribution. This work shows that apart from the Chicxulub meteoric impact, the Deccan Traps eruptions might have also contributed to extinctions patterns and/or enhanced ecological pressures on the biota in this time. The results indicate that the analyzed fossils register the evidence of temperature and Hg content rise at a global scale, which may be connected to volcanic $CO_2$ and Hg emissions that occurred during the Deccan eruptive activity in the Cretaceous–Paleogene boundary interval.

## 3.3. GEOLOGICAL SETTINGS

### 3.3.1. THE SILURIAN–DEVONIAN BOUNDARY INTERVAL IN THE PRAGUE BASIN

The Prague Basin is distinguished for being an area with well-exposed sequences of the Silurian–Devonian boundary interval. Importantly, the International Commission on Stratigraphy (ICS) and the International Union of Geological Sciences (IUGS) approved the recognition of the Global Boundary Stratotype Section and Point (GSSP) of this interval in Klonk near Suchomasty, and Budňanská skála near Karlštejn, as an auxiliary type section (parastratotype) in 1972.

This GSSP was the first global stratotype of a system boundary, and it was chosen after worldwide discussions and extensive research. Additionally, the method and procedure of the boundary definition and approvement provided a reference for the standardization of other chronostratigraphic boundaries (Chlupáč & Hladil, 2000).

Before the ratification of the GSSP, many biostratigraphic and paleontological studies were carried out in these sequences. Starting in 1846, Barrande divided these interval sequences in "étages", as lithostratigraphic units (i.e., mainly considering the dominant lithology). These units were considered chronostratigraphic units for many years (see discussion in Manda & Frýda, 2010). The definition of Barrande's étages caused significant controversies, especially because of the position of the S–D boundary (see Chlupáč, 1999; Vacek, 2009, and references therein). The modern biostratigraphic scale of the Přídolí and Lochkovian was defined by Přibyl (1940, 1943) by subdividing this stratigraphic interval into zones of graptolites ( Kříž et al., 1986; Kříž 1991, 1992). In further detailed studies of Chlupáč (1952, 1953), the S–D boundary was located at the boundary between the current Lochkov and Praha formations, which agreed with the hypothesis of that moment that graptolites do not occur in Devonian formations (Vacek, 2009). However, Bouček (1966) discovered new graptolite fauna in the Early Devonian Praha Formation and clearly showed that the concept of the Silurian–Devonian boundary based on the last occurrence of graptolites is unusable. In 1955, Horný suggested a division of the carbonate sequences into horizons according to the common content of fossils (e.g., brachiopod *Dayia bohemica*, or crinoid *Scyphocrinites*) (see discussion in Manda & Frýda, 2010). Following the recommendations that resulted from the first meeting of the S–D boundary in Prague in 1958, a Committee on the S–D boundary was established during the 21st International Geological Congress in Copenhagen, 1960.

Later on, the redefinition of the S–D boundary was established at the base of the *Monograptus uniformis* graptolite Biozone (i.e., at the level of the first occurrence of *Monograptus uniformis*) and the Lochkovian stage was assigned to the Devonian Period. After exhaustive research, the Committee confirmed the decision to recognize the S–D boundary GSSP at the Klonk section, which was later approved by the ICS and the IUGS, in 1972. Among the authors who described the stratotype in detail were Chlupáč et al., (1972), and Chlupáč & Kukal (1977) among others.

After 1972, the interest in studying the Klonk section significantly increased, and the research in this section was mainly focused on sedimentology and paleontology of chitinozoans, conodonts, and trilobites (see Horný, 1961; Chlupáč & Hladil, 2000, for references). Some of the paleontological studies revealed distinct changes in faunal communities of trilobites, brachiopods, bivalves, cephalopods, and gastropods, although

such investigations did not evaluate these changes quantitatively, therefore it was not possible to determine if such changes were significant if compared to “normal” levels of extinction rate (Manda & Frýda, 2010).

### 3.3.2. SILURIAN VOLCANISM IN THE PRAGUE BASIN

The Prague Basin (Teplá–Barrandian Unit, Bohemian Massif) was a continental rift basin, probably located on the Perunica microplate (**Figure 7**) (see Havlíček, 1980; Fatka & Mergl, 2009; Tasáryová et al., 2014, for details). As with other peri-Gondwana terrains, it preserves evidence of intense volcanic activity during the Silurian (Stampfli et al., 2002). The Silurian volcanism is probably related with a major episode of regional extension-related rifting of the Teplá‑Barrandian Unit (Kříž, 1998; Štorch, 1998; Tasáryová et al., 2018). This volcanic activity was controlled by deep faults that provided routes for magma ascendance (Kříž 1991, 1992; Štorch, 1998; Elbra et al., 2015).

The Silurian volcanism is restricted to the Aeronian stage-Ludlow series, with a significant peak at the Wenlock–Ludlow interval (Fiala, 1970; Patočka et al., 1993, 2003; Štorch 1998; Tasáryová et al., 2018). According to the latter authors, the trigger for this peak might be related to the closure of the Iapetus Ocean (slab-pull force). The latest phase of the Silurian volcanism was registered to the Suchomasty Volcanic Center (**Figure 3**) in basalts from Gorstian deposits, and it was concluded during the Ludlow series (Tasáryová et al., 2014).

Other extensive volcanic accumulations are concentrated in proximities to the Tachlovice fault (Svatý Jan Volcanic Centre, **Figure 3**), and a basalt intrusion into Telychian shales of the Motol Formation evidences the onset of the volcanic activity in this Volcanic Center (Kříž 1991, 1992; Elbra et al., 2015).

The occurrence of local volcanic products in Silurian sediments of the Prague Basin may obscure the record of a distinct global volcanic event from the large volcanic province. Therefore, the Hg-chemostratigraphy seems to be a suitable proxy for the determination of an intense volcanic event (causing Hg-anomaly), possibly influencing environmental and faunal changes.

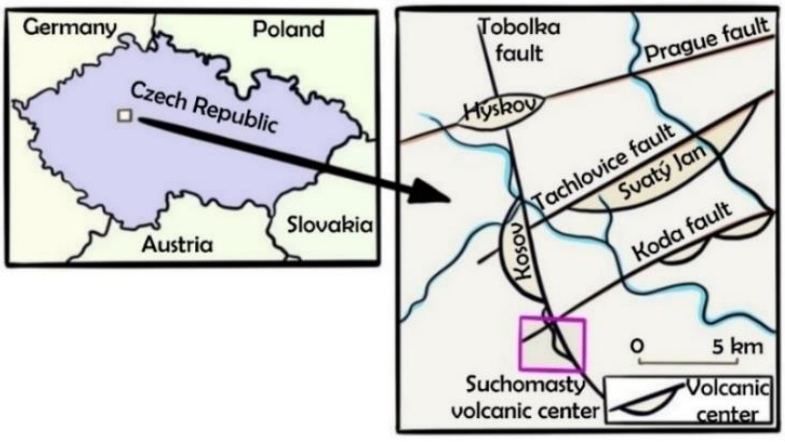


**Figure 3.** Location of volcanic centers of the Prague Basin and faults associated with the magma ascent in the Silurian. Modified from (Tasáryová et al., 2014).

### 3.3.3. OPATŘILKA SECTION

#### 3.3.3.1. LITHOLOGY AND BIOSTRATIGRAPHY

The Opatřilka section was described by Chlupáč (1972) as a key section for the study of the Silurian–Devonian boundary. Later, several studies provided more detailed information on the section, including microfacies analysis of its sedimentary record (Vacek, 2007) and carbon isotope chemostratigraphy (Manda & Frýda, 2010). The latest author's research covered the whole stratigraphic range that is studied in the present thesis. Therefore, both papers were taken as a reference for the lithological and paleontological description of the Opatřilka section.

The S–D boundary is marked in the section by the first occurrence of the index trilobite *Warburgella rugulosa rugulosa*, which was reported for the first time by Chlupáč et al. (1972). According to Chlupáč (1972), the lowest part of the Opatřilka section (**Figure 4**) is formed by the shallow-water facies (Kotýs limestones) of the Lochkov Formation. The latter facies occur in the NW flank of the Prague Basin and is mainly characterized by bioclastic limestones (Vacek, 2007).

The base of the measured section is located approximately 18 m below the S–D boundary (**Figure 4**) and belongs to the *M. bouceki* Biozone. The sample collected at this level corresponds to L40. This part is mainly dominated by an alternation of mudstones with shales and the base of the above-mentioned biozone consists of a crinoidal limestone with the dominant brachiopod species *Dayia minor*. Upwards, within *M. transgrediens* Biozone (**Figure 4**), cephalopod limestone or crinoidal limestone beds are alternated with mudstones. The limestone beds bear a distinct faunal community of cephalopods, bivalves, and gastropods. The next upper levels contain limestones with the brachiopods *Septatrypa* and *Dayia bohemica.* Intercalations of mudstones with limestones containing *Dayia bohemica* follow the latest layers. The uppermost Silurian (latest Přídolí) contains the index trilobite fossil *Tetinia minuta.* The earliest part of the section (Lochkovian) consists of crinoidal limestones.

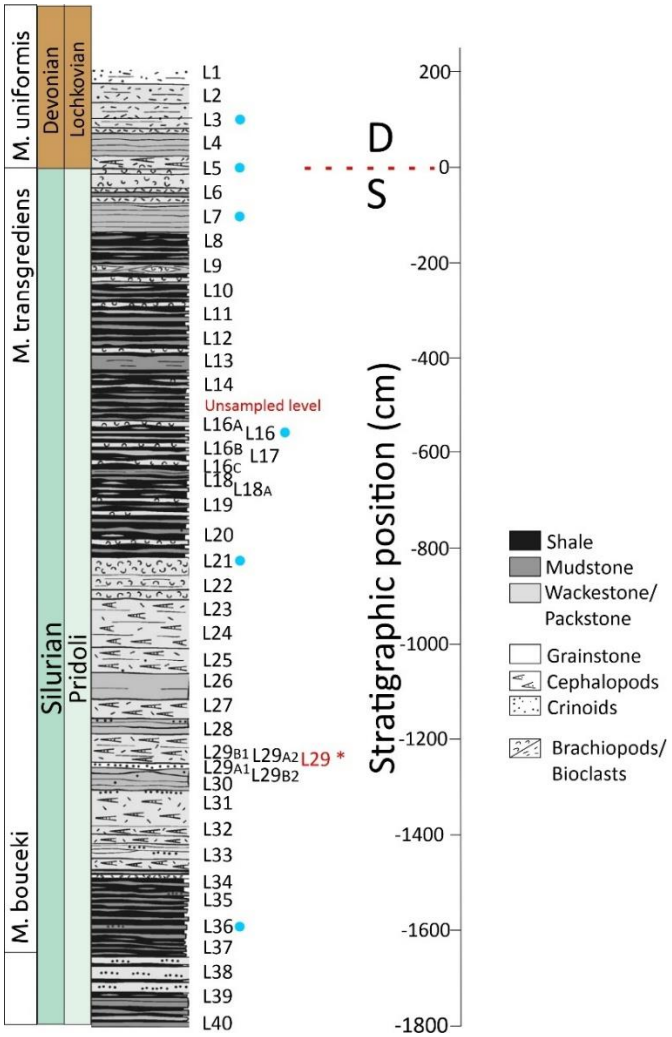


**Figure 4.** Stratigraphic column from the Opatřilka section showing zones defined by the index fossils from the S–D interval, lithology, fossils content, and location of the samples. Blue dots indicate levels chosen for thin sections analysis. The S–D boundary corresponds to the reference level (0 cm). Negatives positions correspond to samples collected below and positive ones to samples collected above the boundary. Modified from (Manda & Frýda, 2010).

### 3.3.3.2. PREVIOUS STUDIES: CARBON ISOTOPES AND EXTINCTIONS

Carbon isotope record from the Opatřilka section was studied by Manda and Frýda (2010). The latter study aimed to compare changes in the global carbon cycle in the ocean (inferred from the $\delta^{13}C$ record) with changes in the species-level diversity of cephalopods using a precise biostratigraphic division of the Silurian–Devonian interval.

In addition to the Opatřilka section, the Zadní Kopanina and Bílá skála sections were studied by Manda and Frýda (2010). The $\delta^{13}C$ results from all three sections were combined to generate a general trend for this interval in the Prague Basin. The results obtained from this composite signal, evidenced an increasing trend of the $\delta^{13}C$ signal within the latest Silurian reaching its highest values during early Lochkovian (early Devonian). Manda and Frýda (2010) reported the highest biodiversity of cephalopods during the rising trend of the $\delta^{13}C$ anomaly, likely connected with a shallowing in the upwelling system which provided water rich in nutrients. Such upwelling was reported

based on trace element geochemical data in sediments from the same stratigraphic interval in Poland (Porebska & Sawlowicz, 1997). Moreover, a progressive cooling tendency was reported by (Joachimski et al., 2009) during the latest Přídolí, which might have generated a deepening of cooler and denser water at high latitudes, affecting the global oceanic circulation (Manda & Frýda, 2010).

On the other hand, more than 80% of the cephalopod species become extinct before the last appearance of *M. transgrediens*, and high extinction rates also occurred during the latest Silurian and early Lochkovian. Manda and Frýda (2010) noted that the extinction affected benthic and demersal cephalopod species with relatively large eggs and long incubation times. The change in dynamics of the global carbon cycle thus coincides with the beginning of this extinction. Therefore, the above-mentioned anoxic or hypoxic events in the period between the last appearance datum of the *Monograptus transgrediens* (Transgrediens Bioevent) in the latest Přídolí and the base of the Devonian *Monograptus uniformis* Biozone was suggested to be a cause for the extinction of non-pelagic cephalopods (Manda & Frýda, 2010). The lack of oxygen was likely caused by the high productivity of cyanobacteria, depleting the available oxygen in the water, which also affected graptolites communities from the successions studied by Porebska & Salowicz (1997) in Poland.

### 3.3.4. KLONK SECTION

#### 3.3.4.1. LITHOLOGY AND BIOSTRATIGRAPHY

The Klonk section is composed of a thick sequence of rhythmically deposited limestones (Chlupáč et al., 1972, 1998; Chlupáč & Hladil, 2000) from a deep-marine setting in the southwestern part of the Prague Syncline (Hladil 1991, 1992). As defined by Chlupáč et al. (1972), the first appearance of the index graptolite *Monograptus uniformis* (**Figure 5**) determines the S–D boundary in this sequence (Hladil, 1992).

Comprehensive research on the sedimentological and diagenetic analysis of this sequence, and the nature of the boundary itself, was done by Hladil (1992), and authors cited therein. Hladil (1992) contrasted the turbiditic interpretation of the sequence given by Chlupáč & Kukal (1977). According to him, the shaly limestones from Klonk rather represent hemipelagic laminites rarely bioturbated with some presence of semilithified surfaces and hardgrounds. Regarding the boundary (bed No. 20 in the GSSP), it represents several laminated rhythms and is not of turbiditic origin either, although turbidite origin in a few beds from the upper part of the Přídolí was accepted. However, a later study on Sr isotopes from the GSSP (Frýda et al., 2002) reported higher $^{87}Sr/^{86}Sr$ values in the Devonian part of the boundary (Bed No. 20 GSSP), which may indicate an exotic material influx of recycled sediment and supports Hladil´s (1992) interpretation.

The Přídolí consists of rhythms of dark and shaly limestones which resemble regular climatic rhythms (Hladíková et al., 1997). Larger repetitive sets mostly composed of clayey interbeds, and carbonaceous beds were interpreted by Chlupáč (1988) as climatic microcycles that lasted around 15 Ka on average each (Hladil, 1992). This microcycle alternation is 0.25 m thick on average (Chlupáč & Hladil, 2000). According to the latter authors, the limestones beds contain only 15 from the 180 subordinated rhythms, while

the clayey interbeds contain the remaining ones, and the rate of sedimentation is about 20m/Ma. The limestones commonly contain fragments of the crinoid *Scyphocrinites*, and the shaly limestones interbed are rather rich in graptolites (Chlupáč & Hladil, 2000).

The earliest Devonian strata do not display distinct facies changes. Accumulation of cysts of prasinophycean algae was documented in the lower part of the boundary interval as well as changes in the direction of currents were also evidenced in Hladil's (1992) study. The latest Přídolí and earliest Lochkovian beds consist of platy bituminous limestones mostly of fine grain intercalated with mudstones interbed with sporadic crinoidal limestone stringers. The rhythmic accumulation of this alternated sequence displays thickening and coarsening upward.

Numerous biostratigraphic studies have been carried out in the Klonk section, and a summary of the investigations on biostratigraphy and identification of the boundary is provided by Chlupáč et al. (1972, 1998), Hladil (1991, 1992), Chlupáč & Vacek (2003), Hušková & Slavík (2019), and references therein. A generalized stratigraphic column with some of the index fossils and biostratigraphic zones defined within the interval can be observed in **Figure 5**.

The study of chitinozoans of the boundary interval was initially done by Paris et al. (1981), and a later study on acritarchs and prasinophytes was carried out by Brocke et al. (2006). The S–D boundary at the GSSP is established by the first appearance datum (FAD) of *Angochitina chlupaci* and by *Urnochitina urna*. The basal Lochkovian is characterized by the FAD of *Eisenackitina bohemica.*

Conodonts were initially studied by Jeppsson (1988, 1989) who defined the latest Přídolí part by the zone of *Ozarkodina steinhornensis eosteinhornensis*. This zone can be correlated with the late part of the *Monograptus transgrediens* zone and the *Ligonodina elegans detorta* zone, covering the short interval from the highest range of *Monograptus transgrediens* up to the boundary (Chlupáč & Hladil, 2000). However, given some discrepancies within the conodont zonation, a further review on conodonts (Carls et al., 2007) found that the use of a *detorta* Biozone for global correlation is not convenient since it is not limited to the final Přídolí. According to this revision, this zone enters before the *eostinhornensis* Biozone. Additionally, new conodont species (*Zieglerodina? ivochlupaci sp. nov., Zieglerodina? klonkensis sp. nov.* and *Zieglerodina? zellmeri sp. nov.)* with stratigraphical potential were described by the latest author. Recently, new conodont biostratigraphy of the Silurian–Devonian boundary interval was discussed by Hušková & Slavík (2019).

Prasinophytes are widely distributed, especially within the boundary interval, and they were assigned to the taxa *Leiosphaeridia* spp., ? *Pleurozonaria* and *Pterospermella* sp (Brocke et al., 2006).

Trilobites are scarce in the Pridolian part of the boundary interval (Přibyl & Vaněk, 1962), where they are concentrated in coarser bioclastic layers (Chlupáč & Hladil, 2000). Trilobites of the lowest part of the Lochkovian belong to the assemblage of *Warburgella* which is confined into the zone of the index graptolite *M. uniformis.*

Among the ostracods identified in the Silurian part of the interval are *Parahippa rediviva* (Barrande), *Craspedobolbina* (Harper), *Mirochilina jarovensis* (Bouček). According to Hansch (1993), the ostracods from the Přídolí are part of a mixture of diverse forms of deeper and pelagic environments (Chlupáč & Hladil, 2000).

The phyllocarids of the late Přídolí contain the index *Ceriatocaris (Bohemicaris) bohemica* (Barrande), and the lowest Lochkovian part contains *Ceratiocaris*

*cornwallisensis damesi* and *Aristozoe* (Chlupáč & Hladil, 2000). Some fish remains occurred in the late Přídolí and lower Lochkovian.

### 3.3.4.2. CHEMOSTRATIGRAPHY

Studies on carbon isotopes from the Klonk section have been done by Hladil (1992), Hladikova et al. (1997), and Buggisch & Mann (2004) among others. According to their results, there is a positive excursion at the S–D boundary, and this excursion can be also noted worldwide, therefore it is considered as a global trend.

In Hladil (1992) study, a few beds from Klonk were sampled for oxygen and carbon isotopes analyses. Results on carbon isotopes showed a general trend of more positive $\delta^{13}C$ values in the Devonian than in the Silurian. The author explained this shift as possible occurrences of abundant algal material with a subsequent rapid burial of organic matter. This explanation was further discussed in Hladiková et al. (1997). The latest authors also observed a general trend with a stepwise increase in the $\delta^{13}C$ values in the Lochkovian. The positive shift was interpreted as higher productivity, shallowing of the basin, and as reported by Hladil (1992), and rapid burial of organic matter enriched in $^{12}C$. Moreover, a moderate shallowing of the basin during the late Přídolí and early Lochkovian was evidenced by Chlupáč et al. (1992), and magnetic susceptibility studies by Crick et al. (2001). This shallowing contributed to the deposition of carbonate material, which might have increased the $\delta^{13}C$ values during this interval.

Similarly, data obtained by Buggisch and Mann (2004) from an analyzed core from the Klonk section, exhibited an increase in the $\delta^{13}C_{carb}$ values above the S–D boundary, and a drop 10 m above. The authors stated that some minor documented bioevents correlate to carbon isotopes excursions, among which is the Klonk event. This correlation between carbon isotopes excursions and bioevents was also discussed by Manda & Frýda (2010). A fall in the sea level, likely connected with the final Caledonian collision, caused the erosion of the large Silurian carbonate platforms (Buggisch & Mann, 2004). The same interpretation was given by Saltzman (2002) who also reported a $\delta^{13}C$ excursion in sections from North America. Moreover, the erosion of the Caledonian orogen, documented by an increase of $^{87}Sr/^{86}Sr$ values in marine carbonates (Veizer et al. 1999 in Buggisch & Mann, 2004 ) led to an increased nutrient flux, and bioproductivity, also contributing to the positive shift. Similarly, further study of Sr isotope variations from the GSSP (Frýda et al., 2002) reported higher $^{87}Sr/^{86}Sr$ values in the first Devonian bed (Bed No. 20 GSSP). This finding was interpreted as exotic material input of recycled sediment.

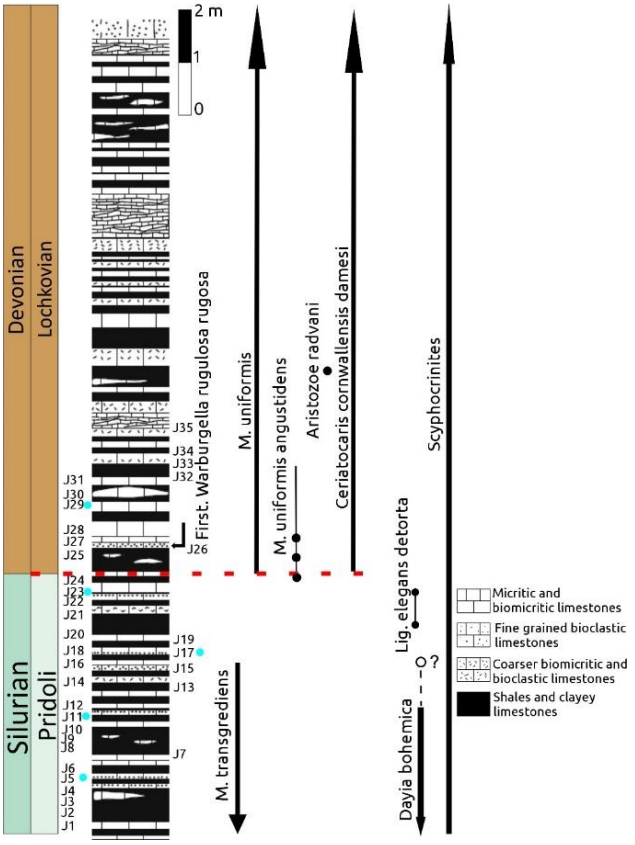


**Figure 5.** Generalized stratigraphic column of the Klonk section with occurrences of some fossils, location of samples analyzed in this study, and blue dots indicating samples chosen for thin section analysis. (Modified from Chlupáč, 2000. Originally in Chlupáč et al. 1972; Paris et al. 1981; Jeppsson, 1988).

# 4. METHODOLOGY

## 4.1. CHARACTERISTICS OF THE STUDY AREA

This study examines the well-exposed Silurian–Devonian boundary section in the Opatřilka quarry and the International stratotype section at the Klonk section. The Opatřilka section is located in an abandoned quarry on the north slope of the Daleje valley, about 750 m to the NW from an old chapel in the Holyně village. The Klonk stratotype section is located NE of the village Suchomasty, about 7 km S of the town Beroun and 40 km SW of Prague (**Figure 6**).

The sections are located in the Prague Basin, an eo-Variscan deformation structure (Vacek, 2007) that is part of the Barandian Unit of the Bohemian Massif. The Basin has an axis oriented in a NE-SW direction and is affected by several faults (Kříž, 1991). This crustal segment is composed of Neoproterozoic to Middle Devonian sedimentary and volcanic successions deformed during the Cadomian and Variscan (Havlíček, 1980; Kříž, 1992; Chlupáč et al., 1998; Vacek et al., 2018).

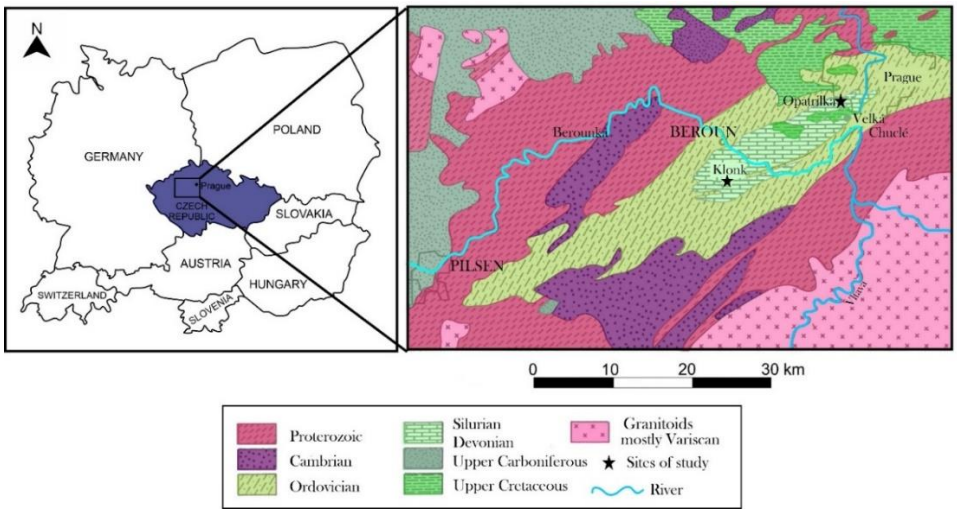


**Figure 6.** Location and geological setting of the area of the studied sections. Modified from (Chlupáč & Hladil, 2000).

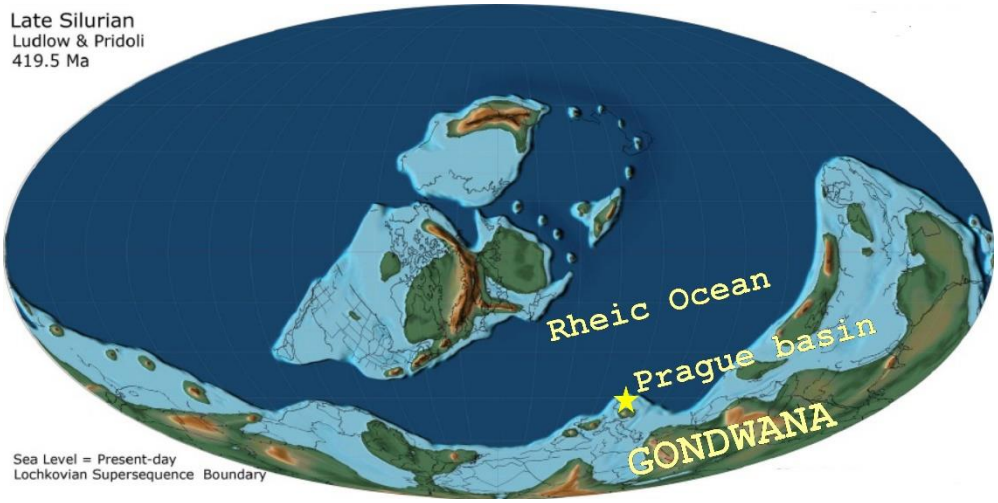


**Figure 7.** Paleogeography of the Late Silurian. The yellow star indicates an approximate location of the Prague Basin. Modified from Scotese (2014).

## 4.2. SAMPLE PREPARATION

A total of 48 rock samples were collected from the Opatřilka section with the help of the supervisor Jiří Frýda. The rocks were sampled approximately every 50 cm, starting from the youngest levels (Devonian). They were labeled with the letter "L" together with the number of the sample. The youngest one corresponds to sample L1, and the sequence continues down to sample L40 (**Figure 4**). At some levels in the Opatřilka section, duplicate samples were collected to corroborate the high values obtained in the Hg analysis.

The rock collection in the Klonk outcrop was done by both the supervisor and the author of this work, and a total of 35 samples were taken from this section. Bed No. 20 (where the S–D boundary was established) was taken as the reference level (**Figure 5**), and the samples were labeled under the letter "J" with a number. The sample J1 corresponds to the oldest collected sample (Silurian), and it is located 485 cm below the S–D boundary.

The subsequent samples were taken considering the interbedded sequence of shales, marls, and limestones. The youngest sample corresponds to J35 which is located at bed 28 (considering the stratigraphic labeling of the stratotype that was done during its recognition). The sample J24 is approximately located at the middle of Bed No. 20 (The S–D boundary), thus the subsequent samples belong to the Devonian. The distances between them were registered, as well as their stratigraphic position considering the number of beds given by the description of the stratotype section.

Once the fieldwork was done, all samples were taken to the Czech Geological Survey in Barrandov (Prague) for their preparation for the geochemical analyses. Firstly, all samples were carefully washed and dried to remove any piece of soil, vegetation, or fragment that could represent a source of contamination for the sample, and therefore affect the geochemical analyses. Afterward, the samples were carefully broken into smaller pieces with a geological hammer. These samples were later ground with the help of a hydraulic crusher. After this procedure, each sample was carefully sorted to ensure the selection of small rock pieces from fresh parts of the rock (i.e., weathered fragments or fragments with calcite veins). 30 grams of each sample were weighed after the sorting for complete pulverization/homogenization as required for the equipment for geochemical analyses. The latter process was done by using an agate mill (**Figure 9**). This process was done with the help and under the supervision of a technician of the Czech Geological Survey.

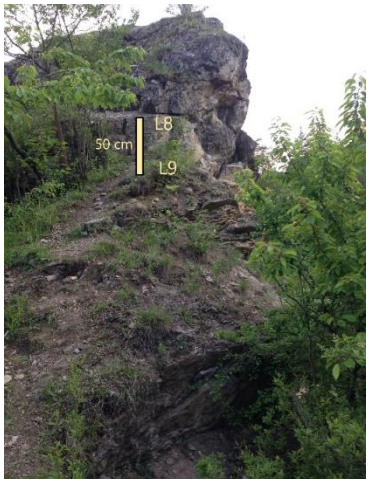


**Figure 8.** Opatřilka section. Samples L8 and L9 (Silurian)

**Figure 9.** Left: Agate balls. Right: Mill for homogenization of samples.


**Figure 10.** Klonk outcrop and approximate location of the S–D boundary at Bed No. 20.

## 4.3. MICROFACIES ANALYSES

A total of six samples were selected for thin section analysis from the Opatřilka section, mainly considering samples with different lithology. Therefore, the selected samples (L3, L5, L7, L16, L21, and L36) cover all main limestone types from the Opatřilka section. The samples L3 and L5 come from the Devonian strata, and the sample L5 is located very close to the S–D boundary (**Figure 4**). The rest of the samples belong to the Silurian part of the section.

At the Klonk section, a total of five samples were selected for microfacies analysis. The Klonk section represents a deposition in a deeper environment what is manifested by the high occurrence of shale beds interbedding the limestone beds. The selected samples (J5, J11, J17, J23, and J29) include all main rock types (**Figure 5**).

The sample J29 comes from the Devonian part of the section. The rest of the samples are of the Silurian age. Classification of Dunham (1962) was used for rock description of microfacies. Thin sections were prepared in laboratories of the Czech Geological Survey (Prague).

## 4.4. ELEMENTAL ANALYSIS

Major and trace element analyses were performed on aliquots of rock powder samples. Concentrations of major ($Al_2O_3$, CaO, $Fe_2O_3$, $K_2O$, MgO, MnO, $Na_2O$, $P_2O_5$, $SiO_2$, $TiO_2$) and trace elements (Ba, Cd, Ce, Co, Cr, Cu, Ga, La, Mo, Nb, Nd, Ni, Pb, Rb, Sc, Sr, Th, U, V, Y, Zn, Zr) were analyzed by using X-Ray Fluorescence method (XRF; Rigaku WD-XRF Primus 4). Several international carbonate or shale standards (GeoPT 40, GeoPT

40A, GeoPT 44, GeoPT 44A, GeoPT 42-Q1, GeoPT 6A-CAL-S, DC73302, DC73306) were used as reference standards. Accuracy and precision were controlled by replicate measurements of laboratory standards, and they were better than ±5%.

All results obtained from the elemental analysis in this thesis (ppm, wt %) represent mass fractions.

## 4.5. TOTAL CARBON (TC) AND TOTAL SULFUR (TS) ANALYSES

For TC (or TS) analyses, about 150 mg of rock were first heated and dried at 80 ◦C for 1 h to remove water. Then, the samples were burned in a ceramic tube in an oxygen stream at 1350–1450◦C to $CO_2$ (or $SO_2$). Moisture and dust were removed from the gas by passing it through drying and sorption columns filled with anhydrone and sodium hydroxide. Then ($CO_2$ or $SO_2$) analyses of the cleaned and dried were performed by using an ELTRA CS 500. Accuracy and precision were controlled by replicate measurements of laboratory standards and were better than ±5% for TC analyses (for concentration range 0.05–50 wt% of carbon) and about 10% for low S concentration (for 0.05–0.50 wt% S) and about 5% for higher S concentration.

All results obtained from TC and TS analysis in this thesis represent mass fractions (wt %).

## 4.6. THE CARBONATE CARBON ANALYSIS

The carbonate carbon was released from the sample by reaction with concentrated phosphoric acid. The $CO_2$ was dried together with the carrier gas in drying columns with anhydrone and sodium hydroxide. The dried $CO_2$ is introduced into the measuring cells of the ELTRA CS 500 analyzer. The absorption of $CO_2$ in the infrared region was measured.

The wt% content of total organic (TOC) was calculated from total carbon and $CO_2$ concentrations as follows:

$$IC\ (wt\ \%) = CO_2(wt\ \%) * {}^{C\ atomic\ mass}/_{CO_2\ atomic\ mass} =$$

$$CO_2(wt\ \%) * 0.2727$$

$$TOC = TC - IC$$

The wt% content of $CaCO_3$ to determine the lithology of each sample (limestone, marl, or shale) was calculated as follows:

$$CaCO_3(wt\ \%) = CO_2(wt\ \%) * {}^{atomic\ mass\ CaCO_3}/_{atomic\ mass\ CO_2} =$$

$$CO_2(wt\ \%) * 2.272$$

All results obtained from carbonate carbon analysis in this thesis (wt %) represent mass fractions.

## 4.7. MERCURY ANALYSIS

The mercury concentration of rock samples was analyzed by AAS, using the AMA254 Advanced Mercury Analyzer (geochemical laboratories of Czech Geological Survey, Prague), which is specifically designed to determine the total mercury content in various

solids and liquids. For Hg analyses, 100 mg of rock powder was used, and about 10% of the samples were duplicated. The limit of determination for solid samples is ~1 ppb, and the blank value was lower than 0.2 ppb. All results obtained from mercury analysis in this thesis (ppb) represent mass fractions.

### 4.8. DATA PROCESSING

Standard parametric, as well as non-parametric statistical methods, were used for the evaluation of relationships between geochemical variables.

The normality of variables was tested by using the Shapiro-Wilk test. The results of the tests rejected a normal distribution in the great majority of obtained variables. Because of that, only a non-parametric statistical method (Spearman) was used for correlation analysis.

Two software were used for data processing: software package Past 4.03 for testing normality for obtained variables, and calculation of Spearman correlation coefficient, and R-studio for construction of the scatter plots illustrating the correlation between chemical variables.

Organic carbon, as well as a sulfur-bearing compound, have been considered to be carriers of mercury within sedimentary rocks. For this reason, the raw Hg data were normalized by TOC, TS, and TOC+TS by dividing Hg concentrations by the latter compounds. Content of total sulfur is general were low (sometimes even close to the lower limit of quantification in the cases of the Opatřilka section). Therefore, calculations of the Hg/TS values may be burdened with a significant error. The normalization by TOC+TS was considered to be more reliable because normalization by solely TS is very sensitive not only to analytical error but also to weathering of iron sulfides.

## 5. RESULTS

### 5.1. MICROFACIES ANALYSES

Broadly, the Opatřilka section is mainly characterized by microfacies of grainstones and packstones with a noticeable presence of pelagic fossils, corresponding to a shallow-water deposition setting. By contrast, the Klonk section corresponds to a deeper depositional setting, and its microfacies consist mainly of laminated mudstones rarely bioturbated, with distinct presence of recrystallized microfossils, and sometimes pelagic fossils redeposited by currents.

In Opatřilka, the following microfacies were identified from the analyzed thin sections (Figs 11, 12):

**Op1: Crinoidal grainstone.** Devonian. This microfacies presents abundant crinoids ossicles, ostracods shells, and disarticulated trilobites. Abundant peloids can be observed especially in the photo from **Figure 11 A**. Moderate to poorly sorted. Photo in **Figure 11 B** shows a feature of diagenetic overgrowth: syntaxial cement in crinoids. Matrix is strongly recrystallized, most of the original mud was washed. Sparite cement is also observed. This microfacies is present in the thin section from sample L3.

**Op2: Brachiopod packstone**. S–D boundary and Silurian: Contains disarticulated brachiopods shells. Fragments of crinoids, ostracods, trilobites, and peloids are also present. Poorly sorted. The matrix may be slightly recrystallized (**Figure 11 C**), and at some parts dolomitized (**Figure 11 D** and **Figure 12 A, B**). This microfacies is present in thin sections from sample L5 (S–D boundary), L16, and L21 (Silurian). A geopetal structure was observed in a thin section from sample L16 (**Figure 12 A, B**). Sample L21 shows an incomplete shell probably of *Dayia bohemica* brachiopod (**Figure 12 D**). This shell is filled with dolomite and calcite.

**Op3: Peloidal packstone:** Silurian. This microfacies is observed in the thin section from sample L7. It is characterized by the presence of crinoids remains, ostracods shells, fragments of trilobites, and abundant peloids. Well- sorted. A stylolite is observed at the top right of the photo in **Figure 11 E**.

**Op4: Laminated packstone:** Silurian. Characterized by horizontal lamination. An alternation of light and dark laminas is observed. Light ones may correspond to sparite cement with some fragments of shells debris of crinoids with infill of sparite (strongly recrystallized) and peloids. Matrix is strongly recrystallized. Poorly sorted and no bioturbation present. This Microfacies is observed in sample L36 (**Figure 12 E, F**).

The following microfacies were identified from the analyzed thin sections coming from the Klonk section, (**Figure 13** and **Figure 14**):

**Kl1: Laminated mudstone with muellerisphaerida:** Silurian. Homogeneous mudstone with no bioturbation, and horizontal lamination. Fine-grained. Well sorted from deep marine background sedimentation (calmed environment). Consists of grains of recrystallized microfossils (muellerisphaerida), and debris of planktonic shells. Present in thin sections from samples J29 (Devonian. **Figure 13 A, B**), J23 (**Figure 13 B**), J17 (**Figure 13 D**), and J5 (Silurian. **Figure 14 A, B**). Cyst of algae (possibly prasinophycean) can be seen from sample J23 (**Figure 13 C**).

**Kl2: Laminated wackestone with crinoids:** Silurian. Moderate to poorly sorted. Presents sub-horizontal lamination and a distinct layer with abundant fragments of crinoids and some graptolites which were possibly redeposited in episodes of stronger currents (storm). Clasts show imbrication within this layer. Observed in sample J11 (**Figure 13 E, F**).

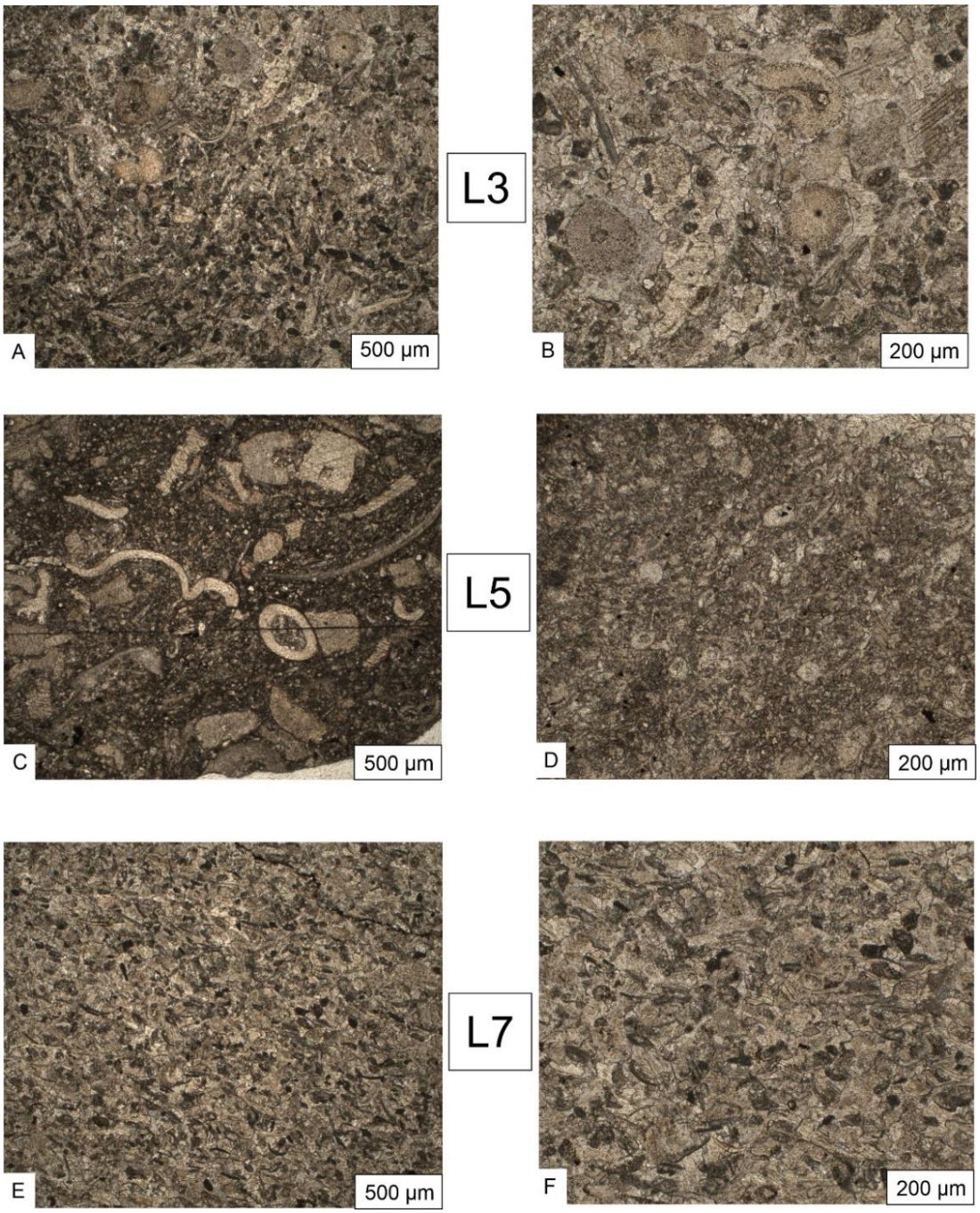


**Figure 11.** Thin section photographs of the samples (L3, L5, and L7) of the Opatřilka section. **A-B:** Devonian. Crinoidal grainstone. **A:** Top part of a thin section from sample L3. **B:** Base part of a thin section from sample L3. **C-D:** Silurian–Devonian boundary. Brachiopod packstone. **C:** Top part of the thin section from sample L5 **D:** Middle part of the thin section from sample L5. **E-F:** Silurian. Peloidal packstone. **E:** Base of the thin section from sample L7. **F:** Middle part of the thin section from sample L7.

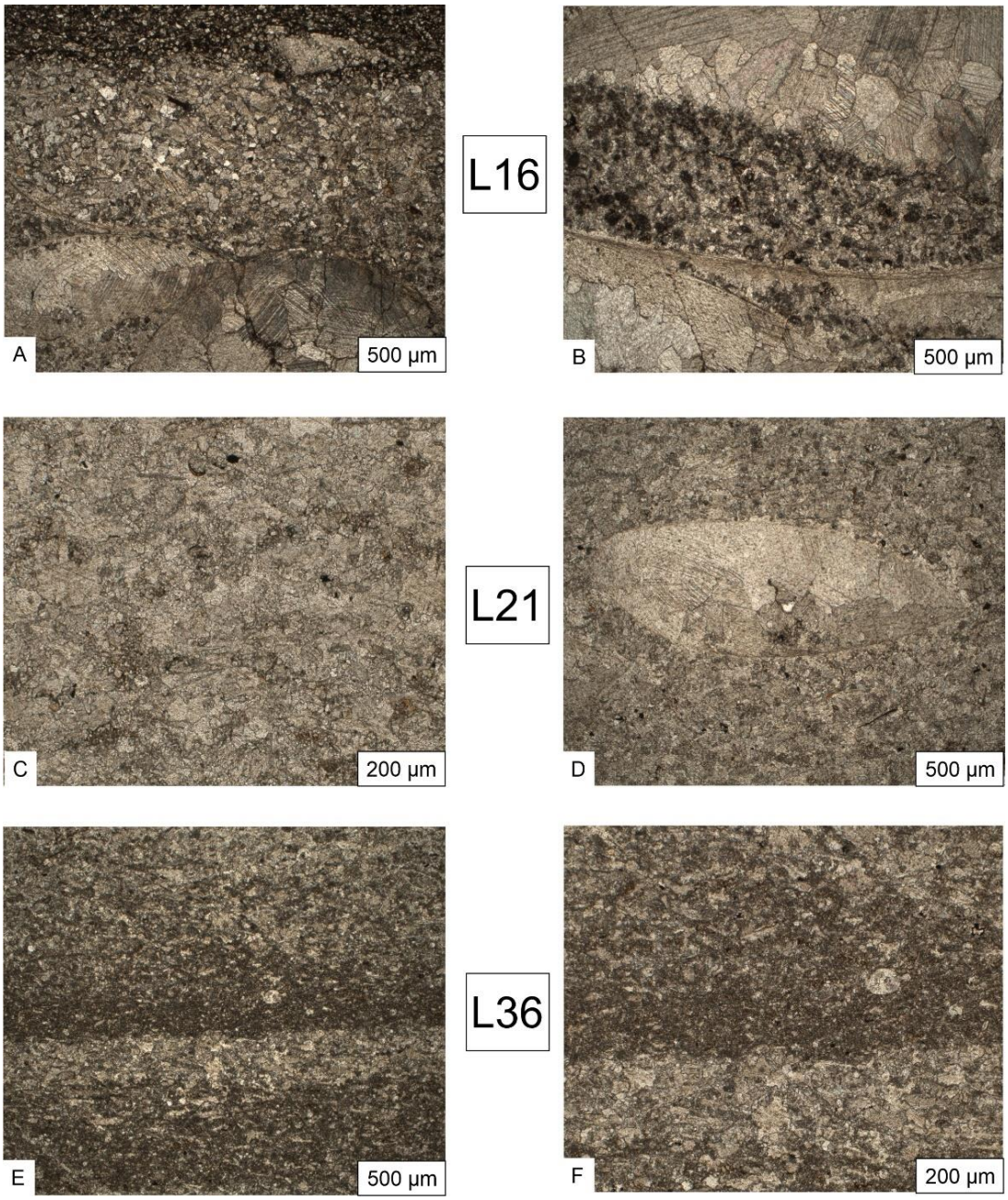


**Figure 12.** Thin section photographs of the samples (L16, L21, and L36) of the Opatřilka section. All samples come from the Silurian strata. **A-B:** Brachiopod packstone. A: Base of the thin section from sample L16. B: Middle part of the thin section from sample L16. **C-D:** Brachiopod packstone. C: Base of the thin section from sample L21. D: Middle part of the thin section showing possibly a shell of *Dayia bohemica*. **E-F:** Laminated packstone. Both photographs belong to the base part of the thin section from sample L36.

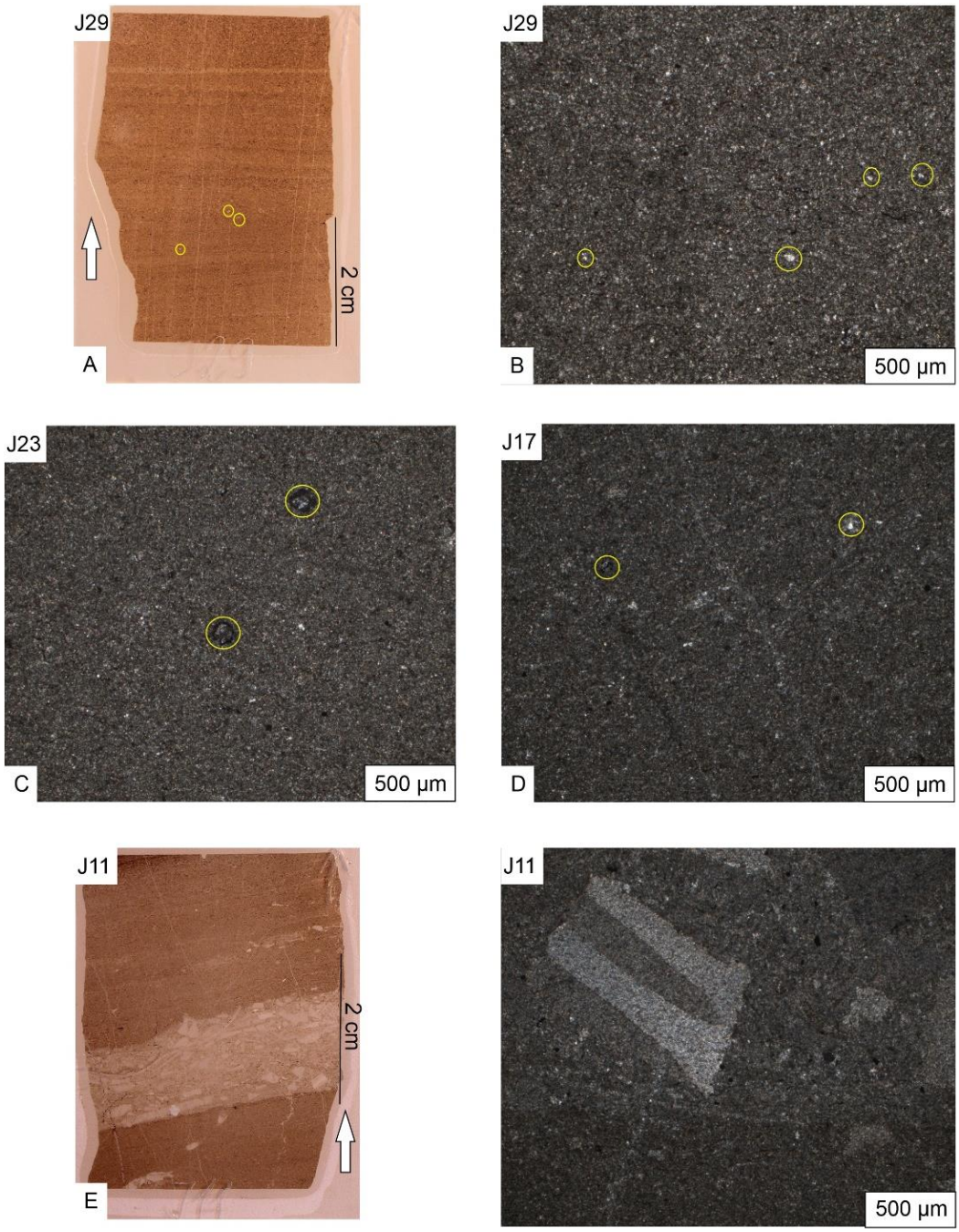


**Figure 13.** Thin section photographs of the samples (J29, J23, J17, and J11) from the Klonk section. **A-B:** Devonian. Laminated mudstone with muellerisphaerida. Photo A shows horizontal lamination with some tiny light layers (sparite). Yellow circles show recrystallized microfossils, a distinct feature of this microfacies. **C-D:** Silurian. Another laminated mudstone with muellerisphaerida. Yellow circles in photo C show cyst of green algae (prasinophycean). **E-F:** Silurian. Laminated wackestone with crinoids. Photo E shows subhorizontal lamination and a distinct layer with disarticulated crinoids and some graptolites that present imbrication. F shows a recrystallized skeletal fragment of a crinoid (possibly *Scyphocrinites*).

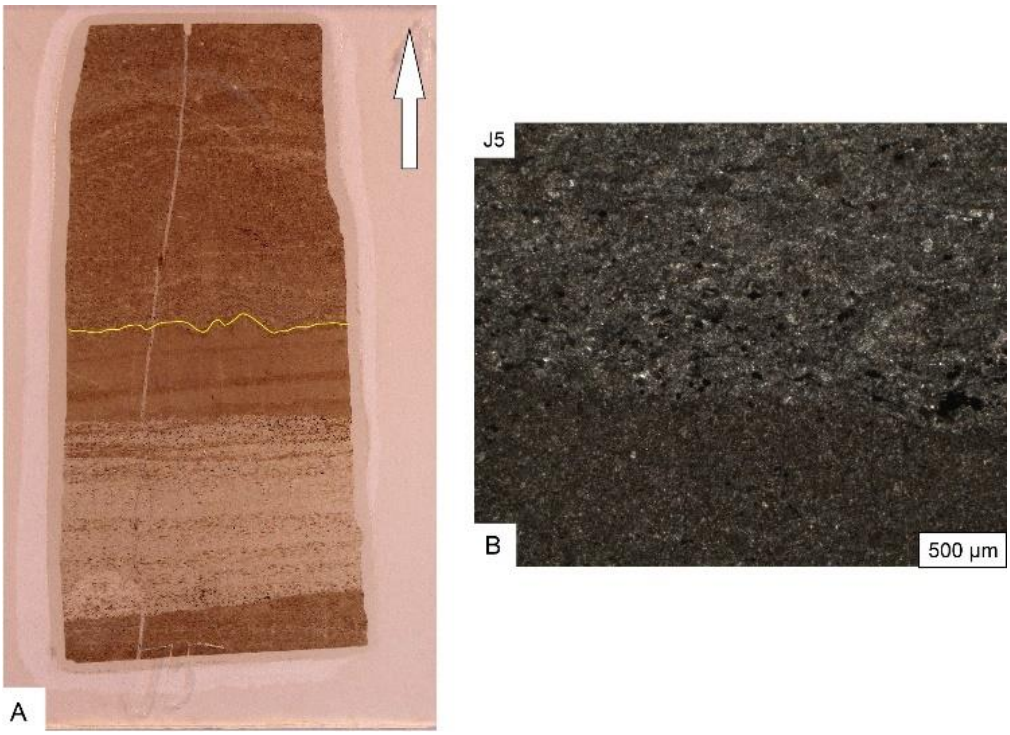


**Figure 14.** Thin section photographs of the sample J5 from the Klonk section. Silurian. The yellow line in photo A shows an erosional surface. Photo B belongs to the base part of the thin section, showing the contact between a lamina of very fine grain and a coarser grain one with stronger recrystallization. Lighter layers contain some pelagic fossils fragments likely redeposited by currents.

## 5.2. MERCURY CHEMOSTRATIGRAPHY

### 5.2.1. OPATŘILKA SECTION

#### 5.2.1.1. MERCURY, TOTAL ORGANIC CARBON, AND TOTAL SULFUR

The Opatřilka section exhibits an anomalous Hg value of 227.2 ppb and 235.7 ppb (there are two anomalous values since the measurement was repeated to corroborate the first obtained value using different fragments of the sample L29). The background values range from 0.6 ppb up to 17.61 ppb (**Table 5**, **Appendix A**). The lowest Hg concentrations are mostly found in the Devonian where thick layers of limestones dominate (**Figure 15**). The highest values, including the anomalous ones, are mainly present in the Silurian levels and close to the base of the section.

The TOC values range from 0.08 wt. % up to 0.46 wt. % (**Table 5**, **Appendix A**). The Devonian samples contain some of the lowest TOC concentrations, and the rest of the lowest ones are found close to the S–D boundary, and at intermediate and lowest levels. The highest contents are mostly found at the lowest stratigraphic levels, very close to the base of the section, and also close to the level where the anomalous Hg concentration was found (**Figure 15**). However, two Devonian samples display high TOC content.

The TS results range from the limit of quantification (~ 0.01 wt %) up to 0.16 wt. % (**Table 5**, **Appendix A**). The lowest TS values are mainly present at the levels close to the S–D boundary and intermediate and lower-intermediate levels. The highest ones coincide with the anomalous Hg concentrations and also with the highest Hg values among the background levels.

The results of the normalization by TOC are highly variable and range from 2.34 ppb/wt.% up to 932.86 ppb/wt.% (**Table 5**, **Appendix A**). The distribution of the lowest values is very much alike to the distribution observed for Hg (**Figure 15**). All the Devonian samples contain the smallest values, and the rest of them are distributed among intermediate and lower stratigraphic levels. The highest results also coincide with the anomalous Hg levels and the highest ones among the background levels. The normalization obtained by TS is extremely variable and displays values from 15.22 ppb/wt. % up to 4866.5 ppb/wt. % (**Table 5**, **Appendix A**). The lowest values are mainly present at Devonian strata (**Figure 15**), and intermediate ones are widely distributed across the section. The highest results correspond to both anomalous Hg samples. Lastly, the normalization by TOC+TS also displays a much alike pattern, an range from 2.25 ppb/wt.% up to 782.80 ppb/wt.%.

#### 5.2.1.2. CORRELATIONS BETWEEN MERCURY AND MAJOR ELEMENTS

For the Opatřilka section, two correlation analyses were carried out: one excluding the sample with the anomalous Hg value, and another one including it. The correlation plots and tables shown in this chapter correspond to the correlation analyses excluding the sample with the Hg anomaly. These outliers were excluded since they affect the correlation analyses results, and for better visualization of the relationships between Hg and the analyzed chemical compounds.

The Shapiro-Wilk test of normality of the major element concentrations from the Opatřilka section (excluding the sample with the Hg anomaly) rejected the normal distribution for all major elements except MnO concentrations (p-value=0.469. **Table 6**, **Appendix B**).

All major elements, except MnO, $Na_2O$, and $P_2O_5$ (p-values >0.05), have a significant statistical correlation with Hg according to the results of the Spearman's correlation coefficient method (**Table 9**). Apart from CaO and $CO_2$, all major elements that have a significant statistical correlation with Hg, display positive correlations (**Figure 16** and **Figure 17**).

**Table 1.** Results of the correlation analysis (Spearman's correlation coefficients and p-values) of mercury (excluding anomalies) and major elements of samples coming from the Opatřilka section. Spearman's correlation coefficients ($r_s$) for mercury are indicated in red color and p-values in blue. Bolded values show correlations that are statistically significant (p-values < 0.05).

| **Hg and major elements** | | | | | | | | | | | | | |
|---|---|---|---|---|---|---|---|---|---|---|---|---|---|
| | **Hg (ppb)** | **$Al_2O_3$ (wt%)** | **CaO (wt%)** | **$Fe_2O_3$ (wt%)** | **$K_2O$ (wt%)** | **MgO (wt%)** | **MnO (wt%)** | **$Na_2O$ (wt%)** | **$P_2O_5$ (wt%)** | **$SiO_2$ (wt%)** | **$TiO_2$ (wt%)** | **$CO_2$ (wt%)** | **Total Sulfurs (wt%)** |
| **Hg (ppb)** | | **2.30E-08** | **5.33E-04** | **6.34E-03** | **5.47E-07** | **1.49E-02** | 0.558 | 0.173 | 0.854 | **3.52E-06** | **1.99E-03** | **4.08E-04** | **2.35E-03** |
| **$Al_2O_3$ (wt%)** | **0.715** | | 1.08E-11 | 1.13E-06 | 8.09E-17 | 3.29E-06 | 0.026175 | 0.003424 | 0.29958 | 3.21E-15 | 1.55E-07 | 5.89E-08 | 0.010268 |
| **CaO (wt%)** | **-0.491** | -0.809 | | 3.43E-07 | 5.52E-18 | 5.48E-18 | 0.097776 | 0.004044 | 0.015522 | 2.43E-20 | 1.19E-06 | 1.19E-07 | 0.0010804 |
| **$Fe_2O_3$ (wt%)** | **0.397** | 0.648 | -0.671 | | 4.62E-06 | 3.99E-04 | 8.21E-04 | 1.80E-03 | 5.92E-01 | 5.55E-07 | 7.33E-09 | 1.18E-11 | 1.81E-02 |
| **$K_2O$ (wt%)** | **0.662** | 0.893 | -0.905 | 0.619 | | 3.51E-09 | 6.93E-02 | 1.65E-03 | 3.54E-02 | 9.67E-28 | 2.78E-09 | 4.84E-08 | 1.24E-04 |
| **MgO (wt%)** | **0.357** | 0.626 | -0.906 | 0.500 | 0.742 | | 4.68E-01 | 2.67E-02 | 7.71E-03 | 1.68E-09 | 4.03E-03 | 1.13E-04 | 7.16E-03 |
| **MnO (wt%)** | 0.089 | 0.328 | -0.247 | 0.476 | 0.270 | 0.110 | | 7.93E-01 | 9.25E-01 | 2.92E-02 | 2.38E-02 | 2.54E-03 | 6.36E-01 |
| **$Na_2O$ (wt%)** | 0.204 | 0.423 | -0.416 | 0.448 | 0.451 | 0.327 | 0.040 | | 2.29E-01 | 2.28E-03 | 2.11E-05 | 3.67E-03 | 4.66E-02 |
| **$P_2O_5$ (wt%)** | -0.028 | -0.156 | 0.355 | 0.081 | -0.311 | -0.388 | -0.014 | 0.181 | | 4.57E-02 | 5.87E-01 | 6.66E-01 | 3.83E-01 |
| **$SiO_2$ (wt%)** | **0.624** | 0.872 | -0.927 | 0.662 | 0.967 | 0.752 | 0.322 | 0.439 | -0.296 | | 2.14E-08 | 6.95E-09 | 1.06E-04 |
| **$TiO_2$ (wt%)** | **0.444** | 0.685 | -0.647 | 0.732 | 0.746 | 0.416 | 0.333 | 0.583 | -0.082 | 0.717 | | 1.30E-08 | 1.05E-02 |
| **$CO_2$ (wt%)** | **-0.500** | -0.701 | 0.689 | -0.808 | -0.704 | -0.539 | -0.435 | -0.420 | -0.065 | -0.733 | -0.724 | | 5.61E-03 |
| **Total Sulfur (wt%)** | **0.438** | 0.375 | -0.467 | 0.347 | 0.536 | 0.391 | -0.072 | 0.295 | -0.132 | 0.540 | 0.374 | -0.402 | |

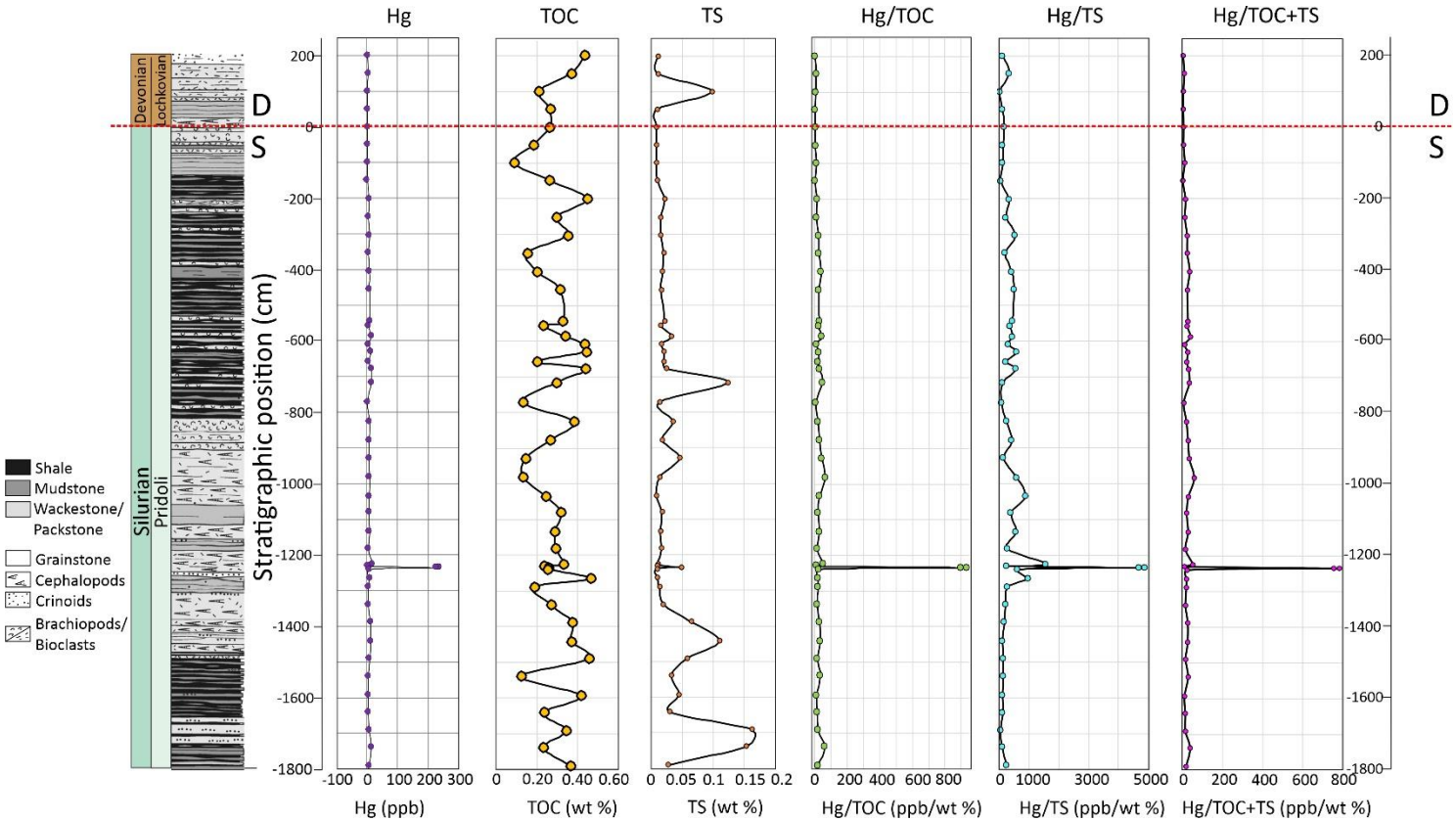


**Figure 15.** Chemostratigraphy of Hg in the Opatřilka section. A. Hg concentrations across the S–D boundary. B. Total Organic Carbon (TOC). C. Total Sulfur (TS). D. Mercury concentrations normalized by TOC (Hg/TOC). E. Mercury concentrations normalized by TS (Hg/TS). F. Mercury concentrations normalized by TOC+TS (Hg/TOC+TS). The stratigraphic position 0 cm corresponds to the reference level (the S–D boundary). Values below are indicated as negative, and values above are indicated as positive. Stratigraphic column modified from (Manda & Frýda, 2010).

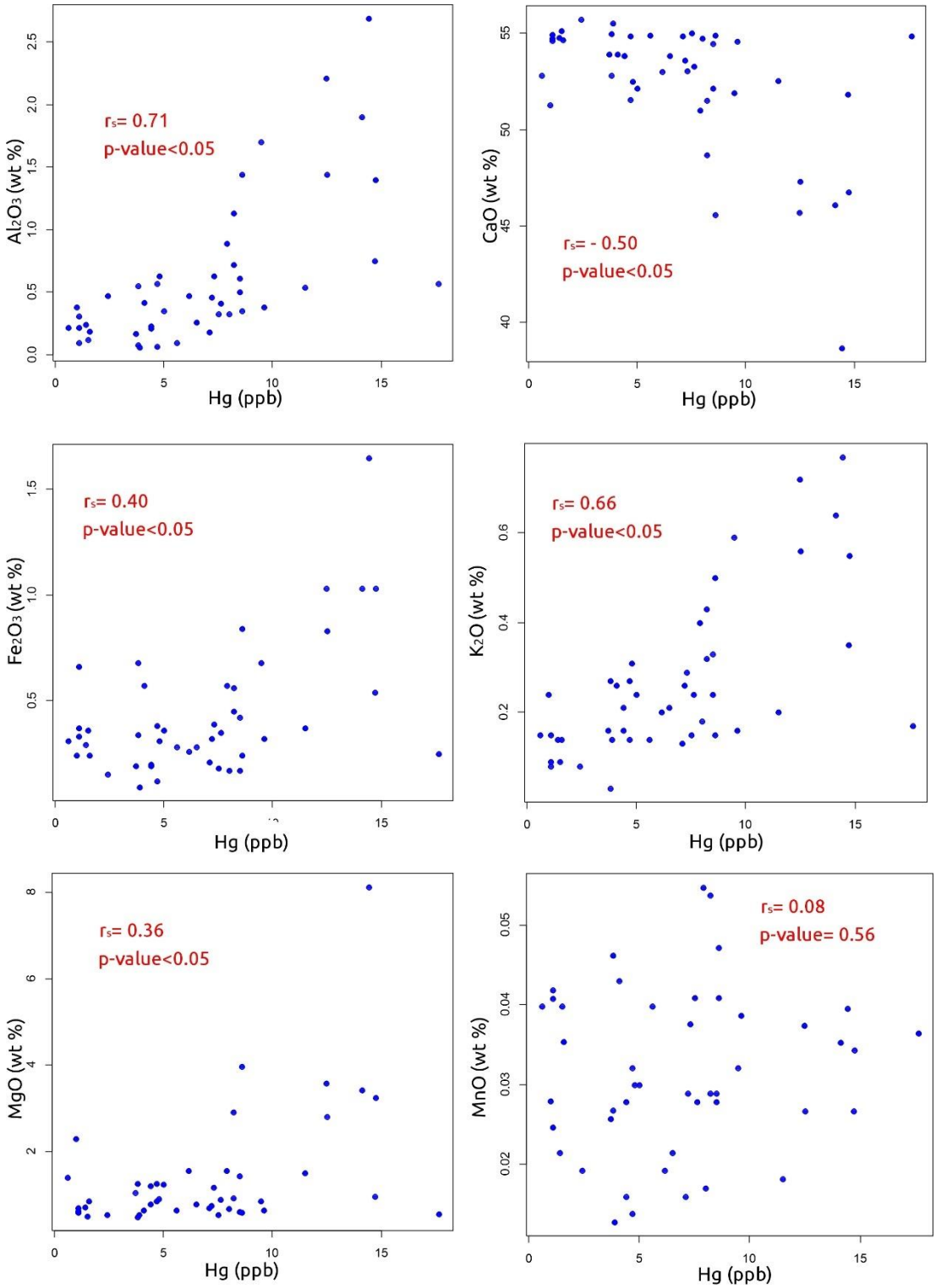


**Figure 16.** Hg and major elements ($Al_2O_3$, CaO, $Fe_2O_3$, $K_2O$, MgO, and MnO) correlations plots from the Opatřilka section (Samples with Hg anomalies are excluded). The $r_s$ values correspond to Spearman's correlation coefficients.

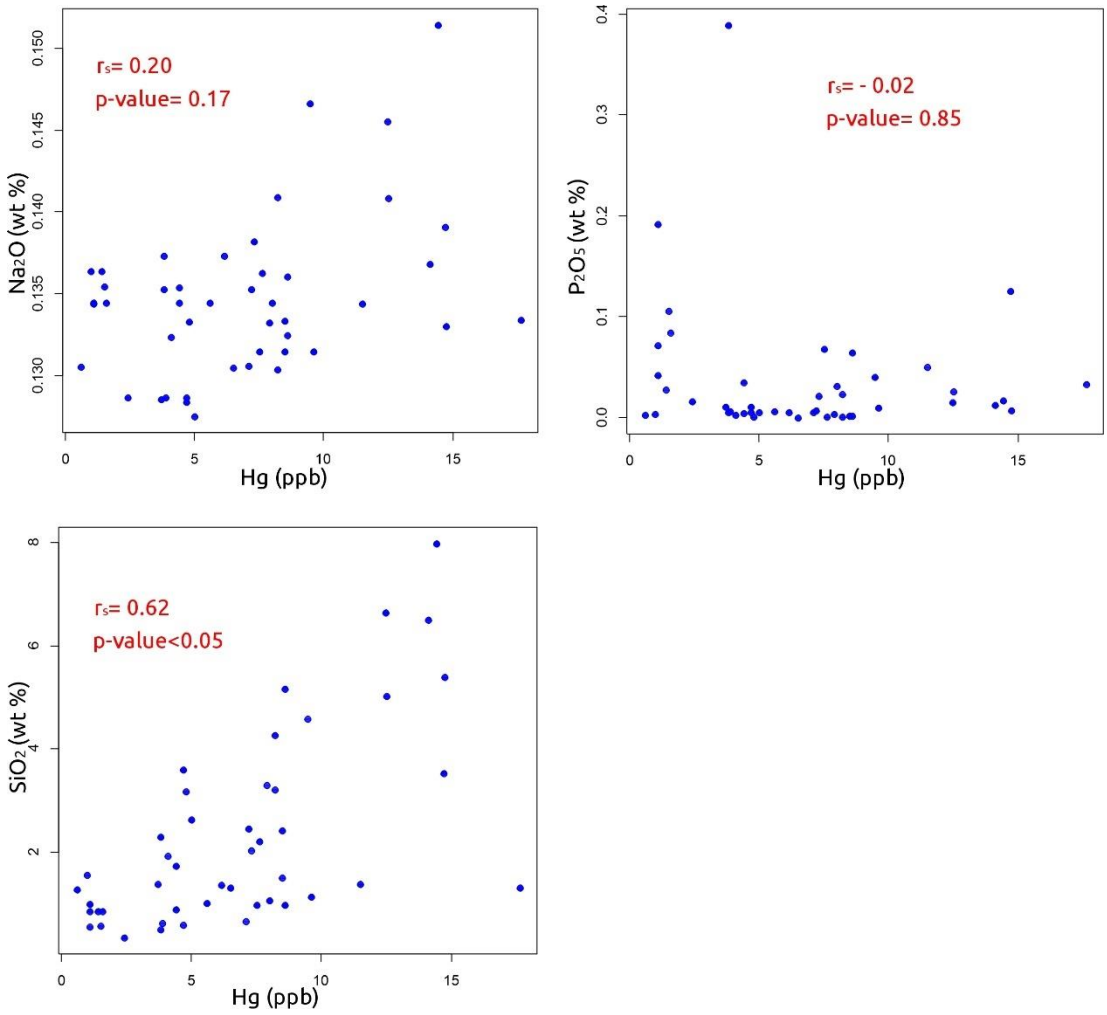


**Figure 17.** Hg and major elements ($Na_2O$, $P_2O_5$, and $SiO_2$) correlations plots from the Opatřilka section. The $r_s$ values correspond to Spearman's correlation coefficients.

### 5.2.1.3. CORRELATIONS BETWEEN HG AND TOTAL SULFUR, TOTAL ORGANIC CARBON, AND CARBON DIOXIDE

The Shapiro-Wilk test of normality of Hg, TS, $CO_2$, and TOC variables from the Opatřilka section rejected the normal distribution for all major elements except TOC concentrations (p-value=0.315. **Table 7**, **Appendix B**).

The results of the correlation analysis (Spearman's correlation) show that all these elements have a significant statistical correlation with Hg (p-values <0.05. **Table 2**). All correlations are positive except for the correlation between mercury and inorganic carbon concentrations (**Figure 18**, **Table 2**).

**Table 2.** Results of the correlation analysis (Spearman's correlation coefficients and p-values) of mercury and TS, TOC, and $CO_2$ of samples coming from the Opatřilka section (excluding samples with anomalous Hg value). Spearman's correlation coefficients ($r_s$) for mercury are indicated in red color, and p-values in blue. Bolded values show correlations that are statistically significant (p-values < 0.05).

| | **Hg (ppb)** | **TS (wt%)** | **$CO_2$ (wt%)** | **TOC (wt%)** |
|---|---|---|---|---|
| **Hg (ppb)** | | **0.0014** | **0.0004** | **0.0009** |
| **TS (wt%)** | **0.4561** | | 0.0041 | 0.0915 |
| **$CO_2$ (wt%)** | **-0.5023** | -0.4152 | | 0.0001 |
| **TOC (wt%)** | **0.4718** | 0.2517 | -0.5360 | |

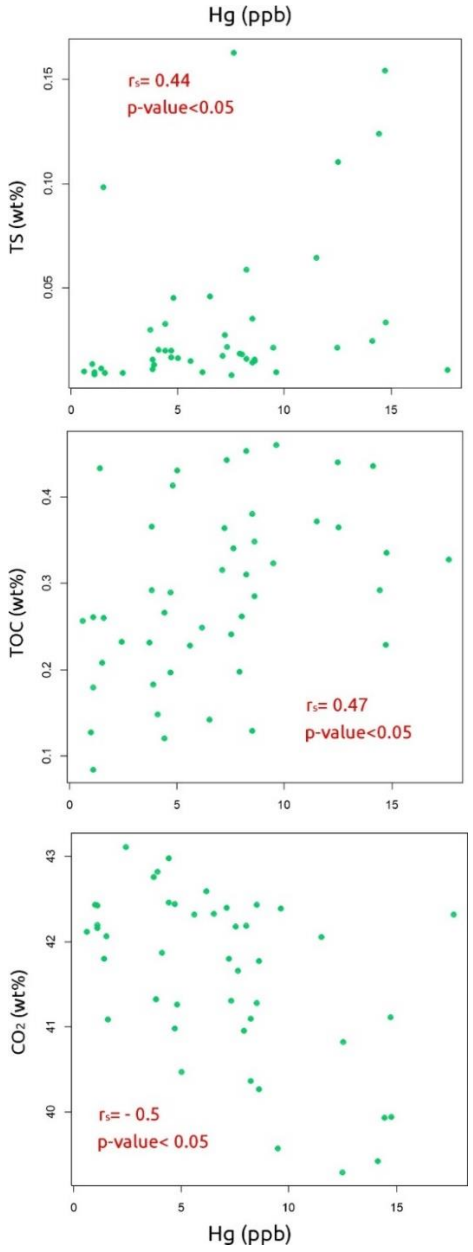


**Figure 18.** Hg and TS, TOC, and $CO_2$ correlation plots of the Opatřilka section (excluding samples with anomalous Hg content). The $r_s$ values correspond to Spearman's correlation coefficients.

#### 5.2.1.4. CORRELATIONS BETWEEN MERCURY AND TRACE ELEMENTS

The Shapiro-Wilk test of normality of the trace element concentrations from the Opatřilka section rejected the normal distribution for all major elements except of Sc concentrations (**Table 8**, **Appendix B**).

Spearman's correlation analysis showed that U, Cd, Sc, Sr, and Th, have p-values >0.05, therefore these elements do not have a significant statistical correlation with Hg in this section (**Table 9**, **Appendix C**).

All the elements (Mo, V, Co, Cr, Cu, Zn, Ni, Pb, Ga, La, Nd, Rb, Y, Zr) that are statistically correlated with Hg have positive correlation coefficients (**Figure 19**, **Figure 20**, **Figure 21**, **Figure 22**).

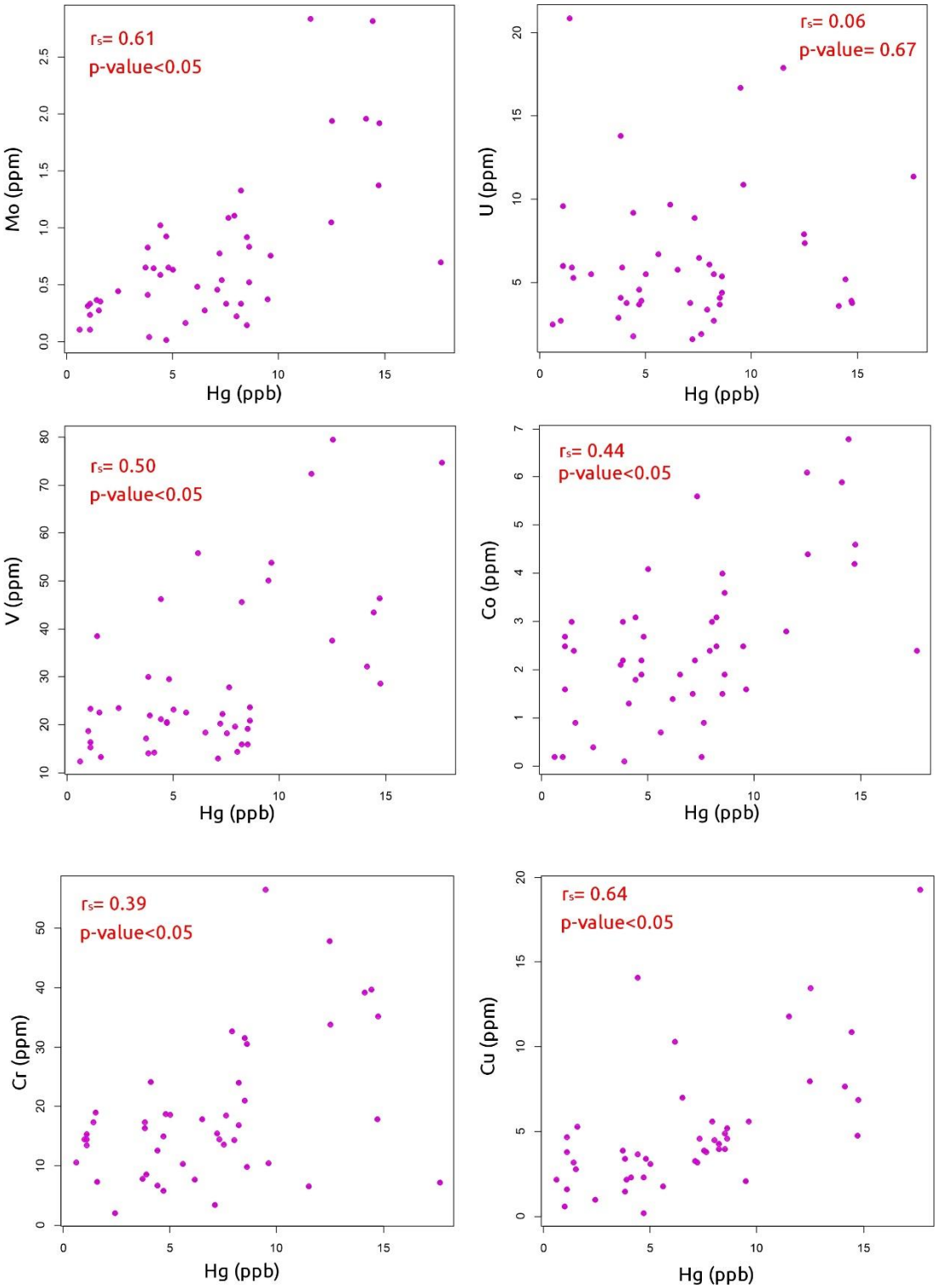


**Figure 19.** Hg and trace elements (Mo, U, V, Co, Cr, Cu,) correlation plots from the Opatřilka section. The $r_s$ values correspond to Spearman's correlation coefficients.

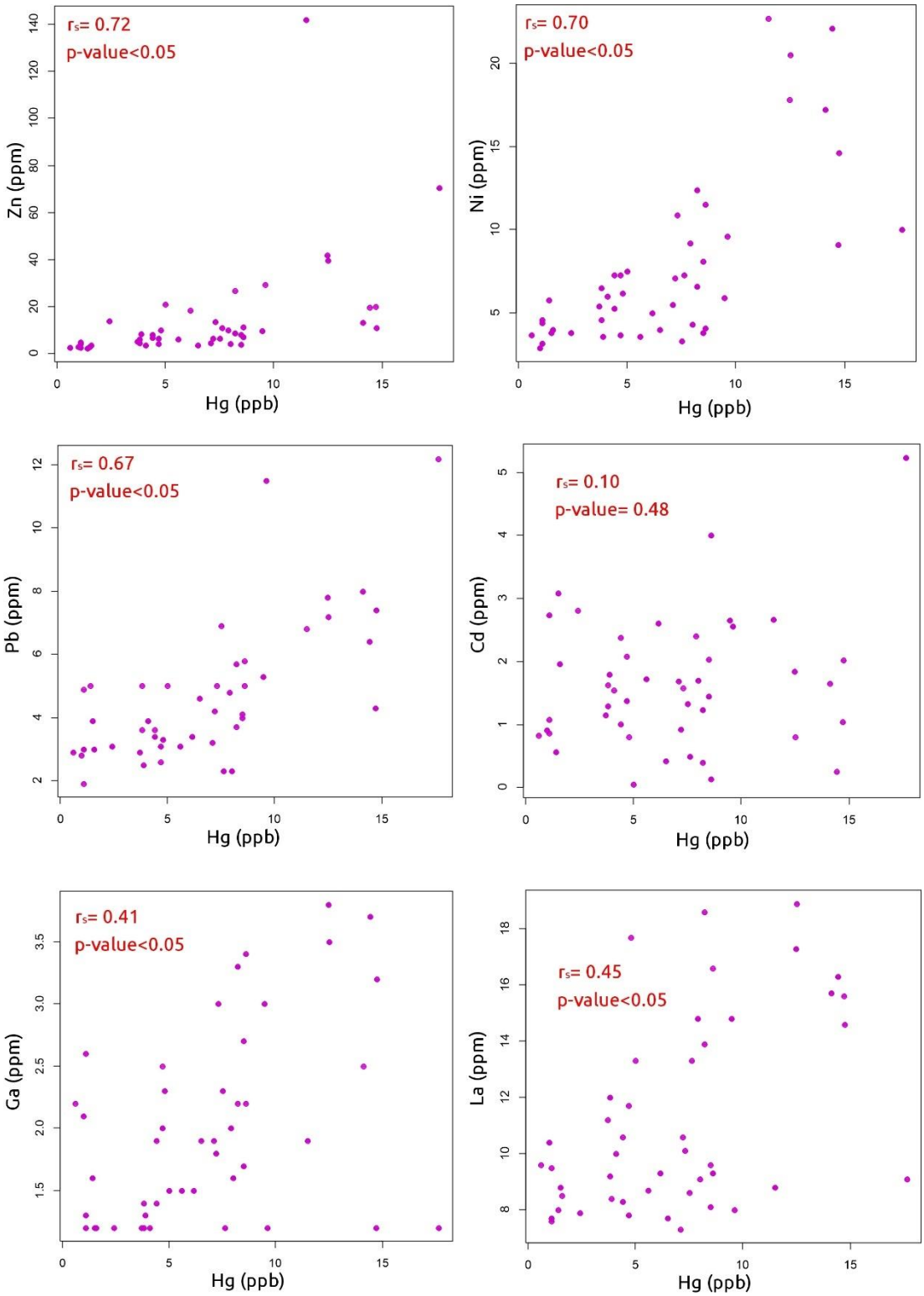


**Figure 20.** Hg and trace elements (Zn, Ni, Pb, Cd, Ga, and La) correlation plots from the Opatřilka section. The $r_s$ values correspond to Spearman's correlation coefficients.

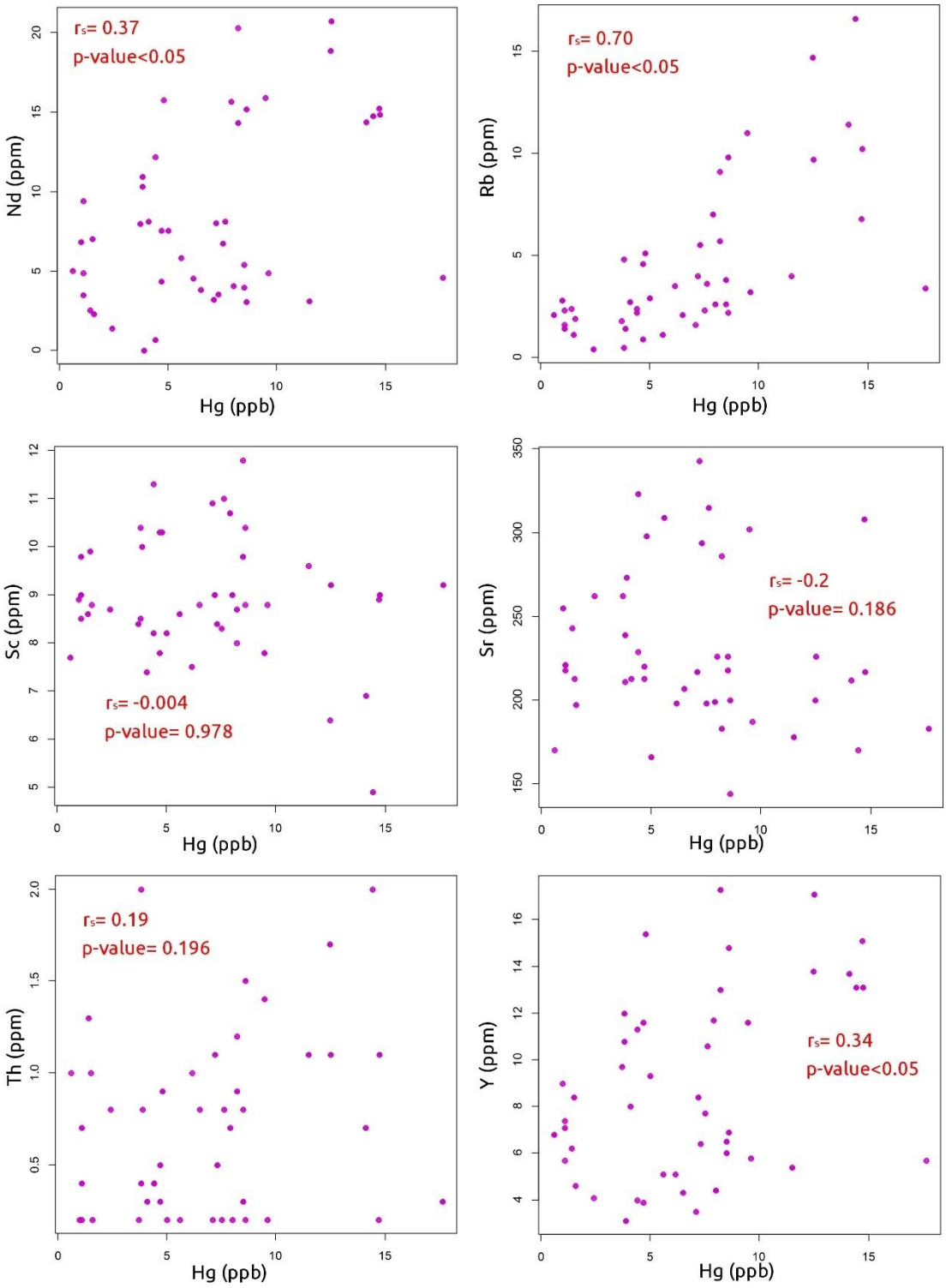


**Figure 21.** Hg and trace elements (Nd, Rb, Sc, Sr, Th, and Y) correlation plots from the Opatřilka section. The $r_s$ values correspond to Spearman's correlation coefficients.

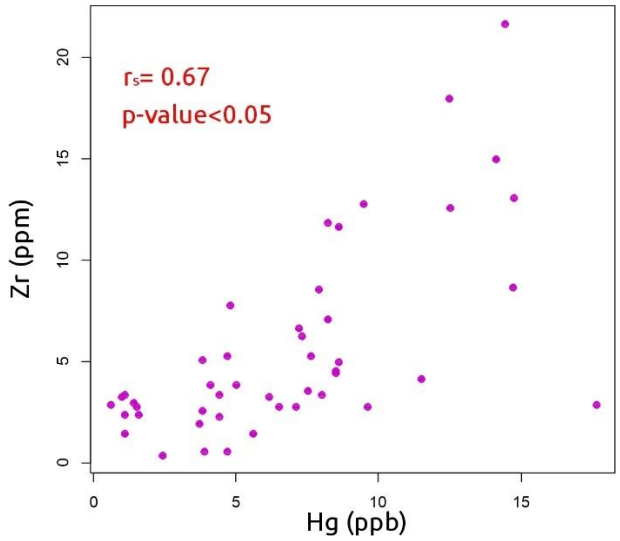


**Figure 22**. Hg and Zr correlation plot from the Opatřilka section. The $r_s$ value correspond to Spearman's correlation coefficient.

### 5.2.2. KLONK SECTION

#### 5.2.2.1. MERCURY, TOTAL ORGANIC CARBON, AND TOTAL SULFUR

There is no big peak of Hg across the Klonk section, although the Silurian part of the section shows slightly higher concentrations than the Devonian part. The raw Hg concentration values range from 11.04 ppb up to 86.69 ppb (**Table 10**, **Appendix D**). Limestones have the lowest values (between 11.04 and 28 ppb) while marls and shales display the highest Hg contents (between 28.68 ppb and 86.69 ppb). Lithologies with the highest organic matter content (black shales) display the highest Hg contents (**Figure 23**).

Similarly, when normalizing Hg content by TOC (Hg/TOC), the limestones show values ranging from 10.2 ppb/wt% up to 29.5 ppb/wt %, while the marls and shales keep showing the highest contents ranging from 15.6 ppb/wt. % for the lowest, up to 44.1 ppb/wt. % for the highest one (**Table 10**, **Appendix D and Figure 24**).

Results of Hg normalized by TS cover a very wide range of values, from 18.45 ppb/wt% up to a significant peak of ~6320.30 ppb/wt% (**Table 10**, **Appendix D**). The high peaks correspond to very small contents of sulfur of the samples, which are mainly observed within shales, probably corresponding to slightly weathered pyrite. Therefore, a normalization by TS and TOC is calculated since TS normalization is very sensitive. Such results display a very much alike pattern to those obtained from TOC normalization. They range from 43.76 ppb/wt% for the highest value, and 8.20 ppb/wt% for the lowest one (**Table 10**, **Appendix D**). Most of the highest values are mainly present in the shales lithologies with just one exception for a limestone. Moderate values (26-23 ppb/wt%) are present in marls and very few shales, and most of the lowest ones are principally present into the limestones and very few cases of marls (**Figure 23**).

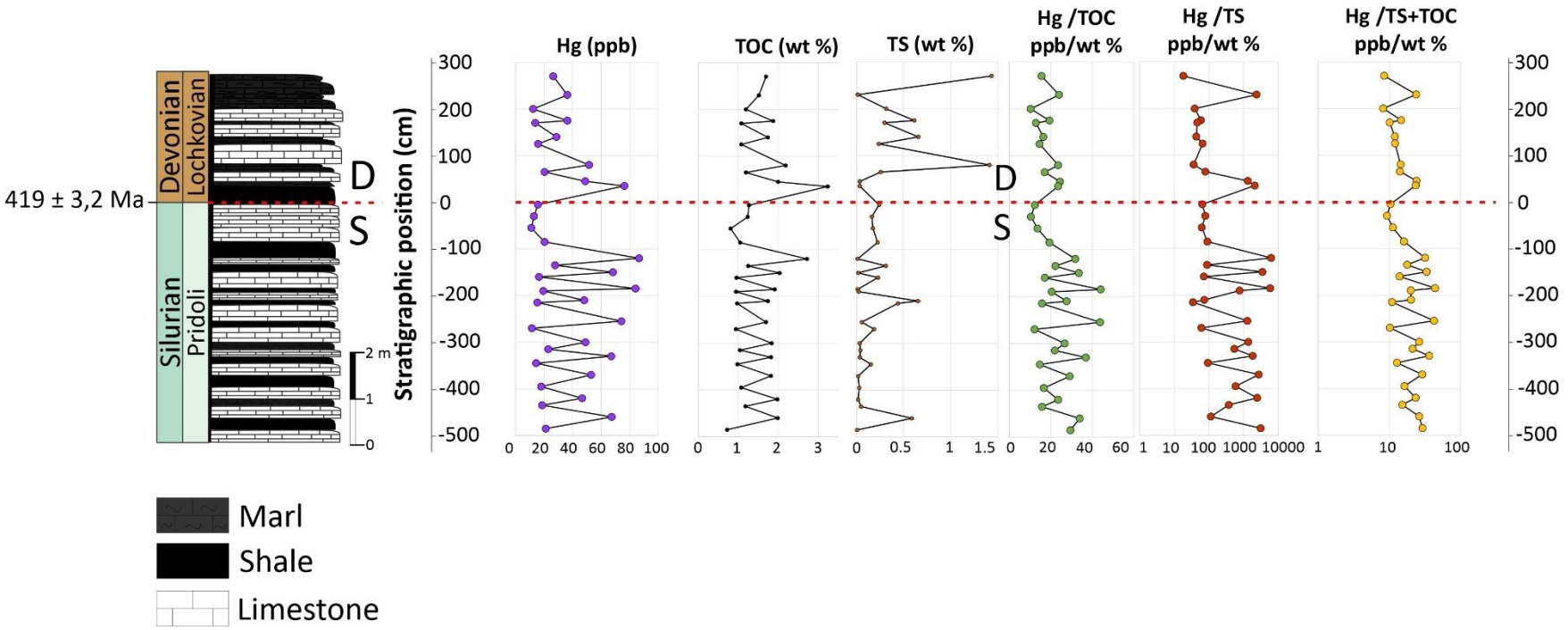


**Figure 23.** Chemostratigraphy of Hg in the Klonk section. A. Hg concentrations across the S–D boundary. B. Total Organic Carbon (TOC). C. Total Sulfur (TS). D. Mercury concentrations normalized by TOC (Hg/TOC). E. Mercury concentrations normalized by TS (Hg/TS). F. Mercury concentrations normalized by TOC+TS (Hg/TOC+TS). The stratigraphic position 0 cm corresponds to the reference level (the S–D boundary). Values below are indicated as negative, and values above are indicated as positive

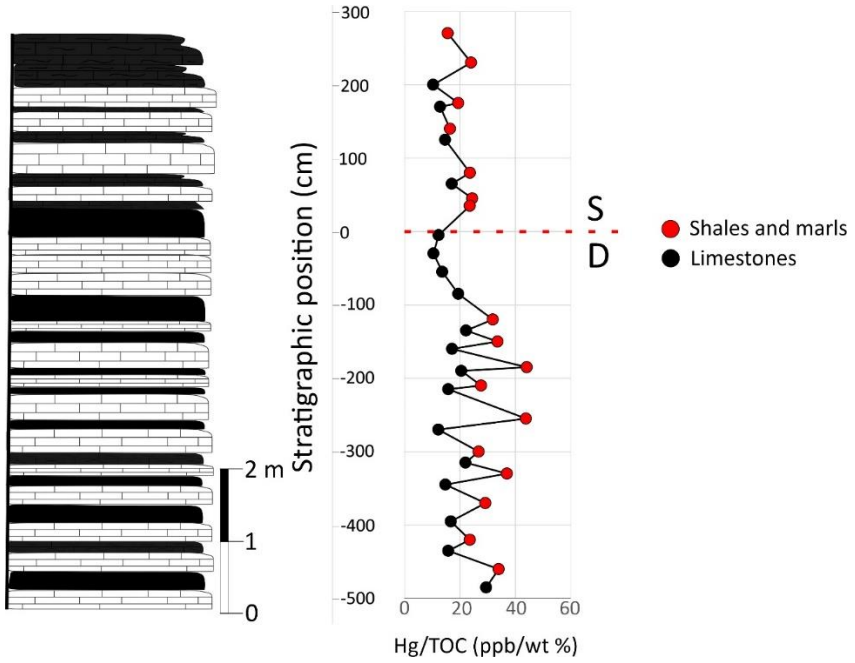


**Figure 24.** Hg chemostratigraphy normalized by TOC in the Klonk section showing the variation of Hg concentrations by lithologies.

### 5.2.2.2. CORRELATIONS BETWEEN MERCURY AND MAJOR ELEMENTS

The Shapiro-Wilk test results rejected a normal distribution for all major elements except MnO concentrations (p-value=0.131. **Table 11**, **Appendix E**).

The correlation analysis (the Spearman's correlation method) shows that all major elements except MnO (p-value > 0.05) have a significant statistical correlation with Hg (**Table 3**). In addition, as in the cases of the Opatřilka section, all major elements display positive correlations with Hg (**Figure 25** and **Figure 26**) except for CaO ($r_s$ = - 0.95).

**Table 3.** Results of the correlation analysis (Spearman's correlation coefficients and p-values) of mercury and major elements of samples coming from the Klonk section. Spearman's correlation coefficients ($r_s$) for mercury are indicated in red color, and p-values in blue. Bolded values show correlations that are statistically significant (p-values < 0.05).

| Hg - Major elements | | | | | | | | | | | | | |
|---|---|---|---|---|---|---|---|---|---|---|---|---|---|
| | Hg (ppb) | $Al_2O_3$ | CaO | $Fe_2O_3$ | $K_2O$ | MgO | MnO | $Na_2O$ | $P_2O_5$ | $SiO_2$ | $TiO_2$ | TS | $CO_2$ |
| | | (wt %) | | | | | | | | | | | |
| **Hg (ppb)** | | **4.2E-19** | **2.4E-18** | **1.4E-18** | **4.2E-18** | **1.7E-12** | 0.145 | **3.3E-05** | **3.8E-08** | **3.2E-15** | **1.3E-18** | 0.062 | **1.1E-16** |
| **$Al_2O_3$ (wt %)** | **0.956** | | 1.5E-21 | 7.0E-21 | 5.5E-32 | 2.9E-14 | 0.113 | 2.9E-06 | 1.10E-08 | 1.8E-17 | 7.4E-26 | 0.041 | 2.1E-18 |
| **CaO (wt %)** | **-0.951** | -0.969 | | 1.6E-21 | 5.7E-22 | 3.5E-11 | 0.105 | 3.7E-06 | 4.29E-08 | 5.1E-29 | 1.8E-24 | 0.099 | 1.3E-30 |
| **$Fe_2O_3$ (wt %)** | **0.952** | 0.966 | -0.969 | | 1.2E-18 | 3.0E-11 | 0.049 | 1.9E-06 | 4.36E-08 | 9.9E-18 | 1.3E-23 | 0.047 | 1.9E-20 |
| **$K_2O$ (wt %)** | **0.949** | 0.993 | -0.971 | 0.953 | | 1.7E-14 | 0.117 | 1.6E-06 | 2.13E-08 | 1.8E-18 | 1.4E-22 | 0.057 | 1.1E-18 |
| **MgO (wt %)** | **0.885** | 0.911 | -0.860 | 0.862 | 0.914 | | 0.517 | 0.001 | 4.21E-08 | 6.5E-10 | 1.6E-11 | 0.373 | 1.5E-10 |
| **MnO (wt %)** | 0.251 | 0.273 | -0.279 | 0.335 | 0.270 | 0.113 | | 5.2E-05 | 0.991 | 0.139 | 0.082 | 1.3E-04 | 0.111 |
| **$Na_2O$ (wt %)** | **0.641** | 0.699 | -0.695 | 0.709 | 0.712 | 0.527 | 0.629 | | 0.027 | 1.2E-05 | 1.2E-06 | 0.002 | 3.6E-06 |
| **$P_2O_5$ (wt %)** | **0.778** | 0.796 | -0.776 | 0.776 | 0.787 | 0.776 | -0.002 | 0.372 | | 6.2E-08 | 1.3E-08 | 0.125 | 5.1E-08 |
| **$SiO_2$ (wt %)** | **0.923** | 0.944 | -0.989 | 0.946 | 0.951 | 0.831 | 0.255 | 0.667 | 0.770 | | 1.4E-19 | 0.143 | 2.2E-30 |
| **$TiO_2$ (wt %)** | **0.953** | 0.983 | -0.979 | 0.977 | 0.973 | 0.867 | 0.298 | 0.718 | 0.793 | 0.958 | | 0.033 | 9.7E-22 |
| **TS (wt %)** | **-0.319** | -0.347 | 0.283 | -0.338 | -0.324 | -0.155 | -0.603 | -0.509 | -0.264 | -0.252 | -0.361 | | 0.147 |
| **$CO_2$ (wt %)** | **-0.937** | -0.951 | 0.991 | -0.963 | -0.953 | -0.846 | -0.274 | -0.695 | -0.773 | -0.991 | -0.969 | 0.250 | |

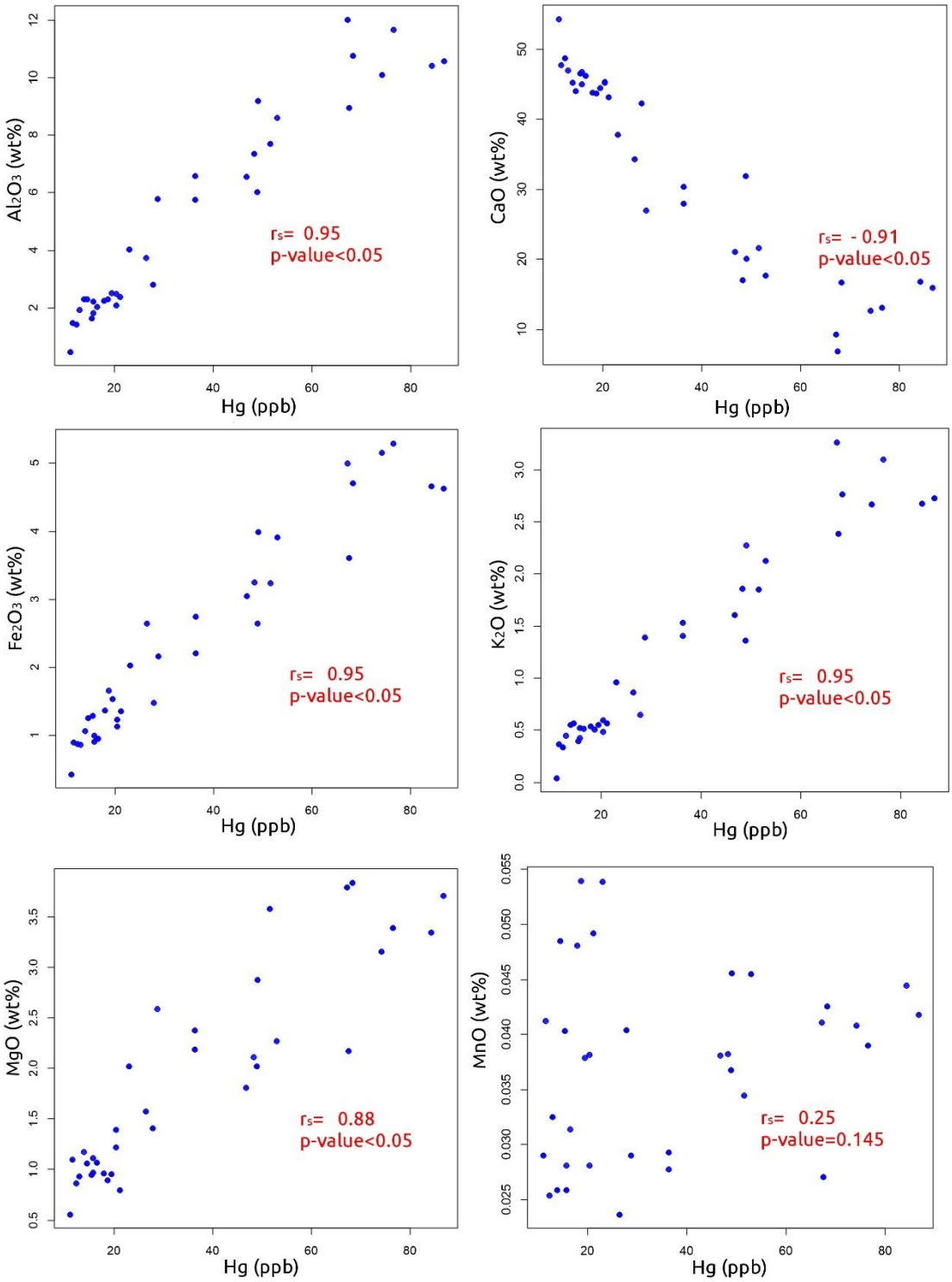


**Figure 25.** Hg and major elements ($Al_2O_3$, CaO, $Fe_2O_3$, $K_2O$, MgO, and MnO) correlation plots of the Klonk section. The $r_s$ values correspond to Spearman's correlation coefficients.

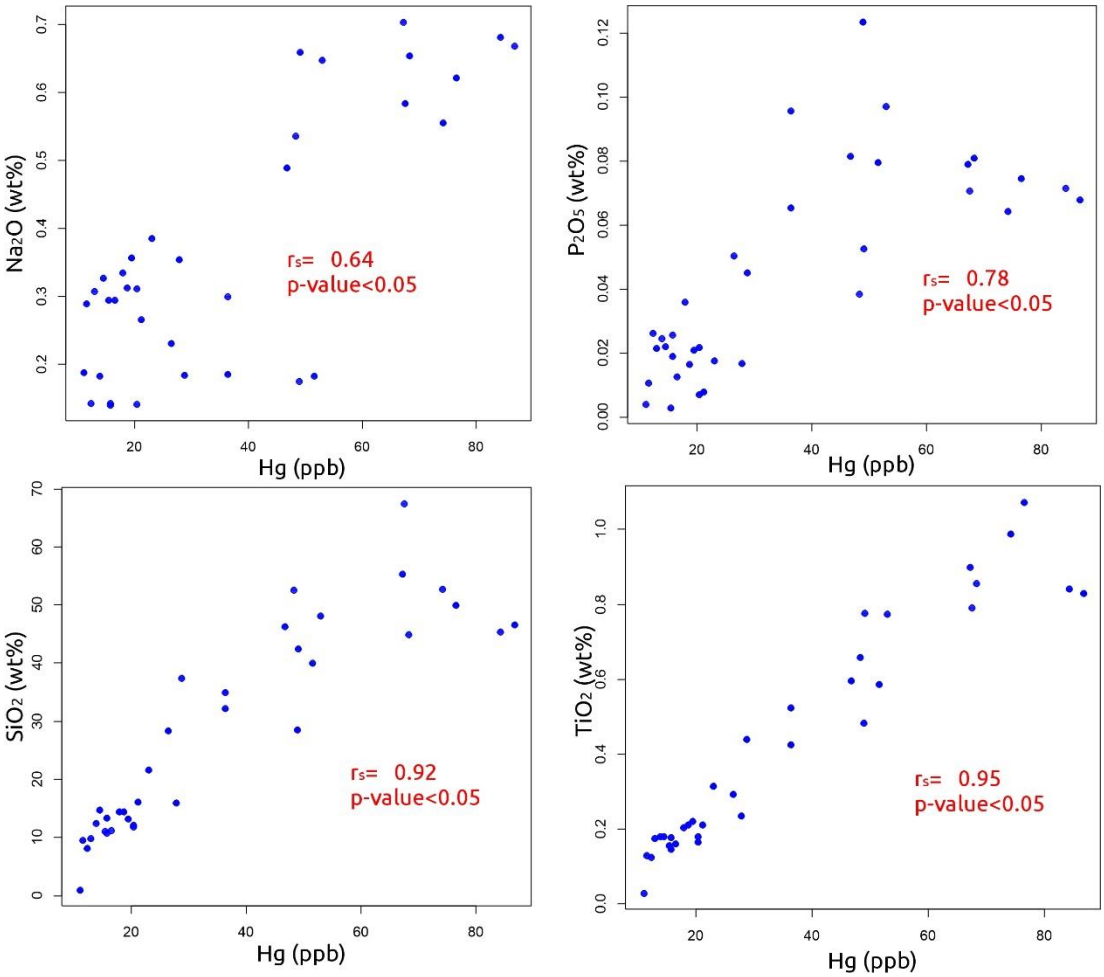


**Figure 26.** Hg and major elements ($Na_2O$, $P_2O_5$, $SiO_2$, and $TiO_2$) correlation plots of the Klonk section. The $r_s$ values correspond to Spearman's correlation coefficients.

### 5.2.2.3. CORRELATIONS BETWEEN MERCURY, TOTAL SULFUR, TOTAL ORGANIC CARBON, AND CARBON DIOXIDE

The Shapiro-Wilk normality test of Hg, TS, TOC, and $CO_2$ concentrations reject a normal distribution for all variables (**Table 12**). The Spearman's correlation results evidence that total organic carbon and carbon dioxide have a statistically significant correlation with Hg in the Klonk section, while total sulfur does not (p-value=0.061. **Table 4**). The relationship with carbon dioxide is negative, and the one with total organic carbon is positive (**Figure 27**, **Table 4**).

**Table 4.** Spearman's correlation coefficients for Hg, TS, TOC, and $CO_2$ in the Klonk section. Correlation coefficients for mercury are indicated in red color, and p-values in blue. Bolded values show correlations that are statistically significant (p-values < 0.05).

| | **Hg (ppb)** | **TS (wt%)** | **TOC (wt %)** | **$CO_2$ (wt %)** |
|---|---|---|---|---|
| **Hg (ppb)** | | 0.061 | **8.7E-10** | **1.1E-16** |
| **TS (wt %)** | -0.319 | | 0.671 | 0.147 |
| **TOC (wt %)** | **0.827** | -0.074 | | 2.1E-08 |
| **$CO_2$ (wt %)** | **-0.937** | 0.250 | -0.786 | |

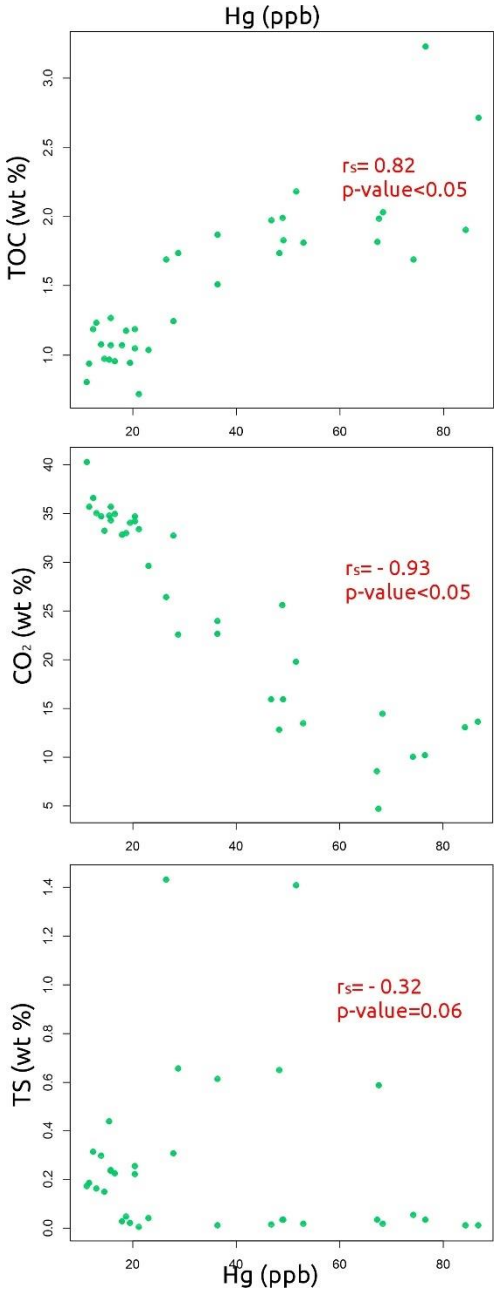


**Figure 27.** Hg and TS, TOC, and $CO_2$ correlation plots of the Klonk section. The $r_s$ values correspond to Spearman's correlation coefficients.

### 5.2.2.4. CORRELATIONS BETWEEN MERCURY AND TRACE ELEMENTS

The Shapiro-Wilk test rejects a normal distribution in all trace elements except Co and Sr (p-values > 0.05; **Table 13**, **Appendix E**).

The results obtained from Spearman's method show that all trace elements have a statistically significant correlation with Hg, except Cd with (p-value=0.21. **Table 14**). All correlations are positive, except for Sr which has a negative correlation coefficient (**Figure 28**, **Figure 29**, **Figure 30**, **and Figure 31**).

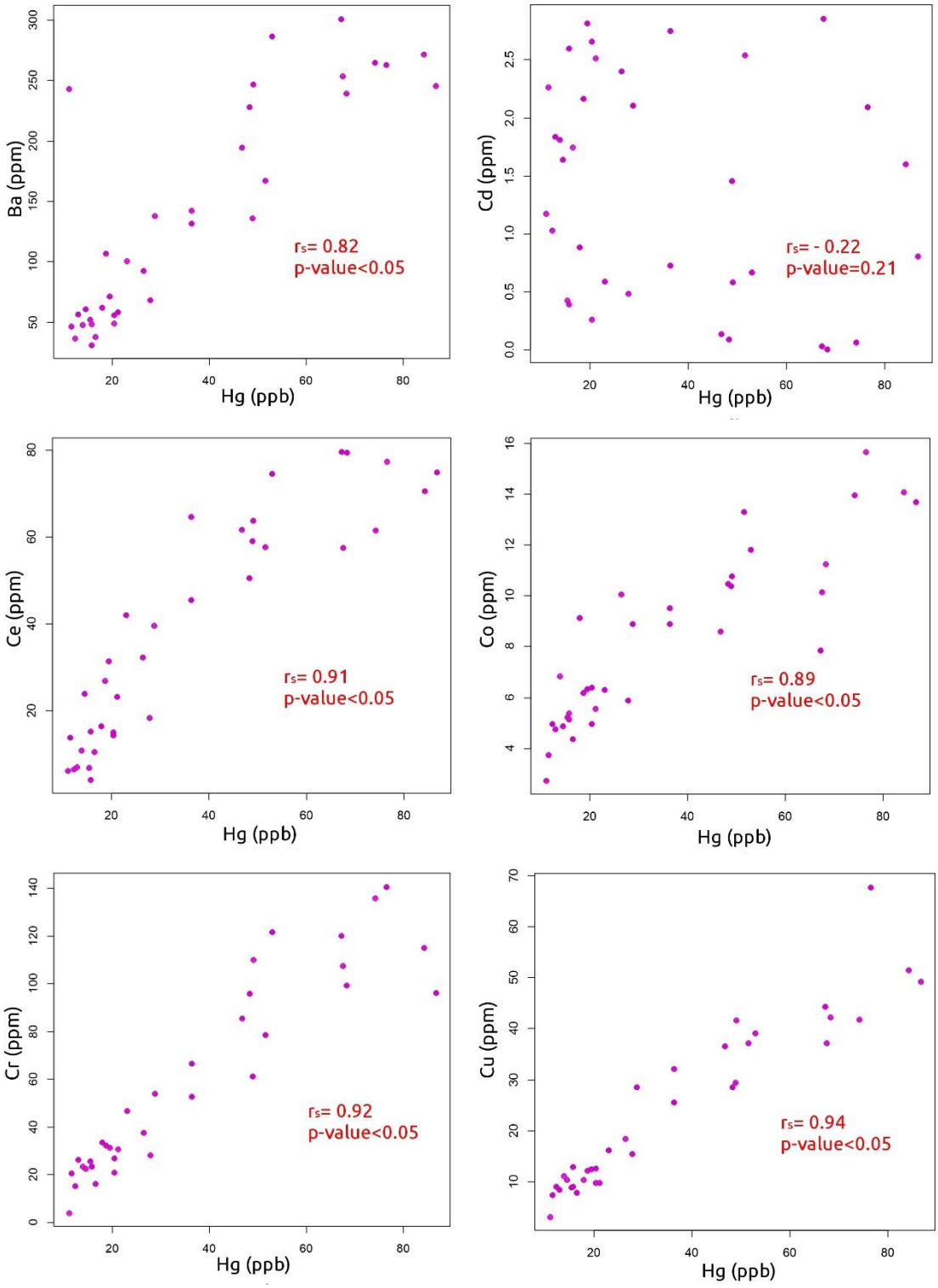


**Figure 28.** Hg and trace elements (Ba, Cd, Ce, Co, Cr, Cu) correlation plots of the Klonk section. The $r_s$ values correspond to Spearman's correlation coefficients.

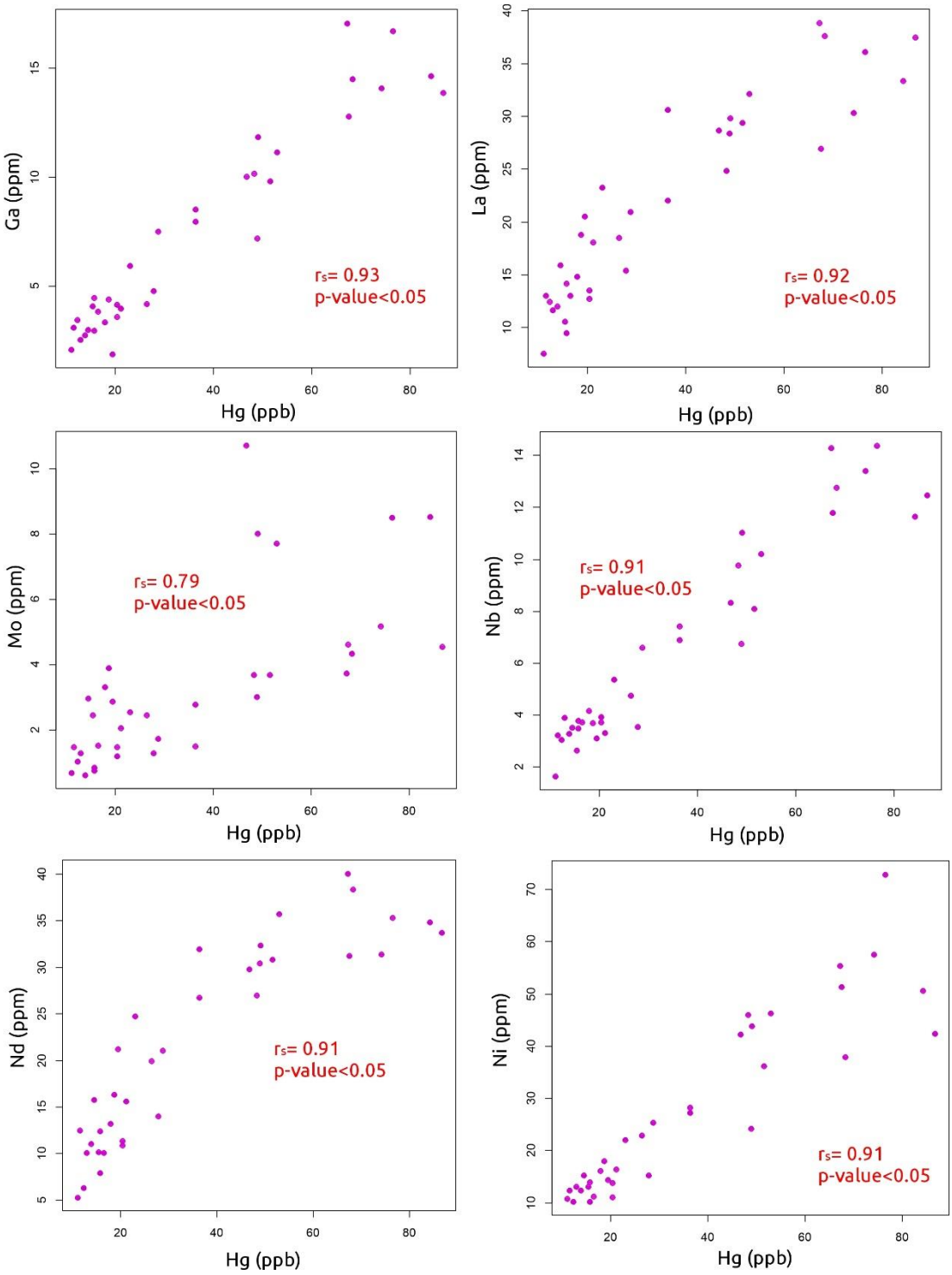


**Figure 29.** Hg and trace elements (Ga, La, Mo, Nb, Nd, Ni) correlation plots of the Klonk section. The $r_s$ values correspond to Spearman's correlation coefficients.

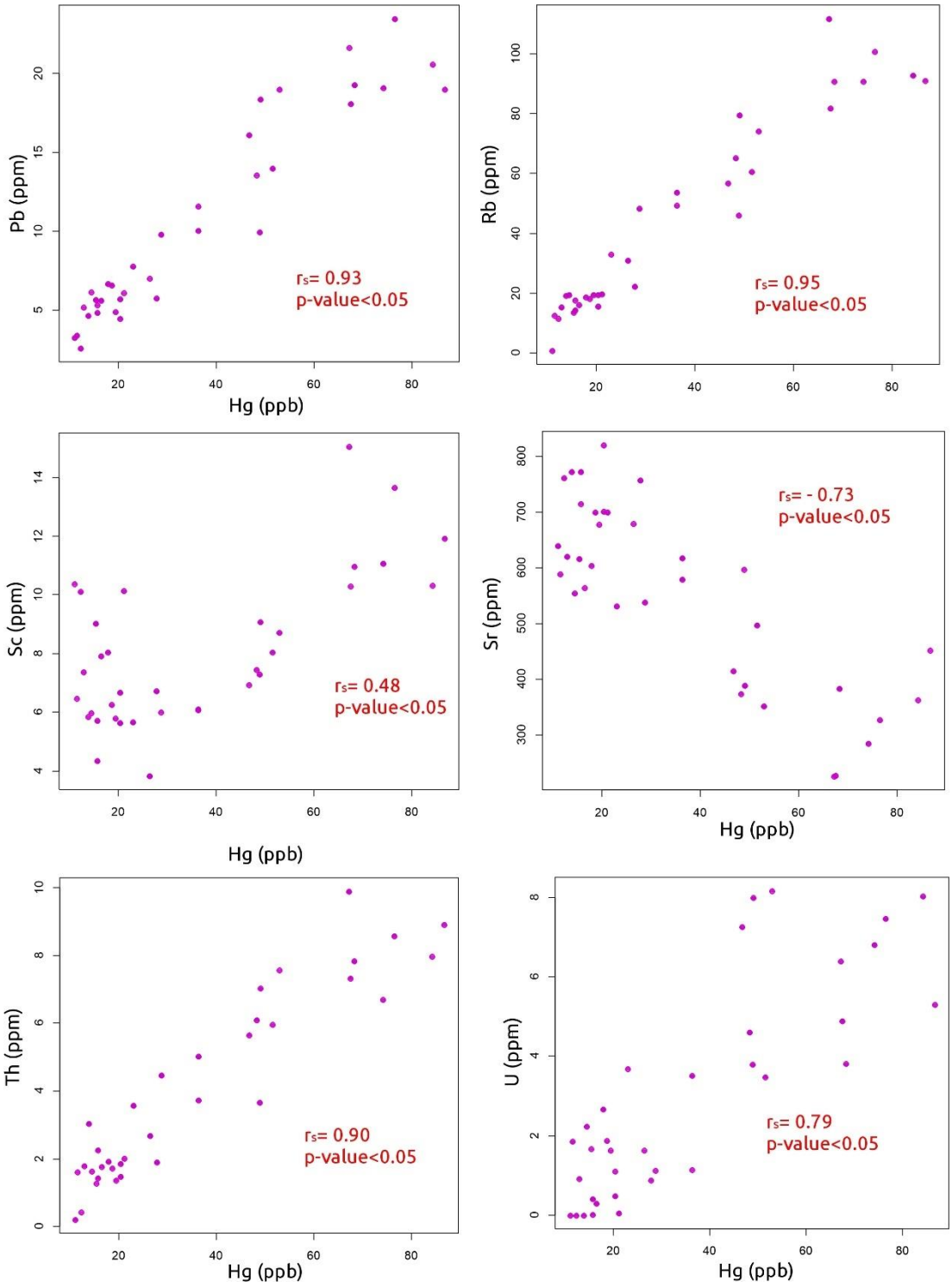


**Figure 30.** Hg and trace elements (Pb, Rb, Sc, Sr, Th, U) correlation plots of the Klonk section. The $r_s$ values correspond to Spearman's correlation coefficients.

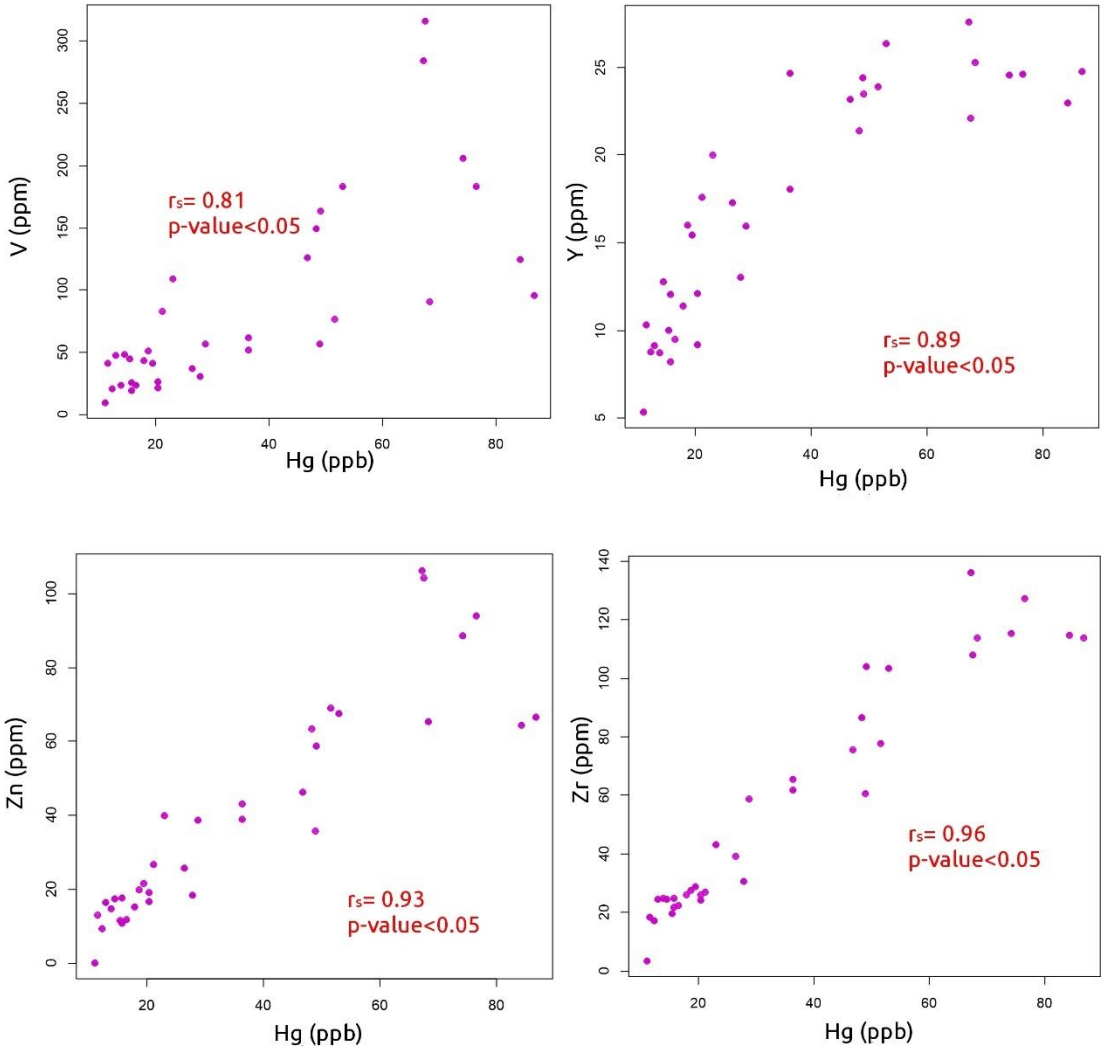


**Figure 31.** Hg and trace elements (V, Y, Zn, Zr) correlation plots of the Klonk section. The $r_s$ values correspond to Spearman's correlation coefficients.

# 6. DISCUSSION

## 6.1. WHAT INFLUENCES THE MERCURY CONTENT OF THE SEDIMENTS STUDIED?

The Opatřilka section presented a very high peak of Hg (227.2 and 235.7 ppb) in the lower part of the Silurian *Monograptus transgrediens* graptolite Biozone that exceeds around 200 times the background concentrations observed through all the section (**Table 5**, **Appendix A**). Such background contents cover a much narrower range when compared to the Klonk section (**Table 10**, **Appendix D**). Excluding the anomalous content from Opatřilka, the range contrast between the sections is of 0.6 up to 17.6 ppb, and 11.0 up to 86.7 ppb for Opatřilka and Klonk respectively (**Table 5**, **Appendix A; and Table 10, Appendix D**). Similarly, there is a contrast in the TS content in both sections. The Klonk section covers a wider range of concentrations (0.01wt. % - 1.43 wt. %) than that of Opatřilka section (0.01 wt. % - 0.16 wt. %).

When normalizing Hg concentrations by TOC in both sections, the range of values for the Klonk section is more moderate, because there is a higher TOC content in this section. On the contrary, Opatřilka displays a wider range of values when normalizing by TOC, due to a lower organic matter content in the section. The Opatřilka section represents limestone deposition in the shallow-water environment, which is probably linked with much lower primary TOC content in comparison with the Klonk section. In addition, the TOC content of samples from the Opatřilka section could be lowered by the mineralization of organic matter during stronger diagenetic overprint (**Figure 32**).

Normalization by TS shows very wide ranges and some peaks for both sections due to low TS values close to the limit of detectability, therefore, this normalization is very sensitive to analytical error. Another reason for the considerable variability in TS and thus Hg/TS values may be the different degrees of weathering of individual samples. Pyrite, as probably the main sulfur carrier in these sediments, is a relatively unstable mineral in the weathering process. Therefore, a normalization by TOC+TS was considered in this analysis. As expected, such normalization moderates the ranges of values for both sections. Excluding the anomalous Hg content from Opatřilka, the range of values from Klonk (8.20 ppb/wt. % - 43.76 ppb/wt. %) is a bit more moderate than in Opatřilka (2.25 ppb/wt. % - 58.93 ppb), which is consistent with the higher content of organic matter and sulfurs in the Klonk section.

In both sections, Hg exhibits statistically significant correlations with most of the major elements except for MnO for both sections, and $P_2O_5$ for Opatřilka. CaO and $CO_2$ have negative correlations with Hg in both sections, and the relationships between Hg and the major elements are stronger in the Klonk section with most coefficients close to 0.95 contrasting the ones in the Opatřilka section which are much more moderate (0.31 up to 0.71). Similarly, the relationships of Hg with TOC and $CO_2$ are much stronger in the Klonk section than in the Opatřilka section. The strong relationship between Hg and TOC in the Klonk section is also consistent with the local variations of Hg within lithologies, where shales and marls contain a much higher content of Hg than limestones (**Figure 24**), which is rational given the fact that Hg is preferably absorbed onto organic matter. On the other hand, the TS does not display a relationship with Hg in the Klonk section, probably because of the high sensitivity of TS to weathering. It should be considered that the Klonk

section is a natural geological outcrop, which is exposed to atmospheric influences and therefore to weathering, for at least thousands of years. In contrast to that, the Opatřilka section is located in a quarry that exposed the studied strata only several decades ago.

The trace elements analysis in the Klonk section revealed that except for Cd, all trace elements have a statistically significant correlation with Hg, and Sr is the only element that has a negative relationship with Hg (**Figure 30**), which can be explained by its presence in the crystal lattice of the calcite. In the Opatřilka section, the relationships between Hg and trace elements differ from those in the Klonk section. On the one hand, the relationships are more moderate in the Opatřilka section for both major and trace elements, and Hg is not statistically correlated with the trace elements U, Cd, Mn, Sc, Sr, and Th.

The Opatřilka section shows similar concentrations of Mn and Sr (**Table 16, Appendix H)**, contrary to the Klonk section which shows a higher content of Sr than Mn **(Table 18**, **Appendix H**). According to Veizer (1983), trace metals such as Mn and Sr in calcium carbonates, are strongly affected by diagenetic alteration. Such alterations typically lead to higher concentrations of Mn and lower concentrations of Sr. In a fluid-buffered system where the carbonate is subject to high water: rock ratio, multiple events of recrystallization, dissolution, and cementation occur, and the geochemistry of the carbonates rather reflects the composition of a diagenetic fluid (Hood et al., 2018).

The contrasts observed in the Sr and Mn contents between both sections reflect that samples from the Opatřilka section likely underwent much stronger diagenetic transformations than those from the Klonk section, according to the variations of Sr and Mn in the limestones (**Figure 32**). This agrees with the fact that Opatřilka belongs to the shallower part of the basin characterized by deposition of coarse-grained limestones which might be more open to meteoric and basinal fluids during diagenesis, causing significant changes in the sediment composition. Moreover, these diagenetic alterations likely decreased the organic carbon content in the Opatřilka section, which is evidenced when compared with the TOC contents of samples from the Klonk section. Such geochemical contrasts between the studied sections, may explain why there are less statistically significant correlations among Hg and trace elements in the Opatřilka section than in the Klonk section, as well as the more moderate strength in the relationships observed among Hg versus trace and major elements in this section.

The different diagenetic overprint of the samples from the Opatřilka section may be also related to the different types of primary carbonate mineralization. Samples from the Klonk section lie on diagenetic trends for low-Mg calcite, whereas samples from the Opatřilka section lie on diagenetic trends for high-Mg calcite (**Figure 32**). As has been documented many times, aragonite and high-Mg calcite are rare minerals in Paleozoic sediments because of their low stability during diagenetic processes. High-Mg calcite is an unstable mineral. Substitution of $Mg^{2+}$ into calcite lattice has a significant influence on the reactivity of carbonates because thermodynamic stability and dissolution/precipitation kinetics are changed (Böttcher et al. 1997). For that reason, high-Mg calcite turns into low magnesium calcite during diagenetic processes. Thus, if the primary carbonate mineralization in the shallow-water environment (Opatřilka section) was mainly composed of high-Mg calcite (**Figure 32**), then it must have changed to low-Mg calcite during diagenetic processes. Recrystallization of high-Mg calcite to stable low-Mg calcite could significantly affect the stability of organic matter and lead to its partial oxidation.

Moreover, this recrystallization could have partially mobilized Hg. Both of the above-mentioned processes may also explain why there are less statistically significant correlations between Hg and trace elements in the Opatřilka section than in the Klonk section.

Taken together, the statistically significant correlations of mercury and TOC contents indicate that organic matter is likely the main carrier of mercury in the studied sediments, as has been documented from many global sites (see chapter 3.1 MERCURY GEOCHEMICAL CYCLING). On the other hand, there are statistically significant correlations between mercury and most major and trace elements at both sites. These correlations are different for the two sites and are likely influenced by the relative abundance of TOC at both sites as well as by the different mineralogical compositions of the detritus. Thus, a statistically significant correlation between Hg and TOC, as well as between TOC and the amount of detrital material, likely produces a statistically significant correlation between most major and trace elements. A detailed analysis of these correlations and a discussion of possible causal relationships between Hg content and individual detritus fractions is beyond the scope of the present thesis and will be the subject of further research. For these reasons, it is not possible to prove that TOC and TS are the only Hg carriers in the rocks studied.

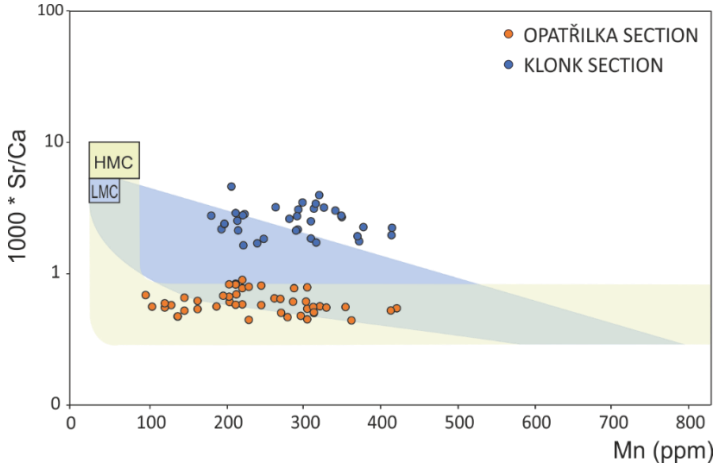


**Figure 32.** Different diagenetic overprint samples from the Opatřilka and Klonk sections. The yellow box represents the primary composition of marine high-Mg calcite, blue box low-Mg calcite. Blue and yellow areas correspond to diagenetic trends for low-Mg calcite and high-Mg calcite with stabilization by meteoritic water. Graph modified from Brand and Veizer (1980).

## 6.2. MERCURY ANOMALY

The present study revealed a very high peak of Hg (227.2 and 235.7 ppb) in the lower part of the Silurian *Monograptus transgrediens* graptolite Biozone at the Opatřilka section which exceeds around 200 times the background concentrations observed through all the section (**Table 5**, **Appendix A**). Cross-plots illustrating the variability in mercury and major, as well as trace element concentrations (**APPENDIX G**), clearly demonstrate that these anomalous Hg values are not from the same population as the other samples from the Opatřilka section. Moreover, this is also clearly evident for TOC and TS (**APPENDIX G, Figure 35**). Therefore the Hg anomaly cannot be explained as of detrital or TOC origin. It is unclear if the Hg anomaly represents an indication of extensive volcanic activity or Hg accumulation resulting from diagenetic/hydrothermal mercury mobilization. Further

investigations of the anomaly in the lower part of the Silurian *Monograptus transgrediens* graptolite Biozone are needed.

In this context, Manda and Frýda (2010) reported that more than 80% of the cephalopod species in the Prague Basin become extinct before the last appearance of *M. transgrediens*. The latter authors noted that the extinction affected benthic and demersal cephalopod species with relatively large eggs and long incubation times. The possible temporal coincidence between the above-mentioned extinction and the observed Hg anomaly in the shallow-water environment may indicate a causal link. On the other hand, this Hg anomaly was not observed in the Klonk section. Whether this absence of Hg anomaly is real or whether it is due to the low sampling density of the Klonk section also needs to be verified by further research.

# 7. CONCLUSIONS.

The main aim of the present study was to analyze mercury chemostratigraphic record in continental shelf sediments of the Silurian–Devonian boundary interval from the Prague Basin as tracers of volcanic activity and to test possible temporal links between extinction events and intense volcanism. The main results are summarized as follows:

a) Different mercury concentrations were found in the sediments coming from different depositional settings. The statistically significant positive correlation between mercury content and total organic carbon content at both study sites (i.e., the Opatřilka section and the Klonk section) is consistent with many published observations that organic matter is the main carrier of mercury in marine sediments. The significantly higher total organic carbon contents in samples from the Klonk section, representing offshore deposition, are consistent with high mercury contents.

b) The statistically significant correlations between Hg and TOC, as well as between TOC and amount of detrital material, likely produce a statistically significant correlation between mercury and most major and trace elements. For these reasons, it is not possible to prove if TOC and TS are the only Hg carriers in the rocks studied.

c) Higher diagenetic overprint of the samples from the Opatřilka section may be related to its type of primary carbonate mineralization. Samples from the Klonk section lie on diagenetic trends for low-Mg calcite, whereas samples from the Opatřilka section lie on diagenetic trends for high-Mg calcite (**Figure *32***). Recrystallization of unstable high-Mg calcite to stable low-Mg calcite could significantly affect the stability of organic matter and lead to its partial oxidation. Moreover, this recrystallization could have partially mobilized Hg. These processes may explain why there are less statistically significant correlations between Hg and trace elements in the Opatřilka section than in the Klonk section.

d) The present study revealed a very high peak of Hg concentration (227.2 and 235.7 ppb) in the lower part of the Silurian *Monograptus transgrediens* graptolite Biozone at the Opatřilka section which exceeds around 200 times the background concentrations observed through all the section. This Hg anomaly cannot be explained as of TOC or detrital origin. It is noteworthy, that this anomaly occurs at the stratigraphic level followed by a worldwide extinction documented by a detailed study of cephalopod biodiversity (Manda and Frýda, 2010). The possible temporal coincidence between the above-mentioned extinction event and the observed Hg anomaly in the shallow-water environment may indicate a causal link. On the other hand, it is unclear if the Hg anomaly represents an indication of extensive volcanic activity or Hg accumulation resulting from diagenetic/hydrothermal mercury mobilization.

e) The present study is the first application of Hg chemostratigraphy in the classic Barrandian area and provides new chemostratigraphic data for the current knowledge of the Prague Basin as well as for the Klonk section, recognized as an International Stratotype (GSSP). The present thesis illustrates the potential of Hg

chemostratigraphy for the study of extinction events in the Prague Basin and raises new scientific questions (i.e., the relationship between observed Hg anomalies and biodiversity decline in the Silurian *Monograptus transgrediens* graptolite Biozone).

## 8. REFERENCES


Benoit, J. M., Gilmour, C. C., Heyes, A., Mason, R. P., & Miller, C. L. 2002. Geochemical and Biological Controls over Methylmercury Production and Degradation in Aquatic Ecosystems. *ACS Symposium Series*, *835*, 262–297. https://doi.org/10.1021/bk-2003-0835.ch019

Böttcher, M.E., Gehlken, P.L., Steele, D.F. 1997. Characterization of inorganic and biogenic magnesian calcites by Fourier transform infrared spectroscopy. Solid State Ionics 101–103:1379–1385

Bouček, B., 1937. Stratigrafie siluru v dalejském údolí u Prahy a v jeho nejbližším okolí. Rozpravy II. 46. Třídy České Akademie, pp. 1–20.

Bouček, B. 1966. Eine neue bisher jüngste Graptolithen Fauna aus dem böhmischen Devon. Neues Jahrbuch für Geologie und Paläontologie, Monatshefte, 3:161–168.

Brocke, R., Fatka, O., & Wilde, V. 2006. Acritarchs and prasinophytes of the Silurian–Devonian GSSP (Klonk, Barrandian area, Czech Republic). *Bulletin of Geosciences*, *81*(1), 27–41. https://doi.org/10.3140/bull.geosci.2006.01.027

Buggisch, W., & Mann, U. 2004. Carbon isotope stratigraphy of Lochkovian to Eifelian limestones from the Devonian of central and southern Europe. *International Journal of Earth Sciences*, *93*(4), 521–541. https://doi.org/10.1007/s00531-004-0407-6

Carls, P., Slavík, L., & Valenzuela-Ríos, J. I. 2007. Revisions of conodont biostratigraphy across the Silurian–Devonian boundary. *Bulletin of Geosciences*, *82*(2), 145–164. https://doi.org/10.3140/bull.geosci.2007.02.145

Chlupáč, I., Havlíček, V., Kříž, J., Kukal, Z., Štorch, P. 1998. Palaeozoic of the Barrandian. Czech Geological Survey, Prague, 183 pp.

Chlupáč I., Jaeger H. & Zikmundová J. 1972: The Silurian–Devonian boundary in the Barrandian. Bull. Canad. Petrol. Geol. 20, 104-174.

Chlupáč, I., & Hladil, J. 2000. *The global stratotype section and point of the Silurian Devonian boundary*. (pp. 1–7).

Chlupáč, I., Kukal, Z., 1988. Possible global events and the stratigraphy of the Paleozoic of the Barrandian (Cambrian-Middle Devonian, Czechoslovakia). Sb. Geol. Věd (Geol.) 43, 83–146.

Chlupáč, I., 1999. Barrande's stratigraphic concepts, palaeontological localities and tradition – comparison with the present state. Journal of the Czech Geological Society 44(1–2), 3–30.

Chlupáč, I., & Vacek, F. 2003. Thirty years of the first international stratotype: The Silurian–Devonian boundary at Klonk and its present status. *Episodes*, *26*(1), 10–15. https://doi.org/10.18814/epiiugs/2003/v26i1/002

Cramer, B.D., Brett, C.E., Melchin, M.J., Männik, P., Kleffner, M.A., McLaughlin, P.I., Lloydell, D.K., Munnecke, A., Jeppsson, L., Corradini, C., Brunton, F.R., Saltzman, M.R., 2011. Revised correlation of Silurian provincial series of North America with global and regional chronostratigraphic and δ13Ccarb chemostratigraphy. Lethaia 44, 185–202.

Crick, R.E., Ellwood, B.B., Hladil, J., El-Hassani, A., Hrouda, F. & Chlupáč, I. 2001. Magnetostratigraphy susceptibility of the Přídolian-Lochkovian (Silurian-Devonian) GSSP (Klonk, Czech Republic) and a coeval sequence in Anti-Atlas Morocco.

Palaeogeography, Palaeoclimatology, Palaeoecology 167, 73–100.

Elbra, T., Schnabl, P., Tasáryová, Z., Čížková, K., & Pruner, P. 2015. New results for Palaeozoic volcanic phases in the Prague Basin - Magnetic and geochemical studies of Lištice, Czech Republic. *Estonian Journal of Earth Sciences*, *64*(1), 31–35. https://doi.org/10.3176/earth.2015.06

Fatka, O. & Mergl, M., 2009. The "microcontinent" Perunica: status and story 15 years after conception. Geol. Soc. Lond., Spec. Publ. 325 (1), 65–101. https://doi.org/10.1144/sp325.4.

Fiala, F., 1970. Silurian and Devonian diabases of the Barrandian Basin. Sborník geologických věd, Řada G 17, 7–89 (in Czech, English summary).

Frýda, J., Hladil, J., & Vokurka, K. 2002. Seawater strontium isotope curve at the Silurian–Devonian boundary: A study of the global Silurian–Devonian boundary stratotype. *Geobios*, *35*(1), 21–28. https://doi.org/10.1016/S0016-6995(02)00006-2

Havlíček, V. 1980. Vývoj paleozoických pánví v Českem masívu (kambrium - spodní karbon); Development of Paleozoic basins in the Bohemian Massif (Cambrian – Lower Carboniferous). Sborník geologických Věd, Geologie, 34, 31–65.

Hladíková, J., Hladil, J., & Kříbek, B. 1997. Carbon and oxygen isotope record across Pridoli to Givetian stage boundaries in the Barrandian basin (Czech Republic). *Palaeogeography, Palaeoclimatology, Palaeoecology*, *132*(1–4), 225–241. https://doi.org/10.1016/S0031-0182(97)00062-X

Hladil, J., 1991. Evaluation of the sedimentary record in the Silurian–Devonian boundary stratotype at Klonk (Barrandian area, Czechoslovakia). Newsl. Stratigr. 115–125.

Hladil, J. (1992). Are there turbidites in the Silurian–Devonian boundary stratotype? (Klonk near Suchomasty, Barrandian, Czechoslovakia). *Facies*, *26*(1), 35–54. https://doi.org/10.1007/BF02539792

Hood, A. v. S., Planavsky, N. J., Wallace, M. W., & Wang, X. 2018. The effects of diagenesis on geochemical paleoredox proxies in sedimentary carbonates. *Geochimica et Cosmochimica Acta*, *232*, 265–287. https://doi.org/10.1016/j.gca.2018.04.022

Horný, R. 1955. Studie o vrstvách budňanských v západní části Barrandienu. Sborník Ústředního ústavu geologického, Oddíl geologický 21, 315–447.

Horný, R. 1961. Hraniční fauna vrstev přídolských a lochkovských v Barrandienu. Věstník Ústředního ústavu geologického 36, 381–384.

Jeppsson, L. 1988. Conodont biostratigraphy of the Silurian-Devonian boundary stratotype at Klonk, Czechoslovakia. Geologica et Palaeontologica 22, 21–31.

Jeppsson, L. 1989. Latest Silurian conodonts from Klonk, Czechoslovakia. Geologica et Palaeontologica 23, 21–37.

Joachimski, M. M., Breisig, S., Buggisch, W., Talent, J. A., Mawson, R., Gereke, M., Morrow, J. R., Day, J., & Weddige, K. 2009. Devonian climate and reef evolution: Insights from oxygen isotopes in apatite. *Earth and Planetary Science Letters*, *284*(3–4), 599–609. https://doi.org/10.1016/j.epsl.2009.05.028

Kalvoda, J., Kumpan, T., Qie, W., Frýda, J., & Bábek, O. 2019. Mercury spikes at the Devonian-Carboniferous boundary in the eastern part of the Rhenohercynian Zone (central Europe) and in the South China Block. *Palaeogeography, Palaeoclimatology, Palaeoecology, 531*.

https://doi.org/10.1016/j.palaeo.2019.05.043

Kerin, E. J., Gilmour, C. C., Roden, E., Suzuki, M. T., Coates, J. D., & Mason, R. P. 2006. Mercury methylation by dissimilatory iron-reducing bacteria. *Applied and Environmental Microbiology*, *72*(12), 7919–7921. https://doi.org/10.1128/AEM.01602-06

Kříž, J., Jaeger, H., Paris F., Schönlaub H.P., 1986. Přídolí - the Fourth Subdivision of the Silurian. Jahrbuch der Geologischen Bundesanstalt 129 (2), 291–360.

Kříž, J., 1991. The Silurian of the Prague Basin (Bohemia): Tectonic, eustatic, and volcanic controls on facies and faunal development. Special Papers in Palaeontology 44, 179–204.

Kříž, J., 1992. Silurian Field Excursions: Prague Basin (Barrandian), Bohemia. National Museum of Wales, Cardiff, Geological Series 13, 111pp.

Li, C., Shen, J., Zhang, J., Lei, P., Kong, Y., Zhang, J., Tang, W., Chen, T., Xiang, X., Wang, S., Zhang, W., & Zhong, H. 2021. The silver linings of mercury: Reconsideration of its impacts on living organisms from a multi-timescale perspective. *Environment International*, *155*(June), 106670. https://doi.org/10.1016/j.envint.2021.106670

Manda, Š., & Frýda, J. 2010 Silurian–Devonian boundary events and their influence on cephalopod evolution: Evolutionary significance of cephalopod egg size during mass extinctions. *Bulletin of Geosciences*, *85*(3), 513–540. https://doi.org/10.3140/bull.geosci.1174

Melchin, M.J., Sadler, P.M., Cramer, B.D., 2012. The Silurian period. In: Gradstein, F.M., Ogg, J.G., Smith, A.G. (Eds.), A Geologic Time Scale 2012. Elsevier, Amsterdam, pp. 525–558.

Melchin, M.J., Sadler, P.M., Cramer, B.D., 2021. Chapter 21 - The Silurian period. In: Gradstein, F.M., Ogg, J.G., Schmitz, M.D., Ogg, G.M. (Eds.), The Geological Time Scale 2020. Elsevier B.V, pp. 695–732. ISBN: 978-0-12-824363-3.

Meyer, K. W., Petersen, S. V., Lohmann, K. C., Blum, J. D., Washburn, S. J., Johnson, M. W., Gleason, J. D., Kurz, A. Y., & Winkelstern, I. Z. 2019. Biogenic carbonate mercury and marine temperature records reveal global influence of Late Cretaceous Deccan Traps. *Nature Communications*, *10*(1), 1–8. https://doi.org/10.1038/s41467-019-13366-0

Morel, F. M. M., Kraepiel, A. M. L., & Amyot, M. 1998. The chemical cycle and bioaccumulation of mercury. *Annual Review of Ecology and Systematics*, *29*, 543–566. https://doi.org/10.1146/annurev.ecolsys.29.1.543

Munnecke, A., Samtleben, C., Bickert, T., 2003. The Ireviken event in the Lower Silurian of Gotland, Sweden—Relation to similar Palaeozoic and Proterozoic events. Palaeogeogr. Palaeoclimatol. Palaeoecol. 195, 99–124. https://doi.org/10.1016/S0031-0182(03)00304-3.

Paris, F., Laufeld, S., Chlupáč, I., 1981. Chitinozoa of the Silurian–Devonian boundary stratotypes in Bohemia. Sver. Geol. Unders. 4, 1–29.

Patočka, F., Vlašímský, P., Blechová, K., 1993. Geochemistry of Early Paleozoic volcanics of the Barrandian Basin (Bohemian Massif, Czech Republic): implications for paleotectonic reconstructions. Jb Geol B-A 136, 873–896.

Patočka, F., Pruner, P., Štorch, P., 2003. Palaeomagnetism and geochemistry of Early

Palaeozoic rocks of the Barrandian (Teplá–Barrandian Unit, Bohemian Massif): palaeotectonic implications. Physics and Chemistry of the Earth 28:735–749

Porebska, E. & Sawlowicz, Z. 1997. Palaeoceanographic linkage of geochemical and graptolite events across the Silurian–Devonian boundary in Bardzkie Mountains (Southwest Poland). Palaeogeography, Palaeoclimatology, Palaeoecology 132, 343–354. DOI 10.1016/S0031-0182(97)00048-5

Přibyl, A., Vaněk, J., 1962. Die Trilobiten-Fauna aus dem bohmischen Obersilur (Budnanium and Lochkovium) and ihre biostratigraphische-Bedeutung. In: Sborník Národního muzea v Praze. 18. pp. 25–46.

Pyle, D. M., & Mather, T. A. 2003. The importance of volcanic emissions for the global atmospheric mercury cycle. *Atmospheric Environment*, *37*(36), 5115–5124. https://doi.org/10.1016/j.atmosenv.2003.07.011

Racki, G. 2019. Big 5 Mass Extinctions. In *Encyclopedia of Geology* (2nd ed.). Elsevier Inc. https://doi.org/10.1016/b978-0-12-409548-9.12028-7

Racki, G. 2020. A volcanic scenario for the Frasnian–Famennian major biotic crisis and other Late Devonian global changes: More answers than questions? *Global and Planetary Change*, *189*(March), 103174. https://doi.org/10.1016/j.gloplacha.2020.103174

Racki, G., Andrzej Baliński, Ryszard Wrona, Krzysztof Małkowski, Daniel Drygant, and Hubert Szaniawski. 2012. aunal dynamics across the Silurian–Devonian positive isotope excursions ($\delta^{13}C$, $\delta^{18}O$) in Podolia, Ukraine: Comparative analysis of the Ireviken and Klonk events, Acta Palaeontologica Polonica 57 (4): 795-832. doi: http://dx.doi.org/10.4202/app.2011.0206

Rakociński, M., Marynowski, L., Pisarzowska, A., Bełdowski, J., Siedlewicz, G., Zatoń, M., Perri, M. C., Spalletta, C., & Schönlaub, H. P. 2020. Volcanic related methylmercury poisoning as the possible driver of the end-Devonian Mass Extinction. *Scientific Reports*, *10*(1), 1–9. https://doi.org/10.1038/s41598-020-64104-2

Saltzman, M. R. 2002. Carbon isotope ($\delta^{13}C$) stratigraphy across the Silurian–Devonian transition in North America: Evidence for a perturbation of the global carbon cycle. *Palaeogeography, Palaeoclimatology, Palaeoecology*, *187*(1–2), 83–100. https://doi.org/10.1016/S0031-0182(02)00510-2

Scotese, C. R. 2014. Atlas of Cambrian and Early Ordovician Paleogeographic Maps (Mollweide Projection), Maps 81-88, Volumes 5, The Early Paleozoic, PALEOMAP Atlas for ArcGIS. *Paleomap Atlas, Volume 5, The Early Paleozoic*, *5*(May), 11. https://doi.org/10.13140/2.1.1087.2324

Selin, N. E. (2009). Global biogeochemical cycling of mercury: A review. *Annual Review of Environment and Resources*, 43–63. https://doi.org/10.1146/annurev.environ.051308.084314

Shen, J., Chen, J., Algeo, T. J., Feng, Q., Yu, J., Xu, Y. G., Xu, G., Lei, Y., Planavsky, N. J., & Xie, S. 2021. Mercury fluxes record regional volcanism in the South China craton prior to the end-Permian mass extinction. *Geology*, *49*(4), 452–456. https://doi.org/10.1130/G48501.1

Skyllberg, U., Qian, J., Frech, W., Xia, K., & Bleam, W. F. 2003. Distribution of mercury, methyl mercury and organic sulphur species in soil, soil solution and stream of a boreal forest catchment. *Biogeochemistry*, *64*(1), 53–76.

https://doi.org/10.1023/A:1024904502633

Slavík, L., 2017. Summary of conodont data from the GSSP of the Silurian–Devonian boundary at Klonk near Suchomasty. In: Suttner, T.J., Valenzuela-Ríos, J.I., Liao, J.-C., Corradini, C., Slavík, L. (Eds.), International Conodont Symposium 4: Progress on Conodont investigation, Valencia 25–30th June 2017, Field Guide Book. 23. Berichte des Institutes für Erdwissenschaften, Karl-Franzens-Universität Graz, pp. 192–197.

Slavík, L., Carls, P., 2012. Post-Lau Event (late Ludfordian, Silurian) recovery of conodont faunas of Bohemia. Bull. Geosci. 87, 815–832.

Slavík, L., Carls, P., Koptíková, L., Hladil, J., 2009. Lochkovian conodont succession in the Požáry Quarries: prospects for refinement of global zonation of the Lochkovian Stage. In: Berichte der Geologischen Bundesanstalt, Wien. 79. pp. 38–39.

Spiridonov, A., Stankevič, R., Gečas, T., Brazauskas, A., Kaminskas, D., Musteikis, P., Kaveckas, T., Meidle, T., Bičkauskas, G., Ainsaar, L., Radzevičius, S. 2020. Ultra-high resolution multivariate record and multiscale causal analysis of Pridoli (late Silurian): implications for global stratigraphy, turnover events, and climate-biota interactions. Gondwana Research. 10.1016/j.gr.2020.05.015

Stampfli, G. M., Von Raumer, J. F., & Borel, G. D. 2002. Paleozoic evolution of pre-Variscan terranes: From Gondwana to the Variscan collision. *Special Paper of the Geological Society of America*, *364*(January 2005), 263–280. https://doi.org/10.1130/0-8137-2364-7.263

Štorch, P., 1995. Biotic crisis and post-crisis recoveries recorded by Silurian planktonic graptolite faunas of the Barrandian Area (Czech Republic). Geolines 3, 59–70.

Štorch, P. 1998. Volcanism. In: Chlupáč I, Havlíček V, Kříž J, Kukal Z, Štorch P (eds) Palaeozoic of the Barrandian (Cambrian to Devonian). Czech Geological Survey, Prague, pp 149–168

Tasáryová, Z., Janoušek, V., & Frýda, J. 2018. Failed Silurian continental rifting at the NW margin of Gondwana: evidence from basaltic volcanism of the Prague Basin (Teplá–Barrandian Unit, Bohemian Massif). In *International Journal of Earth Sciences* (Vol. 107, Issue 4). https://doi.org/10.1007/s00531-017-1530-5

Tasáryová, Z., Schnabl, P., Čížková, K., Pruner, P., Janoušek, V., Rapprich, V., Štorch, P., Manda, Š., Frýda, J., & Trubač, J. 2014. Gorstian palaeoposition and geotectonic setting of Suchomasty Volcanic Centre (Silurian, Prague Basin, Teplá-Barrandian Unit, Bohemian Massif). *Gff*, *136*(1), 262–265. https://doi.org/10.1080/11035897.2013.879735

Urbanek, A. 1993. Biotic crises in the history of Upper Silurian graptoloids: A palaeobiological model. Historical Biology 7, 29–50. DOI 10.1080/10292389309380442

Vacek, F. 2007. Carbonate microfacies and depositional environments of Silurian–Devonian boundary strata in the Barrandian area (Czech Republic). *Geologica Carpathica*, *58*(6), 497–510.

Vacek, F. 2009. The Silurian–Devonian boundary in the Barrandian (Czech Republic): Sedimentology, magnetic susceptibility and gamma-ray spectrometry stratigraphy. Charles University.

Vacek, F., Hladil, J., Schnabl, P., 2010. Stratigraphic correlation potential of magnetic

susceptibility and gamma-ray spectrometric variations in calciturbiditic facies (Silurian–Devonian boundary, Prague Synclinorium, Czech Republic). Geol. Carpath. 61, 257–272.

Vacek, F., Slavík, L., Sobień, K., & Čáp, P. 2018. Refining the late Silurian sea-level history of the Prague Syncline—a case study based on the Přídolí GSSP (Czech Republic). *Facies*, *64*(4), 0–16. https://doi.org/10.1007/s10347-018-0542-3

Walliser, O.H. 1986. Natural boundaries and Commission boundaries in the Devonian. Courier Forschungsinstitut Senckenberg 75, 401–408.

Wang, X., Cawood, P. A., Zhao, H., Zhao, L., Grasby, S. E., Chen, Z. Q., Wignall, P. B., Lv, Z., & Han, C. 2018. Mercury anomalies across the end Permian mass extinction in South China from shallow and deep water depositional environments. *Earth and Planetary Science Letters*, *496*, 159–167. https://doi.org/10.1016/j.epsl.2018.05.044

WHO. 2000. Chapter 6.9 Mercury General description. *Air Quality Guidelines*, *5*, 1–15.

# 9. APPENDICES.

## APPENDIX A

**Table 5**. Chemostratigraphy of mercury. Opatřilka section. IC: Inorganic Carbon. TOC: Total Organic Carbon. TS: Total Sulfur. S–D boundary is taken as the reference level (0 cm) for the stratigraphic position. Negatives values are below the S–D boundary and positives above. All data is generated in this study. All fractions represent mass fractions. This table continues on the next page.

| Position | Lithology | Hg | $CO_2$ | C | IC | TOC | TS | Hg/TOC | Hg/TOC+TS |
|---|---|---|---|---|---|---|---|---|---|
| | | (ppb) | (wt %) | | | | | ppb/ wt % | |
| 150 | Limestone | 3.800 | 41.33 | 11.64 | 11.27 | 0.366 | 0.011 | 10.38 | 10.06 |
| 100 | Limestone | 1.500 | 42.07 | 11.68 | 11.47 | 0.208 | 0.099 | 7.206 | 4.891 |
| 50 | Limestone | 1.100 | 42.17 | 11.76 | 11.50 | 0.262 | 0.010 | 4.205 | 4.050 |
| 0 | Limestone | 1.600 | 41.09 | 11.47 | 11.21 | 0.260 | 0.010 | 6.145 | 5.927 |
| -50 | Limestone | 1.100 | 42.43 | 11.75 | 11.57 | 0.180 | 0.009 | 6.128 | 5.833 |
| -100 | Limestone | 1.100 | 42.20 | 11.59 | 11.51 | 0.084 | 0.009 | 13.035 | 11.73 |
| -150 | Limestone | 0.600 | 42.12 | 11.74 | 11.49 | 0.257 | 0.010 | 2.338 | 2.248 |
| -202 | Limestone | 7.300 | 41.31 | 11.71 | 11.27 | 0.443 | 0.022 | 16.47 | 15.69 |
| -253 | Limestone | 3.800 | 41.33 | 11.56 | 11.27 | 0.292 | 0.016 | 13.02 | 12.33 |
| -304 | Limestone | 8.600 | 40.27 | 11.33 | 10.98 | 0.348 | 0.016 | 24.69 | 23.60 |
| -353 | Limestone | 4.100 | 41.87 | 11.47 | 11.42 | 0.149 | 0.021 | 27.56 | 24.22 |
| -405 | Limestone | 7.900 | 40.96 | 11.37 | 11.17 | 0.198 | 0.019 | 39.99 | 36.51 |
| -456 | Limestone | 8.200 | 41.10 | 11.52 | 11.21 | 0.311 | 0.016 | 26.40 | 25.07 |
| -544 | Limestone | 9.470 | 39.58 | 11.12 | 10.79 | 0.323 | 0.022 | 29.29 | 27.44 |
| -557 | Limestone | 5.600 | 42.33 | 11.77 | 11.54 | 0.228 | 0.015 | 24.56 | 23.00 |
| -587 | Limestone | 14.72 | 39.95 | 11.23 | 10.90 | 0.336 | 0.034 | 43.81 | 39.82 |
| -609 | Limestone | 5.000 | 40.47 | 11.47 | 11.04 | 0.431 | 0.017 | 11.61 | 11.17 |
| -630 | Limestone | 12.47 | 39.30 | 11.16 | 10.72 | 0.441 | 0.022 | 28.29 | 26.97 |
| -658 | Limestone | 4.700 | 40.98 | 11.37 | 11.18 | 0.197 | 0.020 | 23.89 | 21.64 |
| -678 | Limestone | 14.11 | 39.43 | 11.19 | 10.75 | 0.436 | 0.025 | 32.36 | 30.62 |
| -716 | Limestone | 14.40 | 39.94 | 11.19 | 10.89 | 0.293 | 0.124 | 49.21 | 34.57 |
| -772 | Limestone | 1.000 | 42.44 | 11.70 | 11.57 | 0.127 | 0.014 | 7.848 | 7.07 |
| -825 | Limestone | 8.500 | 41.29 | 11.64 | 11.26 | 0.381 | 0.036 | 22.32 | 20.41 |
| -878 | Limestone | 8.000 | 42.19 | 11.77 | 11.51 | 0.262 | 0.019 | 30.55 | 28.52 |
| -928 | Limestone | 6.500 | 42.33 | 11.69 | 11.54 | 0.143 | 0.046 | 45.59 | 34.42 |
| -982 | Limestone | 8.500 | 42.44 | 11.70 | 11.57 | 0.130 | 0.015 | 65.63 | 58.93 |
| -1035 | Limestone | 7.500 | 42.19 | 11.74 | 11.51 | 0.241 | 0.009 | 31.13 | 30.06 |
| -1080 | Limestone | 7.100 | 42.40 | 11.88 | 11.56 | 0.316 | 0.018 | 22.47 | 21.27 |
| -1134 | Limestone | 8.600 | 41.78 | 11.67 | 11.39 | 0.286 | 0.015 | 30.12 | 28.59 |
| -1182 | Limestone | 4.700 | 42.44 | 11.86 | 11.57 | 0.290 | 0.017 | 16.23 | 15.32 |
| -1225 | Limestone | 17.61 | 42.32 | 11.87 | 11.54 | 0.328 | 0.011 | 53.64 | 51.87 |
| -1230 | Limestone | 2.420 | 43.12 | 11.99 | 11.76 | 0.232 | 0.010 | 10.42 | 9.99 |
| -1235 | Limestone | 227.2 | 42.04 | 11.72 | 11.47 | 0.253 | 0.048 | 899.2 | 754.57 |

| | | | | | | | | | |
|---|---|---|---|---|---|---|---|---|---|
| -1235 | Limestone | 235.7 | 42.04 | 11.72 | 11.47 | 0.253 | 0.048 | 932.9 | 782.80 |
| -1240 | Limestone | 6.140 | 42.59 | 11.87 | 11.62 | 0.249 | 0.010 | 24.63 | 23.70 |
| -1265 | Limestone | 9.610 | 42.39 | 12.02 | 11.56 | 0.461 | 0.010 | 20.86 | 20.42 |
| -1289 | Limestone | 3.900 | 42.82 | 11.86 | 11.68 | 0.184 | 0.014 | 21.25 | 19.77 |
| -1339 | Limestone | 4.400 | 42.98 | 11.99 | 11.72 | 0.267 | 0.020 | 16.50 | 15.34 |
| -1388 | Limestone | 11.50 | 42.06 | 11.84 | 11.47 | 0.372 | 0.065 | 30.92 | 26.34 |
| -1442 | Limestone | 12.50 | 40.83 | 11.50 | 11.13 | 0.365 | 0.110 | 34.21 | 26.27 |
| -1490 | Limestone | 8.200 | 40.37 | 11.46 | 11.01 | 0.453 | 0.059 | 18.09 | 16.00 |
| -1539 | Limestone | 4.400 | 42.46 | 11.70 | 11.58 | 0.121 | 0.033 | 36.49 | 28.61 |
| -1593 | Limestone | 4.800 | 41.27 | 11.67 | 11.25 | 0.413 | 0.046 | 11.61 | 10.46 |
| -1641 | Limestone | 3.700 | 42.76 | 11.89 | 11.66 | 0.231 | 0.030 | 15.99 | 14.15 |
| -1691 | Limestone | 7.600 | 41.66 | 11.70 | 11.36 | 0.341 | 0.163 | 22.31 | 15.09 |
| -1738 | Limestone | 14.70 | 41.12 | 11.44 | 11.21 | 0.229 | 0.154 | 64.24 | 38.39 |
| -1790 | Limestone | 7.200 | 41.80 | 11.76 | 11.40 | 0.364 | 0.028 | 19.78 | 18.38 |

APPENDIX B

**Table 6.** Shapiro-Wilk test of normality for Hg and major element variables coming from the Opatřilka section (excluding sample with Hg anomaly). Values in red color show variables that do not have a normal distribution (p-values < 0.05).

| Total of samples=46 | | |
|---|---|---|
| **Variable** | **p-value** | **Shapiro-Wilk** |
| **Hg (ppb)** | 0.0323 | 0.946 |
| **$Al_2O_3$ (wt%)** | 5.18E-07 | 0.773 |
| **CaO (wt%)** | 2.50E-07 | 0.758 |
| **$Fe_2O_3$ (wt%)** | 2.30E-06 | 0.803 |
| **$K_2O$ (wt%)** | 4.08E-05 | 0.855 |
| **MgO (wt%)** | 1.21E-09 | 0.622 |
| **MnO (wt%)** | 0.469 | 0.977 |
| **$Na_2O$ (wt%)** | 1.61E-08 | 0.693 |
| **$P_2O_5$ (wt%)** | 5.22E-11 | 0.523 |
| **$SiO_2$ (wt%)** | 1.47E-05 | 0.837 |
| **$TiO_2$ (wt%)** | 7.39E-06 | 0.825 |
| **$CO_2$ (wt%)** | 6.50E-03 | 0.927 |
| **Total Sulfur (wt%)** | 1.59E-09 | 0.630 |

**Table 7**. Shapiro-Wilk test of normality from the Opatřilka section (excluding sample with anomalous Hg value). Red values show variables that do not have a normal distribution.

| **Variable** | **p-normal** | **Shapiro-Wilk** |
|---|---|---|
| **Hg (ppb)** | 0.0323 | 0.946 |
| **TS (wt%)** | 1.62E-09 | 0.630 |
| **TOC (wt%)** | 0.315 | 0.971 |
| **$CO_2$ (wt%)** | 0.006 | 0.927 |

**Table 8.** Shapiro-Wilk test of normality for Hg and trace element variables for samples from the Opatřilka section (excluding sample with Hg anomalous content). Values in red color show variables that do not have a normal distribution (p-values < 0.05).

| Variable | p-normal | Shapiro-Wilk |
|---|---|---|
| Hg (ppb) | 0.0323 | 0.9458 |
| Mo (ppm) | 5.3E-06 | 0.8192 |
| U (ppm) | 4.1E-06 | 0.8145 |
| V (ppm) | 2.5E-06 | 0.8051 |
| Co (ppm) | 0.0249 | 0.9428 |
| Cr (ppm) | 0.0002 | 0.8806 |
| Cu (ppm) | 5.4E-06 | 0.8193 |
| Zn (ppm) | 2.2E-11 | 0.4936 |
| Ni (ppm) | 9.5E-07 | 0.7858 |
| Pb (ppm) | 3.0E-05 | 0.8494 |
| Cd (ppm) | 0.0099 | 0.9319 |
| Ga (ppm) | 0.0003 | 0.8840 |
| La (ppm) | 0.0001 | 0.8629 |
| Nd (ppm) | 0.0033 | 0.9182 |
| Rb (ppm) | 4.0.E-06 | 0.8137 |
| Sc (ppm) | 0.2589 | 0.9692 |
| Sr (ppm) | 0.0118 | 0.9340 |
| Th (ppm) | 0.0002 | 0.8821 |
| Y (ppm) | 0.0175 | 0.9387 |
| Zr (ppm) | 4.6.E-06 | 0.8165 |

APPENDIX C

**Table 9.** Results of the correlation analysis (Spearman's correlation coefficients and p-values) of mercury and trace elements of samples coming from the Opatřilka section (excluding samples with anomalous Hg content). Spearman's correlation coefficients ($r_s$) for mercury are indicated in red color, and p-values in blue. Bolded values show correlations that are statistically significant (p-values < 0.05). This table continues on the next page.

| | Hg (ppb) | Mo (ppm) | U (ppm) | V (ppm) | Co (ppm) | Cr (ppm) | Cu (ppm) | Zn (ppm) | Ni (ppm) | Pb (ppm) | Cd (ppm) |
|---|---|---|---|---|---|---|---|---|---|---|---|
| **Hg (ppb)** | | **6.28E-06** | 0.671 | **4.16E-04** | **3.95E-04** | **6.58E-03** | **1.82E-06** | **1.17E-08** | **7.30E-08** | **2.31E-07** | 0.485 |
| **Mo (ppm)** | **0.612** | | 2.8E-01 | 8.44E-04 | 9.85E-05 | 6.78E-03 | 4.09E-04 | 1.14E-07 | 7.93E-15 | 1.06E-04 | 6.54E-01 |
| **U (ppm)** | 0.064 | -0.162 | | 2.34E-04 | 2.60E-01 | 2.74E-01 | 9.98E-02 | 2.10E-01 | 8.58E-01 | 1.17E-02 | 4.78E-03 |
| **V (ppm)** | **0.499** | 0.475 | 0.517 | | 1.50E-02 | 3.36E-01 | 1.26E-03 | 3.77E-07 | 6.74E-04 | 1.37E-05 | 9.57E-02 |
| **Co (ppm)** | **0.501** | 0.542 | 0.170 | 0.357 | | 9.55E-05 | 3.11E-03 | 1.06E-03 | 1.14E-09 | 5.44E-04 | 2.56E-01 |
| **Cr (ppm)** | **0.395** | 0.394 | -0.165 | 0.145 | 0.543 | | 2.71E-01 | 2.44E-01 | 1.29E-03 | 3.61E-03 | 1.36E-02 |
| **Cu (ppm)** | **0.638** | 0.500 | 0.246 | 0.461 | 0.427 | 0.166 | | 3.24E-04 | 3.04E-05 | 1.24E-05 | 3.26E-01 |
| **Zn (ppm)** | **0.726** | 0.690 | 0.188 | 0.669 | 0.467 | 0.175 | 0.507 | | 1.20E-09 | 9.25E-05 | 5.76E-01 |
| **Ni (ppm)** | **0.697** | 0.866 | 0.027 | 0.483 | 0.757 | 0.460 | 0.574 | 0.756 | | 1.08E-05 | 4.22E-01 |
| **Pb (ppm)** | **0.678** | 0.540 | 0.369 | 0.594 | 0.490 | 0.421 | 0.596 | 0.544 | 0.599 | | 2.80E-01 |
| **Cd (ppm)** | 0.105 | -0.068 | 0.409 | 0.249 | -0.171 | -0.361 | 0.148 | 0.085 | -0.121 | 0.163 | |
| **Ga (ppm)** | **0.412** | 0.272 | -0.057 | 0.084 | 0.500 | 0.460 | 0.180 | 0.276 | 0.408 | 0.314 | -0.243 |
| **La (ppm)** | **0.448** | 0.633 | -0.367 | 0.212 | 0.524 | 0.655 | 0.155 | 0.493 | 0.615 | 0.261 | -0.409 |
| **Nd (ppm)** | **0.369** | 0.468 | -0.325 | 0.149 | 0.416 | 0.729 | 0.055 | 0.320 | 0.454 | 0.265 | -0.422 |
| **Rb (ppm)** | **0.699** | 0.728 | -0.141 | 0.356 | 0.647 | 0.673 | 0.453 | 0.626 | 0.806 | 0.538 | -0.233 |
| **Sc (ppm)** | -0.004 | -0.111 | -0.153 | -0.068 | -0.234 | -0.172 | -0.051 | -0.171 | -0.228 | -0.181 | 0.165 |
| **Sr (ppm)** | -0.199 | -0.083 | -0.096 | 0.095 | -0.101 | -0.008 | -0.369 | -0.138 | -0.208 | -0.339 | -0.053 |
| **Th (ppm)** | 0.194 | 0.302 | 0.032 | 0.278 | 0.381 | 0.491 | 0.103 | 0.262 | 0.410 | 0.244 | -0.217 |
| **Y (ppm)** | **0.343** | 0.583 | -0.326 | 0.218 | 0.482 | 0.729 | 0.124 | 0.326 | 0.508 | 0.371 | -0.431 |
| **Zr (ppm)** | **0.672** | 0.677 | -0.245 | 0.260 | 0.619 | 0.765 | 0.329 | 0.505 | 0.709 | 0.504 | -0.306 |

| | Hg (ppb) | Ga (ppm) | La (ppm) | Nd (ppm) | Rb (ppm) | Sc (ppm) | Sr (ppm) | Th (ppm) | Y (ppm) | Zr (ppm) |
|---|---|---|---|---|---|---|---|---|---|---|
| **Hg (ppb)** | | **4.47E-03** | **1.77E-03** | **1.17E-02** | **6.45E-08** | 0.978 | 0.186 | 0.196 | **1.97E-02** | **3.18E-07** |
| **Mo (ppm)** | **0.612** | 6.77E-02 | 2.37E-06 | 1.03E-03 | 1.02E-08 | 4.63E-01 | 5.83E-01 | 4.12E-02 | 2.13E-05 | 2.46E-07 |
| **U (ppm)** | 0.064 | 7.05E-01 | 1.21E-02 | 2.76E-02 | 3.49E-01 | 3.11E-01 | 5.25E-01 | 8.34E-01 | 2.72E-02 | 1.01E-01 |
| **V (ppm)** | **0.499** | 5.80E-01 | 1.56E-01 | 3.22E-01 | 1.52E-02 | 6.54E-01 | 5.32E-01 | 6.13E-02 | 1.45E-01 | 8.10E-02 |
| **Co (ppm)** | **0.501** | 3.98E-04 | 1.84E-04 | 4.06E-03 | 1.20E-06 | 1.17E-01 | 5.05E-01 | 8.90E-03 | 6.93E-04 | 4.45E-06 |
| **Cr (ppm)** | **0.395** | 1.32E-03 | 7.96E-07 | 9.27E-09 | 3.00E-07 | 2.52E-01 | 9.57E-01 | 5.25E-04 | 9.52E-09 | 6.12E-10 |
| **Cu (ppm)** | **0.638** | 2.32E-01 | 3.04E-01 | 7.17E-01 | 1.58E-03 | 7.37E-01 | 1.17E-02 | 4.96E-01 | 4.13E-01 | 2.54E-02 |
| **Zn (ppm)** | **0.726** | 6.34E-02 | 4.99E-04 | 3.00E-02 | 3.31E-06 | 2.55E-01 | 3.60E-01 | 7.92E-02 | 2.69E-02 | 3.39E-04 |
| **Ni (ppm)** | **0.697** | 4.93E-03 | 5.35E-06 | 1.53E-03 | 1.41E-11 | 1.28E-01 | 1.65E-01 | 4.65E-03 | 3.12E-04 | 3.46E-08 |
| **Pb (ppm)** | **0.678** | 3.33E-02 | 8.00E-02 | 7.51E-02 | 1.14E-04 | 2.29E-01 | 2.11E-02 | 1.02E-01 | 1.12E-02 | 3.54E-04 |
| **Cd (ppm)** | 0.105 | 1.04E-01 | 4.79E-03 | 3.52E-03 | 1.20E-01 | 2.73E-01 | 7.26E-01 | 1.47E-01 | 2.78E-03 | 3.83E-02 |
| **Ga (ppm)** | **0.412** | | 3.66E-04 | 8.70E-03 | 2.15E-05 | 8.12E-02 | 2.78E-01 | 1.69E-03 | 6.19E-03 | 4.87E-07 |
| **La (ppm)** | **0.448** | 0.503 | | 5.24E-14 | 4.88E-11 | 1.06E-01 | 8.71E-01 | 3.36E-03 | 1.76E-16 | 3.57E-13 |
| **Nd (ppm)** | **0.369** | 0.383 | 0.853 | | 1.45E-06 | 3.55E-01 | 8.78E-01 | 7.90E-03 | 1.49E-18 | 1.19E-08 |
| **Rb (ppm)** | **0.699** | 0.583 | 0.793 | 0.643 | | 2.96E-02 | 3.12E-01 | 3.62E-04 | 1.67E-07 | 1.69E-19 |
| **Sc (ppm)** | -0.004 | -0.260 | -0.241 | -0.140 | -0.321 | | 7.64E-02 | 1.53E-01 | 3.45E-01 | 1.80E-01 |
| **Sr (ppm)** | -0.199 | -0.163 | -0.025 | 0.023 | -0.153 | 0.264 | | 6.54E-01 | 9.84E-01 | 5.08E-01 |
| **Th (ppm)** | 0.194 | 0.450 | 0.424 | 0.387 | 0.503 | -0.214 | -0.068 | | 1.06E-02 | 2.55E-04 |
| **Y (ppm)** | **0.343** | 0.398 | 0.888 | 0.911 | 0.683 | -0.142 | -0.003 | 0.373 | | 3.38E-10 |
| **Zr (ppm)** | **0.672** | 0.664 | 0.838 | 0.725 | 0.920 | -0.201 | -0.100 | 0.514 | 0.772 | |

APPENDIX D

**Table 10.** Chemostratigraphy of Hg. Klonk section. IC: Inorganic Carbon. TOC: Total Organic Carbon. TS: Total Sulfurs. S–D boundary is taken as the reference level (0 cm) for the stratigraphic position. Negatives values are below the S–D boundary and positives above. All data is generated in this study.

| Sample | Position | Lithology | Hg | $CO_2$ | C | IC | TOC | TS | Hg/TOC | Hg/TOC+TS |
|---|---|---|---|---|---|---|---|---|---|---|
| | | | (ppb) | wt % | | | | | ppb/ wt % | |
| J35 | 270 | Marl | 26.46 | 26.48 | 8.917 | 7.223 | 1.693 | 1.434 | 15.62 | 8.461 |
| J34 | 230 | Marl | 36.40 | 22.76 | 7.721 | 6.206 | 1.514 | 0.015 | 24.04 | 23.80 |
| J33 | 200 | Limestone | 12.37 | 36.66 | 11.19 | 10.00 | 1.191 | 0.316 | 10.38 | 8.206 |
| J32 | 175 | Marl | 36.42 | 24.01 | 8.420 | 6.548 | 1.872 | 0.615 | 19.45 | 14.64 |
| J31 | 170 | Limestone | 13.88 | 34.81 | 10.57 | 9.493 | 1.078 | 0.299 | 12.88 | 10.08 |
| J30 | 140 | Marl | 28.68 | 22.68 | 7.927 | 6.186 | 1.740 | 0.658 | 16.48 | 11.96 |
| J29 | 125 | Limestone | 15.80 | 35.73 | 10.82 | 9.746 | 1.076 | 0.238 | 14.68 | 12.03 |
| J28 | 80 | Marl | 51.61 | 19.88 | 7.605 | 5.422 | 2.184 | 1.410 | 23.63 | 14.36 |
| J27 | 65 | Limestone | 20.41 | 34.29 | 10.54 | 9.352 | 1.193 | 0.257 | 17.11 | 14.07 |
| J26 | 45 | Marl | 48.93 | 25.72 | 9.013 | 7.015 | 1.998 | 0.036 | 24.49 | 24.05 |
| J25 | 35 | Shale | 76.45 | 10.26 | 6.035 | 2.799 | 3.237 | 0.036 | 23.62 | 23.36 |
| J24 | -5 | Limestone | 15.68 | 34.41 | 10.65 | 9.385 | 1.269 | 0.241 | 12.36 | 10.39 |
| J23 | -30 | Limestone | 12.97 | 35.12 | 10.81 | 9.578 | 1.236 | 0.164 | 10.50 | 9.264 |
| J22 | -55 | Limestone | 11.04 | 40.39 | 11.83 | 11.02 | 0.809 | 0.176 | 13.65 | 11.21 |
| J21 | -85 | Limestone | 20.40 | 34.75 | 10.53 | 9.477 | 1.050 | 0.225 | 19.43 | 16.00 |
| J20 | -120 | Shale | 86.69 | 13.68 | 6.449 | 3.730 | 2.719 | 0.014 | 31.89 | 31.73 |
| J19 | -135 | Limestone | 27.80 | 32.81 | 10.20 | 8.949 | 1.249 | 0.311 | 22.25 | 17.82 |
| J18 | -150 | Shale | 68.31 | 14.51 | 5.992 | 3.958 | 2.034 | 0.019 | 33.58 | 33.27 |
| J17 | -160 | Limestone | 16.47 | 35.05 | 10.51 | 9.558 | 0.956 | 0.229 | 17.22 | 13.90 |
| J16 | -185 | Shale | 84.22 | 13.14 | 5.493 | 3.583 | 1.910 | 0.014 | 44.09 | 43.76 |
| J15 | -190 | Limestone | 19.46 | 34.10 | 10.25 | 9.300 | 0.948 | 0.025 | 20.53 | 19.99 |
| J14 | -210 | Shale | 48.22 | 12.91 | 5.262 | 3.520 | 1.742 | 0.652 | 27.68 | 20.15 |
| J13 | -215 | Limestone | 15.36 | 34.85 | 10.47 | 9.505 | 0.970 | 0.440 | 15.83 | 10.89 |
| J12 | -255 | Shale | 74.23 | 10.07 | 4.440 | 2.746 | 1.694 | 0.057 | 43.82 | 42.39 |
| J11 | -270 | Limestone | 11.50 | 35.74 | 10.69 | 9.746 | 0.940 | 0.188 | 12.23 | 10.19 |
| J10 | -300 | Marl | 49.14 | 16.04 | 6.210 | 4.375 | 1.835 | 0.036 | 26.77 | 26.26 |
| J9 | -315 | Limestone | 22.97 | 29.74 | 9.151 | 8.110 | 1.042 | 0.042 | 22.05 | 21.20 |
| J8 | -330 | Shale | 67.20 | 8.59 | 4.162 | 2.343 | 1.819 | 0.036 | 36.95 | 36.23 |
| J7 | -345 | Limestone | 14.48 | 33.31 | 10.06 | 9.083 | 0.978 | 0.153 | 14.81 | 12.80 |
| J6 | -370 | Shale | 53.02 | 13.56 | 5.517 | 3.699 | 1.818 | 0.019 | 29.16 | 28.86 |
| J5 | -395 | Limestone | 17.97 | 32.91 | 10.05 | 8.975 | 1.074 | 0.030 | 16.73 | 16.27 |
| J4 | -420 | Marl | 46.72 | 16.04 | 6.354 | 4.376 | 1.978 | 0.019 | 23.62 | 23.40 |
| J3 | -435 | Limestone | 18.70 | 33.07 | 10.20 | 9.019 | 1.180 | 0.049 | 15.85 | 15.21 |
| J2 | -460 | Black shale | 67.50 | 4.76 | 3.285 | 1.297 | 1.988 | 0.587 | 33.96 | 26.21 |
| J1 | -485 | Limestone | 21.23 | 33.47 | 9.848 | 9.128 | 0.720 | 0.007 | 29.50 | 29.22 |

APPENDIX E

**Table 11.** Shapiro-Wilk test of normality for Hg and major element variables coming from the Klonk section. Values in red color show variables that do not have a normal distribution (p-values < 0.05).

| Hg vs major elements. N=35 | | |
|---|---|---|
| **Variable** | **p-(normal)** | **Shapiro-Wilk** |
| Hg (ppb) | 4.4.E-04 | 0.862 |
| $Al_2O_3$ | 0.001 | 0.873 |
| CaO | 0.002 | 0.884 |
| $Fe_2O_3$ | 0.002 | 0.891 |
| $K_2O$ | 0.001 | 0.869 |
| MgO | 0.002 | 0.887 |
| MnO | 0.131 | 0.952 |
| $Na_2O$ | 0.001 | 0.879 |
| $P_2O_5$ | 0.014 | 0.920 |
| $SiO_2$ | 0.003 | 0.898 |
| $TiO_2$ | 0.001 | 0.870 |

**Table 12.** Shapiro-Wilk test of normality for Hg, TS, TOC, and $CO_2$ variables coming from the Klonk section. Values in red color show variables that do not have a normal distribution (p-values < 0.05).

| **Variable** | **p-normal** | **Shapiro-Wilk** |
|---|---|---|
| **Hg (ppb)** | 4.4E-04 | 0.862 |
| **TS (wt %)** | 3.3E-07 | 0.696 |
| **TOC (wt %)** | 0.005 | 0.904 |
| **$CO_2$ (wt %)** | 0.001 | 0.878 |

**Table 13.** Shapiro-Wilk test of normality for Hg and trace element variables coming from the Klonk section. Values in red color show variables that do not have a normal distribution (p-values < 0.05). The table continues on the next page.

| Hg vs Trace elements (N = 35) | | |
|---|---|---|
| **Trace element** | **p-(normal)** | **Shapiro-Wilk** |
| Ba | 4.1E-04 | 0.8608 |
| Cd | 0.012 | 0.917 |
| Ce | 0.004 | 0.899 |
| Co | 0.072 | 0.944 |
| Cr | 0.001 | 0.877 |
| Cu | 0.002 | 0.887 |
| Ga | 0.001 | 0.877 |
| La | 0.037 | 0.934 |
| Mo | 2.4E-04 | 0.850 |
| Nb | 4.7E-04 | 0.863 |
| Nd | 0.014 | 0.920 |
| Ni | 4.7E-04 | 0.863 |
| Pb | 4.8E-04 | 0.864 |
| Rb | 0.001 | 0.873 |
| Sc | 0.037 | 0.934 |
| Sr | 0.117 | 0.950 |
| Th | 0.003 | 0.896 |
| U | 0.001 | 0.883 |
| V | 3.8E-05 | 0.814 |
| Y | 0.010 | 0.915 |
| Zn | 0.002 | 0.886 |
| Zr | 4.5E-04 | 0.862 |

APPENDIX F

**Table 14.** Results of the correlation analysis (Spearman's correlation coefficients and p-values) of mercury and trace elements of samples coming from the Klonk section. Correlation coefficients for mercury are indicated in red color, and p-values in blue. Bolded values show correlations that are statistically significant (p-values < 0.05). The table continues on the next page.

| | Hg (ppb) | Ba (ppm) | Cd (ppm) | Ce (ppm) | Co (ppm) | Cr (ppm) | Cu (ppm) | Ga (ppm) | La (ppm) | Mo (ppm) | Nb (ppm) |
|---|---|---|---|---|---|---|---|---|---|---|---|
| **Hg (ppb)** | | **1.3E-09** | 0.210 | **1.9E-14** | **2.9E-13** | **9.4E-16** | **7.7E-18** | **8.7E-16** | **1.9E-08** | **1.9E-08** | **1.8E-14** |
| **Ba (ppm)** | **0.823** | | 0.099 | 1.8E-10 | 2.1E-07 | 6.7E-12 | 1.1E-09 | 2.6E-08 | 3.6E-08 | 3.6E-08 | 1.4E-08 |
| **Cd (ppm)** | -0.217 | -0.284 | | 0.163 | 0.504 | 0.131 | 0.174 | 0.094 | 0.293 | 0.293 | 0.145 |
| **Ce (ppm)** | **0.914** | 0.845 | -0.241 | | 2.5E-10 | 3.6E-15 | 1.3E-17 | 7.6E-11 | 2.7E-10 | 2.7E-10 | 7.4.E-12 |
| **Co (ppm)** | **0.897** | 0.750 | -0.117 | 0.841 | | 5.2E-13 | 5.4E-14 | 5.5E-09 | 1.2E-07 | 1.2E-07 | 2.3.E-10 |
| **Cr (ppm)** | **0.929** | 0.874 | -0.260 | 0.922 | 0.893 | | 4.0E-15 | 1.8E-12 | 1.2E-10 | 1.2E-10 | 3.7.E-14 |
| **Cu (ppm)** | **0.947** | 0.825 | -0.235 | 0.945 | 0.908 | 0.922 | | 5.8E-13 | 3.3E-08 | 3.3E-08 | 1.2.E-13 |
| **Ga (ppm)** | **0.929** | 0.783 | -0.287 | 0.853 | 0.805 | 0.885 | 0.893 | | 1.6E-07 | 1.6E-07 | 6.6.E-15 |
| **La (ppm)** | **0.917** | 0.832 | -0.241 | 0.992 | 0.831 | 0.918 | 0.935 | 0.858 | 3.2E-10 | 3.2E-10 | 1.8.E-11 |
| **Mo (ppm)** | **0.788** | 0.779 | -0.183 | 0.841 | 0.760 | 0.849 | 0.780 | 0.755 | | | 9.2.E-08 |
| **Nb (ppm)** | **0.914** | 0.793 | -0.251 | 0.874 | 0.842 | 0.910 | 0.903 | 0.919 | 0.764 | 0.764 | |
| **Nd (ppm)** | **0.908** | 0.849 | -0.217 | 0.989 | 0.843 | 0.936 | 0.935 | 0.851 | 0.845 | 0.845 | 0.861 |
| **Ni (ppm)** | **0.916** | 0.889 | -0.220 | 0.931 | 0.869 | 0.961 | 0.922 | 0.880 | 0.867 | 0.867 | 0.899 |
| **Pb (ppm)** | **0.932** | 0.860 | -0.305 | 0.930 | 0.848 | 0.959 | 0.910 | 0.923 | 0.862 | 0.862 | 0.928 |
| **Rb (ppm)** | **0.955** | 0.851 | -0.269 | 0.948 | 0.862 | 0.948 | 0.952 | 0.890 | 0.791 | 0.791 | 0.908 |
| **Sc (ppm)** | **0.481** | 0.588 | -0.269 | 0.422 | 0.399 | 0.463 | 0.407 | 0.528 | 0.518 | 0.518 | 0.466 |
| **Sr (ppm)** | **-0.733** | -0.809 | 0.274 | -0.772 | -0.633 | -0.808 | -0.706 | -0.771 | -0.817 | -0.817 | -0.799 |
| **Th (ppm)** | **0.906** | 0.799 | -0.303 | 0.908 | 0.843 | 0.916 | 0.922 | 0.870 | 0.721 | 0.721 | 0.916 |
| **U (ppm)** | **0.794** | 0.795 | -0.249 | 0.853 | 0.765 | 0.869 | 0.803 | 0.797 | 0.940 | 0.940 | 0.816 |
| **V (ppm)** | **0.814** | 0.821 | -0.258 | 0.857 | 0.720 | 0.912 | 0.795 | 0.814 | 0.858 | 0.858 | 0.819 |
| **Y (ppm)** | **0.898** | 0.811 | -0.269 | 0.971 | 0.799 | 0.910 | 0.893 | 0.840 | 0.809 | 0.809 | 0.837 |
| **Zn (ppm)** | **0.931** | 0.851 | -0.194 | 0.933 | 0.830 | 0.943 | 0.923 | 0.864 | 0.798 | 0.798 | 0.888 |
| **Zr (ppm)** | **0.957** | 0.867 | -0.273 | 0.951 | 0.877 | 0.972 | 0.958 | 0.894 | 0.805 | 0.805 | 0.918 |

| | Hg (ppb) | Nd (ppm) | Ni (ppm) | Pb (ppm) | Rb (ppm) | Sc (ppm) | Sr (ppm) | Th (ppm) | U (ppm) | V (ppm) | Y (ppm) | Zn (ppm) | Zr (ppm) |
|---|---|---|---|---|---|---|---|---|---|---|---|---|---|
| **Hg (ppb)** | | **4.7E-14** | **1.1E-14** | **4.36E-16** | **5.2E-19** | **3.5E-03** | **5.4E-07** | **6.9E-14** | **1.3E-08** | **2.7E-09** | **2.8E-13** | **5.0E-16** | **2.3E-19** |
| **Ba (ppm)** | **0.823** | 1.1E-10 | 9.4E-13 | 3.5E-11 | 9.2E-11 | 2.0E-04 | 3.9E-09 | 8.8E-09 | 1.2E-08 | 1.6E-09 | 3.5E-09 | 9.3E-11 | 1.7E-11 |
| **Cd (ppm)** | -0.217 | 0.210 | 0.203 | 0.074 | 0.118 | 0.118 | 0.111 | 0.077 | 0.149 | 0.134 | 0.118 | 0.265 | 0.113 |
| **Ce (ppm)** | **0.914** | 5.6E-29 | 5.4E-16 | 6.6E-16 | 6.4E-18 | 0.012 | 5.7E-08 | 5.1E-14 | 7.9E-11 | 5.2E-11 | 4.2E-22 | 3.2E-16 | 2.5E-18 |
| **Co (ppm)** | **0.897** | 2.1E-10 | 1.3E-11 | 1.3E-10 | 3.0E-11 | 0.018 | 4.4E-05 | 2.0E-10 | 8.8E-08 | 1.1E-06 | 8.6E-09 | 7.4E-10 | 4.7E-12 |
| **Cr (ppm)** | **0.929** | 1.5E-16 | 6.5E-20 | 1.2E-19 | 5.8E-18 | 0.005 | 4.4E-09 | 1.3E-14 | 1.3E-11 | 2.6E-14 | 3.4E-14 | 2.3E-17 | 2.9E-22 |
| **Cu (ppm)** | **0.947** | 2.3E-16 | 3.8E-15 | 3.6E-14 | 1.3E-18 | 0.015 | 2.1E-06 | 4.1E-15 | 6.6E-09 | 1.2E-08 | 5.2E-13 | 3.1E-15 | 2.0E-19 |
| **Ga (ppm)** | **0.929** | 9.1E-11 | 3.2E-12 | 2.9E-15 | 8.2E-13 | 0.001 | 6.0E-08 | 1.2E-11 | 9.8E-09 | 2.8E-09 | 2.7E-10 | 2.2E-11 | 4.8E-13 |
| **La (ppm)** | **0.917** | 2.8E-27 | 5.4E-15 | 8.6E-16 | 9.8E-18 | 0.008 | 2.7E-08 | 1.3E-13 | 2.4E-10 | 4.7E-11 | 4.7E-23 | 1.5E-16 | 2.3E-18 |
| **Mo (ppm)** | **0.788** | 1.8E-10 | 1.7E-11 | 2.9E-11 | 1.5E-08 | 0.001 | 2.2E-09 | 1.0E-06 | 6.4E-17 | 4.3E-11 | 4.2E-09 | 9.5E-09 | 5.5E-09 |
| **Nb (ppm)** | **0.914** | 3.4E-11 | 2.3E-13 | 1.0E-15 | 5.0E-14 | 0.005 | 8.9E-09 | 1.2E-14 | 2.3E-09 | 1.8E-09 | 3.8E-10 | 1.1E-12 | 7.8E-15 |
| **Nd (ppm)** | **0.908** | | 2.5E-16 | 4.4E-16 | 5.8E-18 | 0.011 | 1.1E-08 | 9.7E-14 | 1.3E-11 | 4.8E-12 | 1.5E-21 | 4.7E-17 | 1.1E-18 |
| **Ni (ppm)** | **0.916** | 0.934 | | 7.0E-18 | 1.1E-17 | 0.003 | 7.1E-10 | 5.9E-14 | 1.5E-11 | 4.7E-16 | 7.7E-14 | 1.4E-18 | 2.3E-19 |
| **Pb (ppm)** | **0.932** | 0.932 | 0.947 | | 7.5E-19 | 0.002 | 9.3E-11 | 7.2E-15 | 1.5E-11 | 2.7E-13 | 1.1E-14 | 5.8E-15 | 1.3E-18 |
| **Rb (ppm)** | **0.955** | 0.948 | 0.946 | 0.954 | | 0.007 | 1.1E-08 | 7.0E-19 | 5.5E-09 | 7.2E-12 | 1.0E-14 | 9.1E-20 | 7.7E-28 |
| **Sc (ppm)** | **0.481** | 0.423 | 0.492 | 0.505 | 0.447 | | 2.0.E-04 | 0.006 | 0.005 | 0.001 | 0.011 | 0.010 | 0.007 |
| **Sr (ppm)** | **-0.733** | -0.796 | -0.830 | -0.851 | -0.795 | -0.589 | | 4.7E-08 | 2.9E-11 | 3.9E-12 | 1.2E-07 | 1.6E-08 | 3.6E-08 |
| **Th (ppm)** | **0.906** | 0.904 | 0.907 | 0.919 | 0.954 | 0.456 | -0.775 | | 1.2E-07 | 1.5E-10 | 3.1E-12 | 7.8E-15 | 1.3E-17 |
| **U (ppm)** | **0.794** | 0.869 | 0.868 | 0.868 | 0.805 | 0.463 | -0.862 | 0.760 | | 1.2E-11 | 1.1E-09 | 6.2E-09 | 2.7E-09 |
| **V (ppm)** | **0.814** | 0.877 | 0.932 | 0.898 | 0.874 | 0.517 | -0.879 | 0.847 | 0.870 | | 1.4E-11 | 2.6E-14 | 3.6E-12 |
| **Y (ppm)** | **0.898** | 0.969 | 0.906 | 0.917 | 0.917 | 0.424 | -0.760 | 0.881 | 0.824 | 0.868 | | 4.6E-16 | 2.1E-15 |
| **Zn (ppm)** | **0.931** | 0.941 | 0.952 | 0.920 | 0.960 | 0.429 | -0.791 | 0.918 | 0.804 | 0.912 | 0.932 | | 1.8E-21 |
| **Zr (ppm)** | **0.957** | 0.953 | 0.957 | 0.953 | 0.987 | 0.448 | -0.779 | 0.945 | 0.814 | 0.879 | 0.925 | 0.968 | |

APPENDIX G

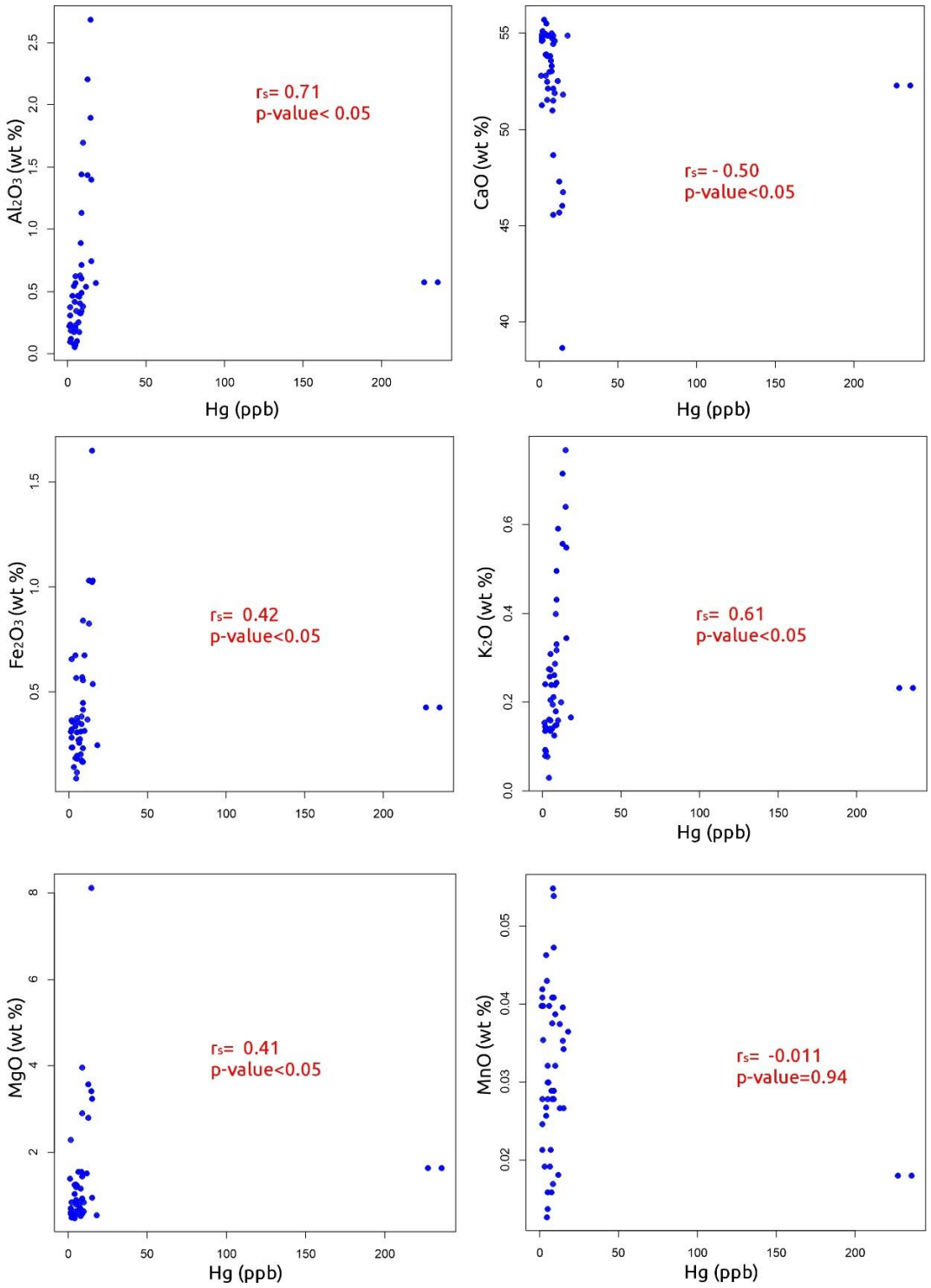


**Figure 33.** Hg and major elements ($Al_2O_3$,CaO, $Fe_2O_3$, $K_2O$, MgO, and MnO) correlations plots from the Opatřilka section (Samples with Hg anomalies are included). The $r_s$ values correspond to Spearman's correlation coefficients.

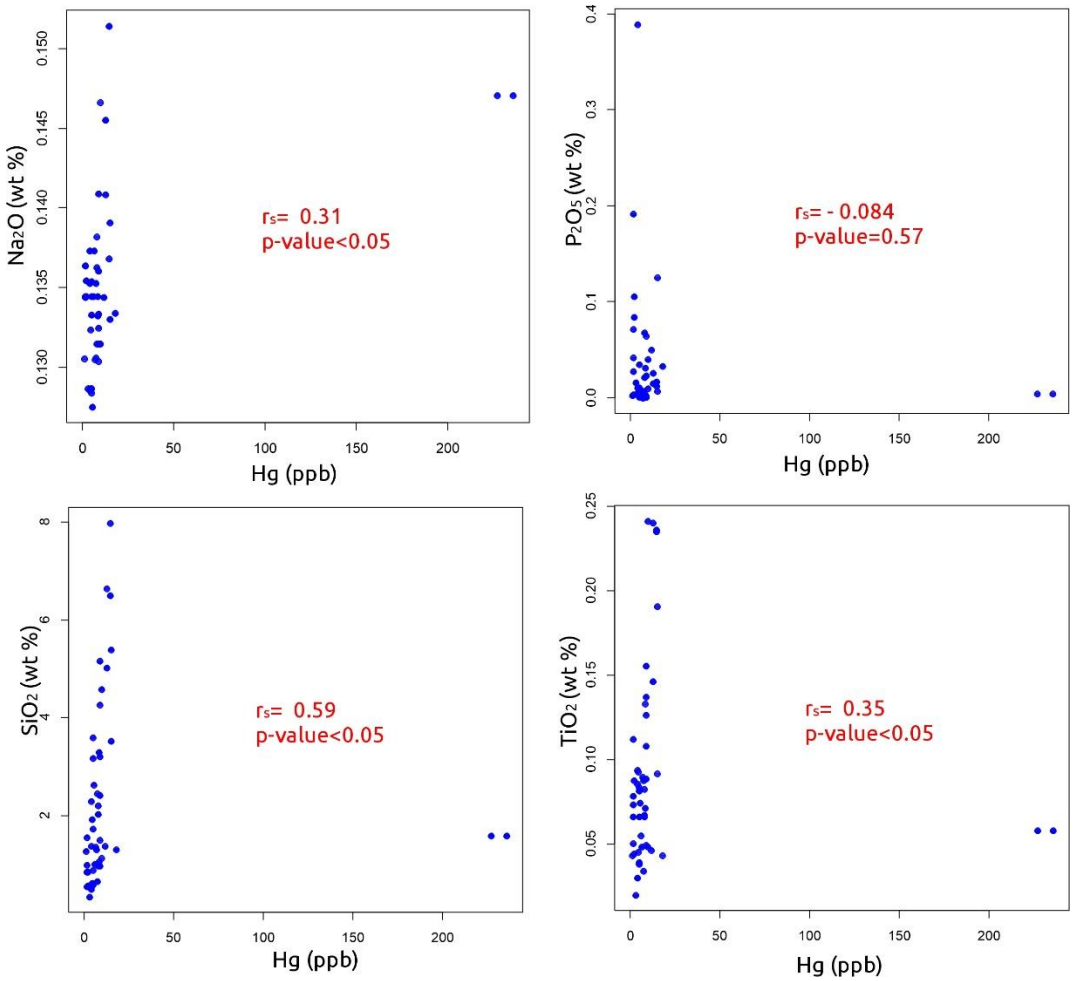


**Figure 34.** Hg and major elements ($Na_2O_3$, $P_2O_5$, $SiO_2$, $TiO_2$) correlations plots from the Opatřilka section (Samples with Hg anomalies are included). The $r_s$ values correspond to Spearman's correlation coefficients.

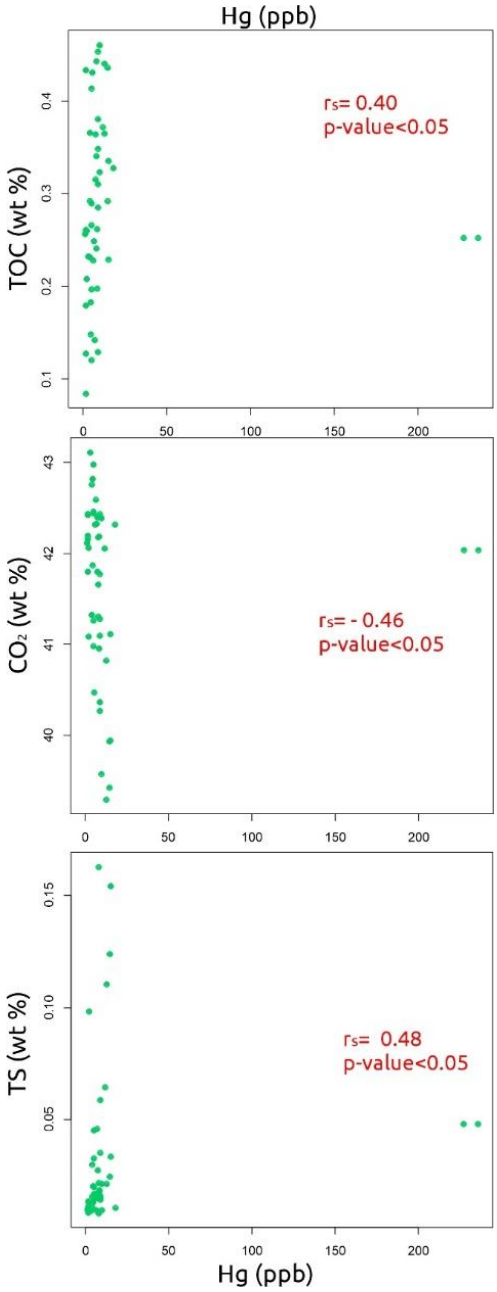


**Figure 35.** Hg and TS, TOC, and $CO_2$ correlation plots of the Opatřilka section (including sample with anomalous Hg content). The $r_s$ values correspond to Spearman's correlation coefficients.

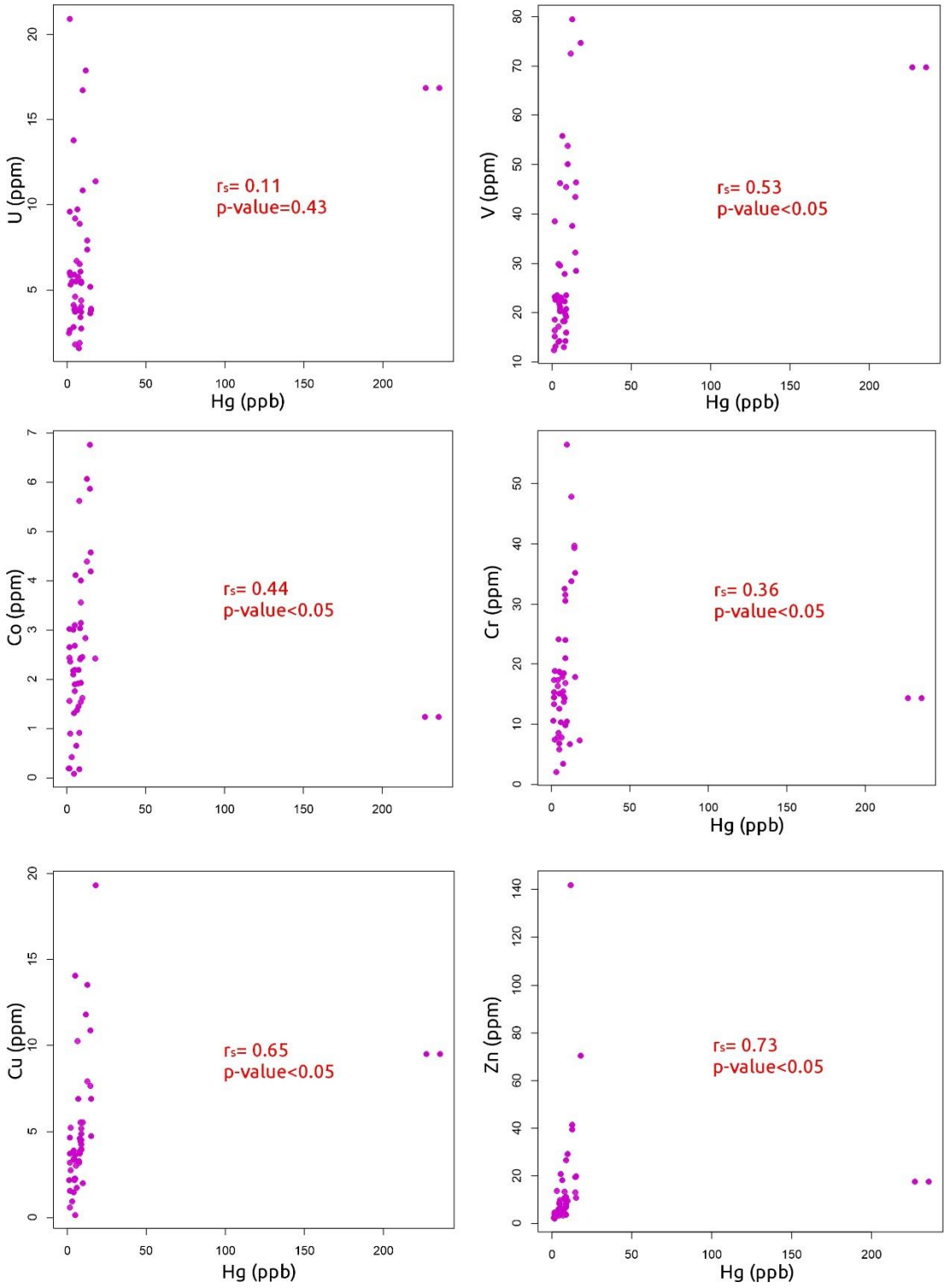


**Figure 36.** Hg and trace elements (U, V, Co, Cr, Cu, and Zn) correlation plots from the Opatřilka section (samples with Hg anomalous content are included).

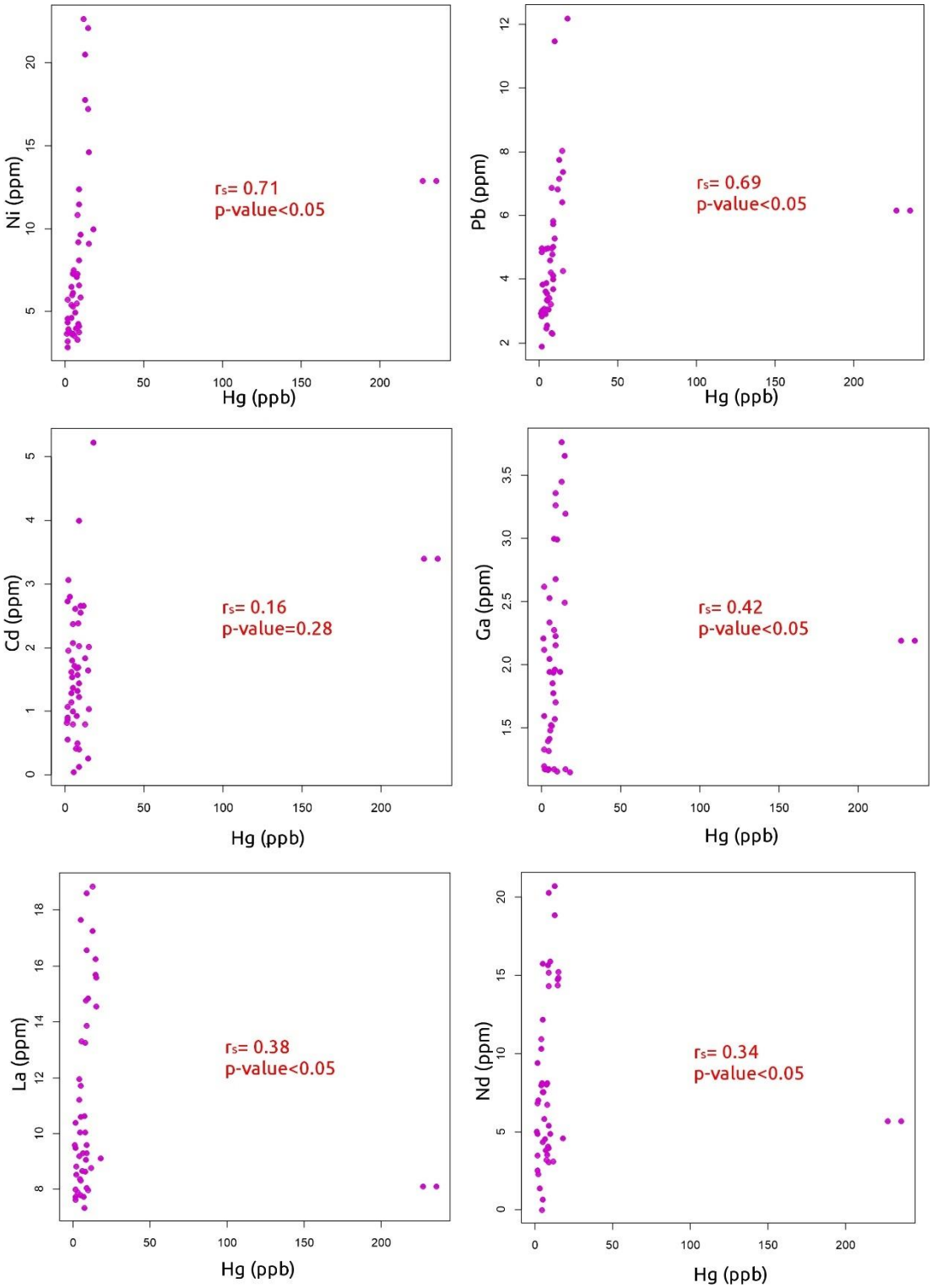


**Figure 37.** Hg and trace elements (Ni, Pb, Cd, Ga, La, and Nd) correlation plots from the Opatřilka section (samples with Hg anomalous content are included).

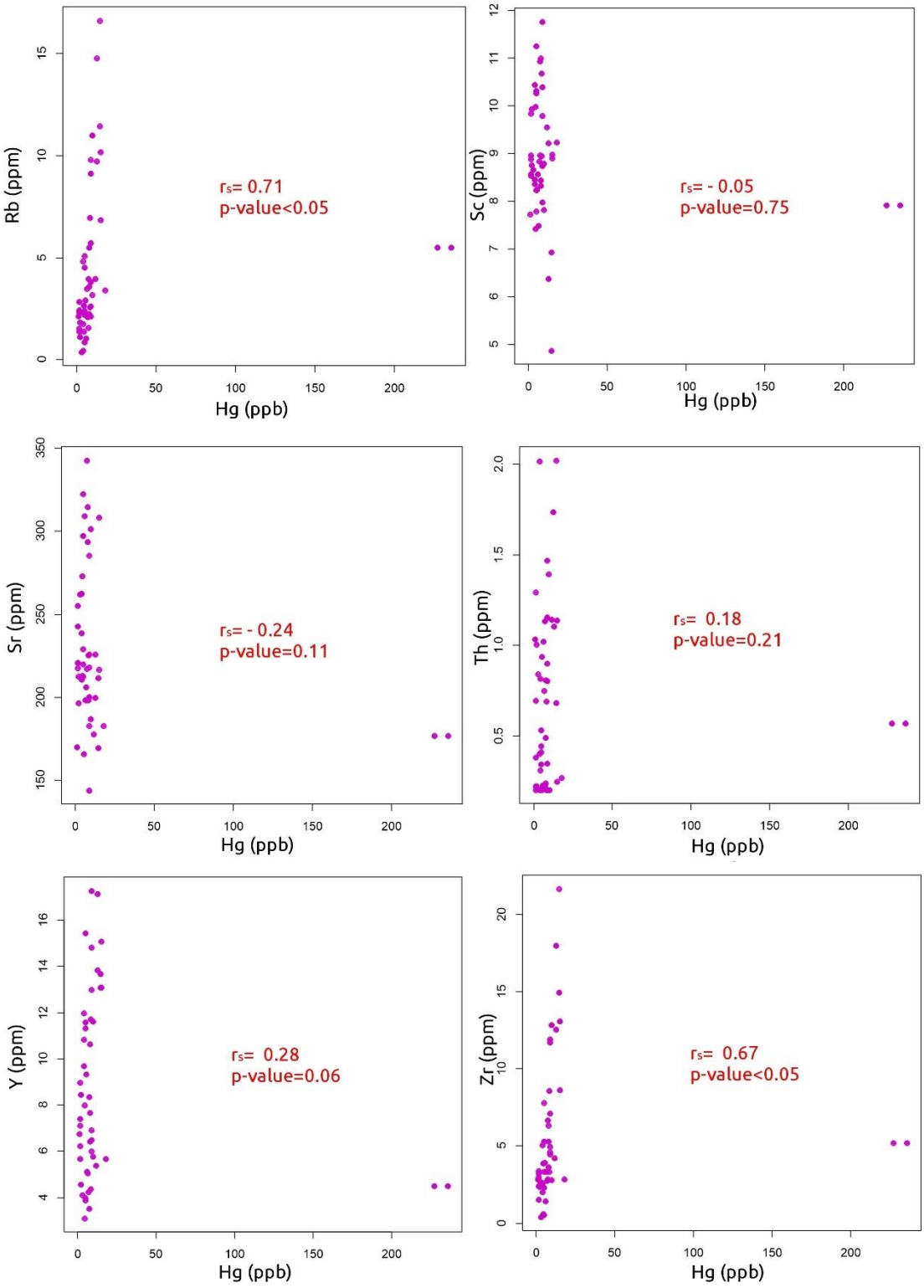


**Figure 38.** Hg and trace elements (Rb, Sc, Sr, Th, Y, and Zr) correlation plots from the Opatřilka section (samples with Hg anomalous content are included).

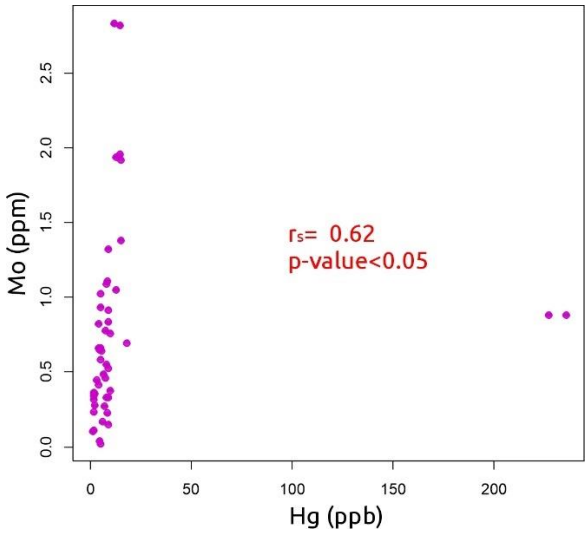


**Figure 39.** Hg and Mo correlation plot from the Opatřilka section (samples with Hg anomalous content are included).

APPENDIX H

**Table 15.** Major elements content from the Opatřilka section. TS: Total Sulfur. TOC: Total organic carbon. $CaCO_3$ is calculated from $CO_2$ content. (Details in chapter 4.6. THE CARBONATE CARBON ANALYSIS). The table continues on the next page.

| Sample | Stratigraphic position | $Al_2O_3$ (wt. %) | CaO (wt. %) | $Fe_2O_3$ (wt. %) | $K_2O$ (wt. %) | MgO (wt. %) | MnO (wt. %) | $Na_2O$ (wt. %) | $P_2O_5$ (wt. %) | $SiO_2$ (wt. %) | $TiO_2$ (wt. %) | $CO_2$ (wt. %) | TS (wt. %) | TC (wt. %) | TOC (wt. %) | $CaCO_3$ (wt%) |
|---|---|---|---|---|---|---|---|---|---|---|---|---|---|---|---|---|
| L1 | 200 | 0.240 | 54.76 | 0.29 | 0.14 | 0.71 | 0.021 | 0.136 | 0.028 | 0.856 | 0.112 | 41.80 | 0.012 | 11.83 | 0.433 | 95.00 |
| L2 | 150 | 0.080 | 54.95 | 0.68 | 0.03 | 0.48 | 0.027 | 0.137 | 0.389 | 0.510 | 0.094 | 41.33 | 0.011 | 11.64 | 0.366 | 93.94 |
| L3 | 100 | 0.123 | 55.11 | 0.36 | 0.09 | 0.50 | 0.040 | 0.135 | 0.105 | 0.571 | 0.088 | 42.07 | 0.099 | 11.68 | 0.208 | 95.61 |
| L4 | 50 | 0.096 | 54.93 | 0.33 | 0.09 | 0.70 | 0.025 | 0.134 | 0.192 | 0.552 | 0.050 | 42.17 | 0.010 | 11.76 | 0.262 | 95.83 |
| L5 | 0 | 0.191 | 54.67 | 0.24 | 0.14 | 0.86 | 0.035 | 0.134 | 0.084 | 0.862 | 0.044 | 41.09 | 0.010 | 11.47 | 0.260 | 93.39 |
| L6 | -50 | 0.224 | 54.75 | 0.37 | 0.15 | 0.62 | 0.042 | 0.134 | 0.072 | 0.861 | 0.067 | 42.43 | 0.009 | 11.75 | 0.180 | 96.42 |
| L7 | -100 | 0.308 | 54.60 | 0.66 | 0.08 | 0.59 | 0.041 | 0.134 | 0.042 | 1.003 | 0.074 | 42.20 | 0.009 | 11.59 | 0.084 | 95.91 |
| L8 | -150 | 0.223 | 52.82 | 0.31 | 0.15 | 1.39 | 0.040 | 0.131 | 0.003 | 1.281 | 0.043 | 42.12 | 0.010 | 11.74 | 0.257 | 95.73 |
| L9 | -202 | 0.635 | 53.03 | 0.39 | 0.29 | 1.17 | 0.038 | 0.138 | 0.021 | 2.028 | 0.083 | 41.31 | 0.022 | 11.71 | 0.443 | 93.89 |
| L10 | -253 | 0.545 | 52.80 | 0.34 | 0.27 | 1.26 | 0.046 | 0.135 | 0.005 | 2.301 | 0.086 | 41.33 | 0.016 | 11.56 | 0.292 | 93.93 |
| L11 | -304 | 1.444 | 45.57 | 0.84 | 0.50 | 3.96 | 0.047 | 0.136 | 0.002 | 5.167 | 0.155 | 40.27 | 0.016 | 11.33 | 0.348 | 91.53 |
| L12 | -353 | 0.419 | 53.89 | 0.57 | 0.26 | 0.64 | 0.043 | 0.132 | 0.003 | 1.936 | 0.093 | 41.87 | 0.021 | 11.47 | 0.149 | 95.16 |
| L13 | -405 | 0.890 | 51.01 | 0.57 | 0.40 | 1.56 | 0.055 | 0.133 | 0.004 | 3.308 | 0.133 | 40.96 | 0.019 | 11.37 | 0.198 | 93.10 |
| L14 | -456 | 0.715 | 48.70 | 0.56 | 0.32 | 2.92 | 0.054 | 0.130 | 0.001 | 3.208 | 0.089 | 41.10 | 0.016 | 11.52 | 0.311 | 93.41 |
| L16a | -544 | 1.702 | 51.92 | 0.68 | 0.59 | 0.85 | 0.032 | 0.147 | 0.041 | 4.595 | 0.241 | 39.58 | 0.022 | 11.12 | 0.323 | 89.96 |
| L16 | -557 | 0.105 | 54.90 | 0.28 | 0.14 | 0.65 | 0.040 | 0.134 | 0.006 | 1.020 | 0.056 | 42.33 | 0.015 | 11.77 | 0.228 | 96.20 |
| L16b | -587 | 1.400 | 46.77 | 1.03 | 0.55 | 3.25 | 0.034 | 0.133 | 0.007 | 5.396 | 0.191 | 39.95 | 0.034 | 11.23 | 0.336 | 90.79 |
| L17 | -609 | 0.348 | 52.13 | 0.36 | 0.24 | 1.24 | 0.030 | 0.128 | 0.005 | 2.630 | 0.075 | 40.47 | 0.017 | 11.47 | 0.431 | 91.99 |
| L16c | -630 | 2.209 | 45.71 | 1.03 | 0.72 | 3.58 | 0.037 | 0.146 | 0.015 | 6.655 | 0.240 | 39.30 | 0.022 | 11.16 | 0.441 | 89.32 |

| | | | | | | | | | | | | | | | | |
|---|---|---|---|---|---|---|---|---|---|---|---|---|---|---|---|---|
| L18 | -658 | 0.569 | 51.56 | 0.38 | 0.27 | 1.25 | 0.032 | 0.128 | 0.011 | 3.609 | 0.082 | 40.98 | 0.020 | 11.37 | 0.197 | 93.14 |
| L18a | -678 | 1.897 | 46.08 | 1.03 | 0.64 | 3.43 | 0.035 | 0.137 | 0.012 | 6.514 | 0.235 | 39.43 | 0.025 | 11.19 | 0.436 | 89.62 |
| L19 | -716 | 2.690 | 38.67 | 1.65 | 0.77 | 8.13 | 0.040 | 0.151 | 0.017 | 7.996 | 0.236 | 39.94 | 0.124 | 11.19 | 0.293 | 90.78 |
| L20 | -772 | 0.376 | 51.27 | 0.24 | 0.24 | 2.29 | 0.028 | 0.136 | 0.003 | 1.559 | 0.079 | 42.44 | 0.014 | 11.70 | 0.127 | 96.45 |
| L21 | -825 | 0.606 | 52.14 | 0.42 | 0.33 | 1.44 | 0.029 | 0.133 | 0.002 | 2.427 | 0.108 | 41.29 | 0.036 | 11.64 | 0.381 | 93.84 |
| L22 | -878 | 0.327 | 54.74 | 0.17 | 0.18 | 0.67 | 0.017 | 0.134 | 0.031 | 1.075 | 0.072 | 42.19 | 0.019 | 11.77 | 0.262 | 95.88 |
| L23 | -928 | 0.255 | 53.82 | 0.28 | 0.21 | 0.78 | 0.021 | 0.131 | 0.000 | 1.321 | 0.090 | 42.33 | 0.046 | 11.69 | 0.143 | 96.20 |
| L24 | -982 | 0.495 | 54.44 | 0.17 | 0.24 | 0.61 | 0.028 | 0.131 | 0.002 | 1.504 | 0.126 | 42.44 | 0.015 | 11.70 | 0.130 | 96.45 |
| L25 | -1035 | 0.330 | 55.02 | 0.18 | 0.15 | 0.53 | 0.041 | 0.132 | 0.068 | 0.974 | 0.067 | 42.19 | 0.009 | 11.74 | 0.241 | 95.88 |
| L26 | -1080 | 0.177 | 54.86 | 0.21 | 0.13 | 0.70 | 0.016 | 0.131 | 0.005 | 0.660 | 0.034 | 42.40 | 0.018 | 11.88 | 0.316 | 96.36 |
| L27 | -1134 | 0.347 | 54.89 | 0.24 | 0.15 | 0.59 | 0.041 | 0.132 | 0.065 | 0.972 | 0.049 | 41.78 | 0.015 | 11.67 | 0.286 | 94.95 |
| L28 | -1182 | 0.074 | 54.87 | 0.12 | 0.14 | 0.86 | 0.014 | 0.129 | 0.005 | 0.595 | 0.038 | 42.44 | 0.017 | 11.86 | 0.290 | 96.46 |
| L29 B1 | -1225 | 0.573 | 54.87 | 0.25 | 0.17 | 0.55 | 0.037 | 0.133 | 0.033 | 1.306 | 0.043 | 42.32 | 0.011 | 11.87 | 0.328 | 96.18 |
| L29 A2 | -1230 | 0.469 | 55.73 | 0.15 | 0.08 | 0.54 | 0.019 | 0.129 | 0.016 | 0.342 | 0.020 | 43.12 | 0.010 | 11.99 | 0.232 | 97.99 |
| L29 REP | -1235 | 0.575 | 52.30 | 0.43 | 0.23 | 1.65 | 0.018 | 0.147 | 0.004 | 1.597 | 0.059 | 42.04 | 0.048 | 11.72 | 0.253 | 95.55 |
| L29 | -1235 | 0.575 | 52.30 | 0.43 | 0.23 | 1.65 | 0.018 | 0.147 | 0.004 | 1.597 | 0.059 | 42.04 | 0.048 | 11.72 | 0.253 | 95.55 |
| L29 A1 | -1240 | 0.469 | 53.01 | 0.26 | 0.20 | 1.55 | 0.019 | 0.137 | 0.005 | 1.364 | 0.048 | 42.59 | 0.010 | 11.87 | 0.249 | 96.81 |
| L29 B2 | -1265 | 0.382 | 54.59 | 0.32 | 0.16 | 0.65 | 0.039 | 0.132 | 0.010 | 1.139 | 0.048 | 42.39 | 0.010 | 12.02 | 0.461 | 96.35 |
| L30 | -1289 | 0.055 | 55.51 | 0.09 | 0.14 | 0.54 | 0.013 | 0.129 | 0.006 | 0.623 | 0.045 | 42.82 | 0.014 | 11.86 | 0.184 | 97.32 |
| L31 | -1339 | 0.209 | 53.83 | 0.20 | 0.16 | 1.20 | 0.016 | 0.134 | 0.004 | 0.899 | 0.039 | 42.98 | 0.020 | 11.99 | 0.267 | 97.69 |
| L32 | -1388 | 0.540 | 52.54 | 0.37 | 0.20 | 1.51 | 0.018 | 0.134 | 0.050 | 1.377 | 0.046 | 42.06 | 0.065 | 11.84 | 0.372 | 95.58 |
| L33 | -1442 | 1.440 | 47.30 | 0.83 | 0.56 | 2.80 | 0.027 | 0.141 | 0.025 | 5.034 | 0.146 | 40.83 | 0.110 | 11.50 | 0.365 | 92.78 |
| L34 | -1490 | 1.134 | 51.53 | 0.45 | 0.43 | 0.93 | 0.029 | 0.141 | 0.023 | 4.267 | 0.137 | 40.37 | 0.059 | 11.46 | 0.453 | 91.76 |
| L35 | -1539 | 0.233 | 53.83 | 0.19 | 0.21 | 0.79 | 0.028 | 0.135 | 0.035 | 1.738 | 0.067 | 42.46 | 0.033 | 11.70 | 0.121 | 96.50 |
| L36 | -1593 | 0.629 | 52.49 | 0.31 | 0.31 | 0.90 | 0.030 | 0.133 | 0.001 | 3.180 | 0.084 | 41.27 | 0.046 | 11.67 | 0.413 | 93.79 |
| L37 | -1641 | 0.175 | 53.90 | 0.19 | 0.16 | 1.05 | 0.026 | 0.129 | 0.011 | 1.386 | 0.030 | 42.76 | 0.030 | 11.89 | 0.231 | 97.18 |

| | | | | | | | | | | | | | | | | |
|---|---|---|---|---|---|---|---|---|---|---|---|---|---|---|---|---|
| L38 | -1691 | 0.410 | 53.30 | 0.35 | 0.24 | 0.88 | 0.028 | 0.136 | 0.001 | 2.209 | 0.068 | 41.66 | 0.163 | 11.70 | 0.341 | 94.68 |
| L39 | -1738 | 0.749 | 51.83 | 0.54 | 0.35 | 0.96 | 0.027 | 0.139 | 0.125 | 3.541 | 0.092 | 41.12 | 0.154 | 11.44 | 0.229 | 93.45 |
| L40 | -1790 | 0.463 | 53.59 | 0.32 | 0.26 | 0.74 | 0.029 | 0.135 | 0.007 | 2.460 | 0.088 | 41.80 | 0.028 | 11.76 | 0.364 | 95.00 |

**Table 16.** Trace elements content from the Opatřilka section. The table continues in the next pages.

| Sample | Stratigraphic position | U (ppm) | V (ppm) | Co (ppm) | Cr (ppm) | Cu (ppm) | Zn (ppm) | Ni (ppm) | Pb (ppm) | Cd (ppm) | Ga (ppm) | La (ppm) | Mn (ppm) |
|---|---|---|---|---|---|---|---|---|---|---|---|---|---|
| L1 | 200 | 20.94 | 38.60 | 3.030 | 17.45 | 3.242 | 2.272 | 5.751 | 4.972 | 0.563 | 1.598 | 8.008 | 165.4 |
| L2 | 150 | 13.80 | 29.96 | 2.183 | 17.39 | 3.437 | 4.502 | 4.629 | 4.959 | 1.629 | 1.176 | 9.208 | 207.3 |
| L3 | 100 | 5.884 | 22.71 | 2.377 | 18.97 | 2.773 | 3.047 | 3.770 | 3.852 | 3.077 | 1.176 | 8.826 | 308.1 |
| L4 | 50 | 9.603 | 23.36 | 1.572 | 13.46 | 4.689 | 2.696 | 3.231 | 4.868 | 2.737 | 1.200 | 7.629 | 190.6 |
| L5 | 0 | 5.321 | 13.31 | 0.907 | 7.44 | 5.252 | 3.641 | 3.977 | 3.041 | 1.963 | 1.174 | 8.530 | 274.5 |
| L6 | -50 | 6.041 | 15.28 | 2.657 | 15.42 | 3.783 | 4.875 | 4.607 | 2.999 | 1.079 | 1.334 | 7.736 | 324.8 |
| L7 | -100 | 5.986 | 16.48 | 2.452 | 14.54 | 1.590 | 4.352 | 4.368 | 1.890 | 0.874 | 2.619 | 9.495 | 316.3 |
| L8 | -150 | 2.481 | 12.44 | 0.209 | 10.67 | 2.225 | 2.731 | 3.698 | 2.949 | 0.830 | 2.208 | 9.587 | 308.0 |
| L9 | -202 | 8.902 | 22.38 | 5.635 | 14.61 | 4.649 | 13.67 | 10.86 | 4.987 | 1.580 | 2.997 | 10.062 | 291.0 |
| L10 | -253 | 4.137 | 14.20 | 3.019 | 16.39 | 1.498 | 6.14 | 6.536 | 3.616 | 1.295 | 1.400 | 11.973 | 358.1 |
| L11 | -304 | 4.389 | 20.86 | 3.576 | 30.63 | 5.207 | 11.50 | 11.50 | 5.028 | 0.131 | 3.361 | 16.576 | 365.8 |
| L12 | -353 | 3.848 | 14.34 | 1.317 | 24.23 | 2.310 | 3.696 | 5.999 | 3.883 | 1.542 | 1.172 | 10.041 | 332.9 |
| L13 | -405 | 3.424 | 19.68 | 2.424 | 32.65 | 5.580 | 9.991 | 9.214 | 4.781 | 2.396 | 1.963 | 14.765 | 424.7 |
| L14 | -456 | 2.749 | 15.98 | 2.455 | 16.86 | 4.040 | 8.758 | 6.604 | 3.708 | 0.405 | 2.157 | 18.630 | 416.6 |
| L16a | -544 | 16.73 | 50.12 | 2.466 | 56.62 | 2.052 | 9.874 | 5.893 | 5.281 | 2.661 | 2.995 | 14.842 | 248.5 |
| L16 | -557 | 6.740 | 22.59 | 0.660 | 10.42 | 1.761 | 6.292 | 3.557 | 3.060 | 1.725 | 1.526 | 8.676 | 308.1 |
| L16b | -587 | 3.812 | 28.59 | 4.593 | 35.21 | 6.941 | 11.07 | 14.62 | 7.379 | 2.024 | 3.195 | 14.555 | 265.3 |
| L17 | -609 | 5.508 | 23.18 | 4.131 | 18.70 | 3.064 | 21.00 | 7.507 | 4.969 | 0.048 | 1.482 | 13.322 | 232.3 |

| | | | | | | | | | | | | | |
|---|---|---|---|---|---|---|---|---|---|---|---|---|---|
| L16c | -630 | 7.929 | 37.73 | 6.084 | 47.88 | 7.966 | 41.76 | 17.77 | 7.759 | 1.843 | 3.765 | 17.263 | 290.0 |
| L18 | -658 | 3.747 | 20.42 | 1.902 | 15.10 | 2.317 | 6.489 | 7.344 | 3.064 | 1.375 | 2.529 | 11.709 | 248.9 |
| L18a | -678 | 3.649 | 32.25 | 5.881 | 39.33 | 7.688 | 13.40 | 17.22 | 8.028 | 1.652 | 2.496 | 15.714 | 273.4 |
| L19 | -716 | 5.210 | 43.54 | 6.775 | 39.78 | 10.908 | 19.58 | 22.08 | 6.424 | 0.260 | 3.656 | 16.261 | 306.9 |
| L20 | -772 | 2.676 | 18.67 | 0.208 | 14.52 | 0.613 | 3.058 | 2.866 | 2.838 | 0.912 | 2.120 | 10.401 | 215.7 |
| L21 | -825 | 4.070 | 15.96 | 4.014 | 21.00 | 3.989 | 8.023 | 8.108 | 3.998 | 2.032 | 2.678 | 9.595 | 223.9 |
| L22 | -878 | 6.091 | 14.36 | 3.047 | 14.38 | 4.486 | 4.273 | 4.281 | 2.293 | 1.704 | 1.572 | 9.061 | 131.8 |
| L23 | -928 | 5.770 | 18.40 | 1.926 | 17.89 | 6.953 | 3.687 | 4.026 | 4.604 | 0.417 | 1.856 | 7.735 | 165.4 |
| L24 | -982 | 3.749 | 19.23 | 1.548 | 31.60 | 4.890 | 3.871 | 3.798 | 4.118 | 1.451 | 1.705 | 8.072 | 215.6 |
| L25 | -1035 | 6.547 | 18.30 | 0.187 | 13.73 | 3.881 | 6.565 | 3.314 | 6.886 | 1.333 | 2.279 | 8.640 | 316.4 |
| L26 | -1080 | 3.845 | 13.10 | 1.460 | 3.54 | 3.328 | 4.643 | 5.501 | 3.217 | 1.690 | 1.942 | 7.339 | 123.5 |
| L27 | -1134 | 5.444 | 23.66 | 1.943 | 9.93 | 4.552 | 7.148 | 4.135 | 5.830 | 3.999 | 2.229 | 9.302 | 316.4 |
| L28 | -1182 | 4.624 | 20.68 | 2.203 | 5.93 | 0.183 | 4.165 | 3.693 | 2.552 | 2.077 | 2.049 | 7.799 | 106.7 |
| L29 B1 | -1225 | 11.41 | 74.68 | 2.425 | 7.34 | 19.336 | 70.60 | 9.984 | 12.20 | 5.237 | 1.150 | 9.131 | 282.7 |
| L29 A2 | -1230 | 5.514 | 23.56 | 0.439 | 2.08 | 0.976 | 14.01 | 3.766 | 3.09 | 2.808 | 1.173 | 7.897 | 148.7 |
| L29 REP | -1235 | 16.86 | 69.86 | 1.246 | 14.38 | 9.538 | 17.79 | 12.917 | 6.157 | 3.408 | 2.191 | 8.105 | 140.2 |
| L29 | -1235 | 16.86 | 69.86 | 1.246 | 14.38 | 9.538 | 17.79 | 12.917 | 6.157 | 3.408 | 2.191 | 8.105 | 140.2 |
| L29 A1 | -1240 | 9.744 | 55.89 | 1.379 | 7.82 | 10.263 | 18.30 | 4.958 | 3.416 | 2.613 | 1.520 | 9.299 | 148.6 |
| L29 B2 | -1265 | 10.88 | 53.87 | 1.628 | 10.50 | 5.588 | 29.43 | 9.647 | 11.48 | 2.562 | 1.155 | 7.977 | 299.6 |
| L30 | -1289 | 5.934 | 21.97 | 0.091 | 8.66 | 2.227 | 8.617 | 3.640 | 2.470 | 1.802 | 1.322 | 8.373 | 98.34 |
| L31 | -1339 | 9.225 | 46.34 | 3.109 | 6.82 | 14.067 | 8.290 | 7.299 | 3.554 | 2.383 | 1.947 | 8.323 | 123.5 |
| L32 | -1388 | 17.88 | 72.54 | 2.850 | 6.73 | 11.811 | 142.1 | 22.66 | 6.829 | 2.665 | 1.944 | 8.787 | 140.2 |
| L33 | -1442 | 7.382 | 79.58 | 4.408 | 33.85 | 13.537 | 39.70 | 20.52 | 7.151 | 0.800 | 3.451 | 18.868 | 206.7 |
| L34 | -1490 | 5.527 | 45.55 | 3.147 | 24.11 | 4.276 | 26.82 | 12.41 | 5.735 | 1.236 | 3.262 | 13.871 | 223.6 |
| L35 | -1539 | 1.808 | 21.31 | 1.776 | 12.64 | 3.671 | 6.957 | 5.313 | 3.359 | 1.011 | 1.418 | 10.607 | 215.7 |
| L36 | -1593 | 3.948 | 29.62 | 2.691 | 18.75 | 3.354 | 9.976 | 6.163 | 3.333 | 0.797 | 2.334 | 17.671 | 232.2 |

| | | | | | | | | | | | | | |
|---|---|---|---|---|---|---|---|---|---|---|---|---|---|
| L37 | -1641 | 2.865 | 17.30 | 2.108 | 7.88 | 3.925 | 5.081 | 5.411 | 2.910 | 1.146 | 1.168 | 11.215 | 199.0 |
| L38 | -1691 | 1.893 | 27.86 | 0.933 | 18.54 | 3.752 | 10.92 | 7.283 | 2.311 | 0.499 | 1.175 | 13.273 | 215.6 |
| L39 | -1738 | 3.893 | 46.43 | 4.206 | 17.95 | 4.760 | 19.98 | 9.122 | 4.271 | 1.041 | 1.175 | 15.601 | 207.0 |
| L40 | -1790 | 1.590 | 20.29 | 2.206 | 15.55 | 3.216 | 6.600 | 7.129 | 4.221 | 0.930 | 1.775 | 10.636 | 223.9 |

Continuation of Table 16.

| Sample | Stratigraphic position | Nd (ppm) | Rb (ppm) | Sc (ppm) | Sr (ppm) | Th (ppm) | Y (ppm) | Zr (ppm) |
|---|---|---|---|---|---|---|---|---|
| L1 | 200 | 2.534 | 2.436 | 8.575 | 243.0 | 1.294 | 6.226 | 3.012 |
| L2 | 150 | 10.96 | 0.451 | 10.44 | 238.7 | 0.402 | 11.97 | 2.643 |
| L3 | 100 | 7.039 | 1.148 | 9.935 | 212.9 | 1.006 | 8.450 | 2.789 |
| L4 | 50 | 3.510 | 1.557 | 9.848 | 220.8 | 0.200 | 7.125 | 1.539 |
| L5 | 0 | 2.304 | 1.863 | 8.755 | 197.0 | 0.220 | 4.560 | 2.365 |
| L6 | -50 | 4.875 | 2.339 | 8.540 | 221.2 | 0.381 | 5.689 | 2.410 |
| L7 | -100 | 9.431 | 1.409 | 8.964 | 217.9 | 0.695 | 7.411 | 3.391 |
| L8 | -150 | 5.020 | 2.128 | 7.731 | 170.5 | 1.032 | 6.753 | 2.853 |
| L9 | -202 | 3.562 | 5.509 | 8.448 | 293.6 | 0.488 | 6.435 | 6.333 |
| L10 | -253 | 10.333 | 4.820 | 8.466 | 211.0 | 2.016 | 10.84 | 5.069 |
| L11 | -304 | 15.193 | 9.804 | 8.784 | 144.2 | 1.471 | 14.84 | 11.72 |
| L12 | -353 | 8.117 | 2.655 | 7.430 | 213.2 | 0.310 | 7.998 | 3.880 |
| L13 | -405 | 15.66 | 6.966 | 10.69 | 198.5 | 0.690 | 11.74 | 8.569 |
| L14 | -456 | 20.298 | 5.716 | 8.747 | 183.1 | 0.899 | 17.29 | 7.105 |
| L16a | -544 | 15.89 | 10.99 | 7.829 | 301.5 | 1.396 | 11.62 | 12.83 |
| L16 | -557 | 5.815 | 1.080 | 8.563 | 309.4 | 0.227 | 5.131 | 1.468 |
| L16b | -587 | 14.85 | 10.16 | 8.981 | 217.1 | 1.139 | 13.11 | 13.11 |
| L17 | -609 | 7.576 | 2.924 | 8.245 | 166.0 | 0.200 | 9.342 | 3.945 |
| L16c | -630 | 18.87 | 14.75 | 6.378 | 199.8 | 1.738 | 13.84 | 18.00 |

| | | | | | | | | |
|---|---|---|---|---|---|---|---|---|
| L18 | -658 | 7.547 | 4.551 | 7.794 | 212.8 | 0.533 | 11.60 | 5.339 |
| L18a | -678 | 14.38 | 11.44 | 6.936 | 211.8 | 0.682 | 13.69 | 14.97 |
| L19 | -716 | 14.78 | 16.60 | 4.865 | 170.0 | 2.024 | 13.09 | 21.66 |
| L20 | -772 | 6.861 | 2.847 | 8.887 | 255.2 | 0.221 | 8.998 | 3.258 |
| L21 | -825 | 3.993 | 3.814 | 9.799 | 218.4 | 0.346 | 6.501 | 4.491 |
| L22 | -878 | 4.092 | 2.580 | 8.950 | 225.7 | 0.200 | 4.372 | 3.370 |
| L23 | -928 | 3.849 | 2.118 | 8.835 | 206.5 | 0.751 | 4.254 | 2.794 |
| L24 | -982 | 5.393 | 2.644 | 11.77 | 226.3 | 0.804 | 6.016 | 4.609 |
| L25 | -1035 | 6.755 | 2.268 | 8.329 | 198.5 | 0.240 | 7.684 | 3.643 |
| L26 | -1080 | 3.194 | 1.575 | 10.93 | 217.5 | 0.220 | 3.522 | 2.849 |
| L27 | -1134 | 3.055 | 2.160 | 10.40 | 200.4 | 0.200 | 6.915 | 4.951 |
| L28 | -1182 | 4.366 | 0.894 | 10.28 | 220.1 | 0.341 | 3.904 | 0.596 |
| L29 B1 | -1225 | 4.581 | 3.407 | 9.230 | 183.1 | 0.269 | 5.683 | 2.871 |
| L29 A2 | -1230 | 1.380 | 0.384 | 8.658 | 262.4 | 0.842 | 4.111 | 0.420 |
| L29 REP | -1235 | 5.686 | 5.512 | 7.923 | 177.3 | 0.568 | 4.513 | 5.207 |
| L29 | -1235 | 5.686 | 5.512 | 7.923 | 177.3 | 0.568 | 4.513 | 5.207 |
| L29 A1 | -1240 | 4.548 | 3.478 | 7.488 | 198.4 | 1.022 | 5.054 | 3.348 |
| L29 B2 | -1265 | 4.875 | 3.203 | 8.792 | 187.4 | 0.200 | 5.780 | 2.807 |
| L30 | -1289 | 0.000 | 1.397 | 9.986 | 273.3 | 0.815 | 3.099 | 0.610 |
| L31 | -1339 | 0.658 | 2.203 | 8.231 | 229.1 | 0.445 | 3.976 | 2.332 |
| L32 | -1388 | 3.102 | 3.970 | 9.553 | 178.2 | 1.142 | 5.392 | 4.244 |
| L33 | -1442 | 20.76 | 9.738 | 9.222 | 226.0 | 1.106 | 17.15 | 12.57 |
| L34 | -1490 | 14.35 | 9.143 | 7.978 | 285.6 | 1.155 | 13.00 | 11.90 |
| L35 | -1539 | 12.20 | 2.420 | 11.26 | 322.8 | 0.409 | 11.34 | 3.385 |
| L36 | -1593 | 15.79 | 5.079 | 10.32 | 297.5 | 0.937 | 15.43 | 7.814 |
| L37 | -1641 | 7.981 | 1.779 | 8.366 | 262.5 | 0.200 | 9.685 | 2.037 |

| | | | | | | | | |
|---|---|---|---|---|---|---|---|---|
| L38 | -1691 | 8.137 | 3.613 | 11.00 | 314.9 | 0.809 | 10.64 | 5.309 |
| L39 | -1738 | 15.26 | 6.844 | 8.909 | 308.3 | 0.246 | 15.09 | 8.654 |
| L40 | -1790 | 8.038 | 3.987 | 8.973 | 342.8 | 1.134 | 8.360 | 6.685 |

**Table 17.** Major elements content from the Klonk section. TS: Total Sulfur. TOC: Total organic carbon. $CaCO_3$ is calculated from $CO_2$ content. (Details in chapter 4.6. THE CARBONATE CARBON ANALYSIS). The table continues on the next page.

| Sample | Stratigraphic position | $Al_2O_3$ (wt. %) | CaO (wt. %) | $Fe_2O_3$ (wt. %) | $K_2O$ (wt. %) | MgO (wt. %) | MnO (wt. %) | $Na_2O$ (wt. %) | $P_2O_5$ (wt. %) | $SiO_2$ (wt. %) | $TiO_2$ (wt. %) | $CO_2$ (wt. %) | TS (wt. %) | TC (wt. %) | TOC (wt. %) | $CaCO_3$ (wt. %) |
|---|---|---|---|---|---|---|---|---|---|---|---|---|---|---|---|---|
| J35 | 270 | 3.741 | 34.36 | 2.650 | 0.864 | 1.576 | 0.024 | 0.231 | 0.051 | 28.38 | 0.294 | 26.48 | 1.434 | 8.917 | 1.693 | 60.19 |
| J34 | 230 | 6.590 | 27.99 | 2.750 | 1.533 | 2.379 | 0.028 | 0.185 | 0.096 | 34.99 | 0.524 | 22.76 | 0.015 | 7.721 | 1.514 | 51.72 |
| J33 | 200 | 1.427 | 48.80 | 0.880 | 0.339 | 0.869 | 0.025 | 0.142 | 0.026 | 8.246 | 0.125 | 36.66 | 0.316 | 11.19 | 1.191 | 83.33 |
| J32 | 175 | 5.775 | 30.37 | 2.214 | 1.406 | 2.190 | 0.029 | 0.300 | 0.066 | 32.21 | 0.426 | 24.01 | 0.615 | 8.420 | 1.872 | 54.57 |
| J31 | 170 | 2.324 | 45.28 | 1.071 | 0.556 | 1.181 | 0.026 | 0.182 | 0.025 | 12.53 | 0.180 | 34.81 | 0.299 | 10.57 | 1.078 | 79.11 |
| J30 | 140 | 5.788 | 27.06 | 2.164 | 1.393 | 2.591 | 0.029 | 0.184 | 0.045 | 37.51 | 0.440 | 22.68 | 0.658 | 7.927 | 1.740 | 51.55 |
| J29 | 125 | 1.846 | 46.75 | 0.916 | 0.430 | 0.976 | 0.028 | 0.139 | 0.026 | 10.82 | 0.147 | 35.73 | 0.238 | 10.82 | 1.076 | 81.21 |
| J28 | 80 | 7.716 | 21.69 | 3.243 | 1.853 | 3.581 | 0.035 | 0.183 | 0.080 | 40.13 | 0.589 | 19.88 | 1.410 | 7.605 | 2.184 | 45.18 |
| J27 | 65 | 2.096 | 45.37 | 1.131 | 0.491 | 1.225 | 0.028 | 0.141 | 0.007 | 12.11 | 0.167 | 34.29 | 0.257 | 10.54 | 1.193 | 77.93 |
| J26 | 45 | 6.026 | 31.93 | 2.645 | 1.368 | 2.026 | 0.037 | 0.175 | 0.124 | 28.58 | 0.483 | 25.72 | 0.036 | 9.013 | 1.998 | 58.46 |
| J25 | 35 | 11.68 | 13.19 | 5.301 | 3.101 | 3.395 | 0.039 | 0.621 | 0.075 | 49.98 | 1.074 | 10.26 | 0.036 | 6.035 | 3.237 | 23.32 |
| J24 | -5 | 2.237 | 45.02 | 0.995 | 0.522 | 1.118 | 0.026 | 0.142 | 0.019 | 13.48 | 0.179 | 34.41 | 0.241 | 10.65 | 1.269 | 78.21 |
| J23 | -30 | 1.940 | 47.04 | 0.866 | 0.453 | 0.935 | 0.033 | 0.307 | 0.022 | 9.858 | 0.176 | 35.12 | 0.164 | 10.81 | 1.236 | 79.82 |
| J22 | -55 | 0.471 | 54.37 | 0.427 | 0.042 | 0.556 | 0.029 | 0.188 | 0.004 | 0.967 | 0.029 | 40.39 | 0.176 | 11.83 | 0.809 | 91.81 |
| J21 | -85 | 2.493 | 45.25 | 1.241 | 0.600 | 1.393 | 0.038 | 0.311 | 0.022 | 11.86 | 0.181 | 34.75 | 0.225 | 10.53 | 1.050 | 78.97 |
| J20 | -120 | 10.58 | 15.98 | 4.636 | 2.730 | 3.712 | 0.042 | 0.668 | 0.068 | 46.65 | 0.830 | 13.68 | 0.014 | 6.449 | 2.719 | 31.08 |
| J19 | -135 | 2.821 | 42.32 | 1.484 | 0.650 | 1.408 | 0.040 | 0.355 | 0.017 | 16.07 | 0.236 | 32.81 | 0.311 | 10.20 | 1.249 | 74.58 |

| | | | | | | | | | | | | | | | | |
|---|---|---|---|---|---|---|---|---|---|---|---|---|---|---|---|---|
| J18 | -150 | 10.77 | 16.82 | 4.710 | 2.771 | 3.841 | 0.043 | 0.654 | 0.081 | 44.97 | 0.857 | 14.51 | 0.019 | 5.992 | 2.034 | 32.99 |
| J17 | -160 | 2.044 | 46.28 | 0.954 | 0.516 | 1.073 | 0.031 | 0.294 | 0.013 | 11.33 | 0.163 | 35.05 | 0.229 | 10.51 | 0.956 | 79.65 |
| J16 | -185 | 10.44 | 16.85 | 4.664 | 2.678 | 3.348 | 0.044 | 0.682 | 0.072 | 45.51 | 0.843 | 13.14 | 0.014 | 5.493 | 1.910 | 29.86 |
| J15 | -190 | 2.520 | 44.54 | 1.538 | 0.559 | 0.957 | 0.038 | 0.357 | 0.021 | 13.22 | 0.221 | 34.10 | 0.025 | 10.25 | 0.948 | 77.50 |
| J14 | -210 | 7.374 | 17.04 | 3.253 | 1.861 | 2.115 | 0.038 | 0.536 | 0.039 | 52.69 | 0.659 | 12.91 | 0.652 | 5.262 | 1.742 | 29.34 |
| J13 | -215 | 1.639 | 46.57 | 1.292 | 0.400 | 0.950 | 0.040 | 0.294 | 0.003 | 11.06 | 0.156 | 34.85 | 0.440 | 10.47 | 0.970 | 79.20 |
| J12 | -255 | 10.10 | 12.76 | 5.158 | 2.674 | 3.160 | 0.041 | 0.556 | 0.064 | 52.81 | 0.989 | 10.07 | 0.057 | 4.440 | 1.694 | 22.88 |
| J11 | -270 | 1.481 | 47.74 | 0.905 | 0.371 | 1.105 | 0.041 | 0.289 | 0.011 | 9.585 | 0.132 | 35.74 | 0.188 | 10.69 | 0.940 | 81.22 |
| J10 | -300 | 9.214 | 20.16 | 3.995 | 2.278 | 2.876 | 0.046 | 0.659 | 0.053 | 42.57 | 0.776 | 16.04 | 0.036 | 6.210 | 1.835 | 36.46 |
| J9 | -315 | 4.047 | 37.85 | 2.035 | 0.961 | 2.021 | 0.054 | 0.385 | 0.018 | 21.62 | 0.316 | 29.74 | 0.042 | 9.151 | 1.042 | 67.58 |
| J8 | -330 | 12.03 | 9.293 | 4.999 | 3.269 | 3.789 | 0.041 | 0.704 | 0.079 | 55.46 | 0.900 | 8.59 | 0.036 | 4.162 | 1.819 | 19.53 |
| J7 | -345 | 2.308 | 44.06 | 1.260 | 0.572 | 1.064 | 0.049 | 0.326 | 0.022 | 14.84 | 0.181 | 33.31 | 0.153 | 10.06 | 0.978 | 75.69 |
| J6 | -370 | 8.624 | 17.77 | 3.917 | 2.128 | 2.275 | 0.046 | 0.648 | 0.097 | 48.25 | 0.775 | 13.56 | 0.019 | 5.517 | 1.818 | 30.82 |
| J5 | -395 | 2.266 | 43.81 | 1.370 | 0.540 | 0.967 | 0.048 | 0.334 | 0.036 | 14.51 | 0.204 | 32.91 | 0.030 | 10.05 | 1.074 | 74.79 |
| J4 | -420 | 6.562 | 21.18 | 3.054 | 1.612 | 1.813 | 0.038 | 0.489 | 0.082 | 46.32 | 0.598 | 16.04 | 0.019 | 6.354 | 1.978 | 36.46 |
| J3 | -435 | 2.300 | 43.77 | 1.662 | 0.509 | 0.900 | 0.054 | 0.313 | 0.017 | 14.44 | 0.212 | 33.07 | 0.049 | 10.20 | 1.180 | 75.16 |
| J2 | -460 | 8.960 | 6.918 | 3.619 | 2.390 | 2.177 | 0.027 | 0.584 | 0.071 | 67.56 | 0.792 | 4.76 | 0.587 | 3.285 | 1.988 | 10.81 |
| J1 | -485 | 2.380 | 43.15 | 1.361 | 0.567 | 0.798 | 0.049 | 0.266 | 0.008 | 16.21 | 0.212 | 33.47 | 0.007 | 9.848 | 0.720 | 76.07 |

**Table 18**. Trace elements content from the Klonk section. The table continues in the next pages

| Sample | Stratigraphic position | Ba (ppm) | Cd (ppm) | Ce (ppm) | Co (ppm) | Cr (ppm) | Cu (ppm) | Ga (ppm) | La (ppm) | Mo (ppm) | Nb (ppm) | Nd (ppm) | Ni (ppm) |
|---|---|---|---|---|---|---|---|---|---|---|---|---|---|
| J35 | 270 | 93.00 | 2.402 | 32.38 | 10.06 | 37.91 | 18.56 | 4.220 | 18.52 | 2.474 | 4.759 | 19.98 | 22.93 |
| J34 | 230 | 131.9 | 2.750 | 64.72 | 9.538 | 66.74 | 32.16 | 8.525 | 30.63 | 2.792 | 7.428 | 31.97 | 28.34 |
| J33 | 200 | 36.46 | 1.035 | 6.513 | 4.968 | 15.57 | 9.101 | 3.458 | 12.46 | 1.057 | 3.058 | 6.345 | 10.21 |
| J32 | 175 | 142.8 | 0.734 | 45.56 | 8.901 | 52.81 | 25.61 | 7.965 | 22.07 | 1.522 | 6.915 | 26.76 | 27.34 |
| J31 | 170 | 47.98 | 1.813 | 10.95 | 6.843 | 23.67 | 11.22 | 2.785 | 12.03 | 0.628 | 3.296 | 11.09 | 12.44 |
| J30 | 140 | 138.1 | 2.106 | 39.73 | 8.913 | 54.26 | 28.66 | 7.523 | 21.00 | 1.745 | 6.615 | 21.06 | 25.44 |
| J29 | 125 | 30.91 | 2.600 | 4.120 | 5.144 | 23.51 | 9.197 | 4.490 | 9.488 | 0.778 | 3.793 | 7.944 | 10.27 |
| J28 | 80 | 167.3 | 2.541 | 57.84 | 13.34 | 78.78 | 37.17 | 9.819 | 29.43 | 3.697 | 8.116 | 30.88 | 36.26 |
| J27 | 65 | 49.00 | 2.659 | 15.16 | 6.406 | 21.06 | 12.66 | 4.187 | 12.77 | 1.480 | 3.952 | 10.92 | 13.92 |
| J26 | 45 | 136.2 | 1.460 | 59.21 | 10.41 | 61.25 | 29.47 | 7.207 | 28.40 | 3.023 | 6.767 | 30.44 | 24.20 |
| J25 | 35 | 263.6 | 2.095 | 77.46 | 15.69 | 140.8 | 67.79 | 16.71 | 36.11 | 8.504 | 14.40 | 35.36 | 72.98 |
| J24 | -5 | 48.27 | 0.394 | 15.35 | 5.381 | 23.51 | 13.01 | 2.993 | 14.18 | 0.860 | 3.509 | 12.41 | 14.02 |
| J23 | -30 | 56.61 | 1.843 | 7.134 | 4.776 | 26.45 | 8.579 | 2.558 | 11.63 | 1.301 | 3.905 | 10.09 | 13.12 |
| J22 | -55 | 243.5 | 1.178 | 6.181 | 2.727 | 4.040 | 3.154 | 2.112 | 7.542 | 0.702 | 1.648 | 5.300 | 10.78 |
| J21 | -85 | 55.77 | 0.263 | 14.41 | 4.959 | 27.16 | 9.899 | 3.612 | 13.53 | 1.223 | 3.744 | 11.37 | 11.17 |
| J20 | -120 | 246.1 | 0.812 | 75.01 | 13.71 | 96.22 | 49.27 | 13.87 | 37.51 | 4.554 | 12.47 | 33.76 | 42.46 |
| J19 | -135 | 68.49 | 0.489 | 18.38 | 5.908 | 28.38 | 15.60 | 4.796 | 15.44 | 1.301 | 3.550 | 14.05 | 15.36 |
| J18 | -150 | 239.6 | 0.008 | 79.54 | 11.26 | 99.36 | 42.30 | 14.50 | 37.61 | 4.359 | 12.78 | 38.37 | 37.94 |
| J17 | -160 | 38.10 | 1.751 | 10.66 | 4.365 | 16.51 | 7.983 | 3.855 | 13.04 | 1.526 | 3.732 | 10.10 | 11.27 |
| J16 | -185 | 272.1 | 1.604 | 70.67 | 14.11 | 115.31 | 51.59 | 14.66 | 33.36 | 8.525 | 11.66 | 34.86 | 50.69 |
| J15 | -190 | 71.26 | 2.817 | 31.42 | 6.343 | 31.45 | 12.58 | 1.896 | 20.55 | 2.886 | 3.112 | 21.27 | 14.48 |
| J14 | -210 | 228.6 | 0.095 | 50.56 | 10.48 | 95.97 | 28.64 | 10.19 | 24.88 | 3.690 | 9.768 | 26.97 | 46.11 |
| J13 | -215 | 51.90 | 0.432 | 6.994 | 5.239 | 25.88 | 9.044 | 4.117 | 10.59 | 2.477 | 2.644 | 10.17 | 13.07 |

| | | | | | | | | | | | | | |
|---|---|---|---|---|---|---|---|---|---|---|---|---|---|
| J12 | -255 | 265.0 | 0.066 | 61.61 | 13.97 | 135.9 | 41.87 | 14.11 | 30.35 | 5.176 | 13.41 | 31.37 | 57.55 |
| J11 | -270 | 46.69 | 2.264 | 13.90 | 3.749 | 20.67 | 7.454 | 3.110 | 13.05 | 1.498 | 3.225 | 12.55 | 12.39 |
| J10 | -300 | 246.9 | 0.587 | 63.82 | 10.79 | 110.0 | 41.74 | 11.84 | 29.87 | 8.017 | 11.05 | 32.37 | 43.92 |
| J9 | -315 | 101.0 | 0.595 | 42.03 | 6.299 | 46.74 | 16.32 | 5.940 | 23.30 | 2.564 | 5.387 | 24.75 | 22.04 |
| J8 | -330 | 301.6 | 0.034 | 79.79 | 7.871 | 120.3 | 44.44 | 17.07 | 38.90 | 3.752 | 14.29 | 40.08 | 55.39 |
| J7 | -345 | 61.07 | 1.644 | 24.08 | 4.891 | 22.69 | 10.50 | 3.033 | 15.95 | 2.982 | 3.525 | 15.77 | 15.26 |
| J6 | -370 | 287.3 | 0.675 | 74.69 | 11.84 | 121.8 | 39.16 | 11.17 | 32.13 | 7.708 | 10.22 | 35.76 | 46.31 |
| J5 | -395 | 62.06 | 0.889 | 16.47 | 9.156 | 33.67 | 10.40 | 3.379 | 14.83 | 3.328 | 4.164 | 13.26 | 16.18 |
| J4 | -420 | 194.6 | 0.142 | 61.73 | 8.607 | 85.43 | 36.66 | 10.04 | 28.70 | 10.721 | 8.337 | 29.78 | 42.38 |
| J3 | -435 | 107.2 | 2.165 | 26.92 | 6.192 | 32.29 | 12.26 | 4.432 | 18.80 | 3.912 | 3.720 | 16.38 | 17.99 |
| J2 | -460 | 253.8 | 2.860 | 57.64 | 10.16 | 107.6 | 37.19 | 12.79 | 26.95 | 4.628 | 11.82 | 31.21 | 51.44 |
| J1 | -485 | 58.74 | 2.516 | 23.29 | 5.561 | 30.91 | 9.832 | 3.987 | 18.06 | 2.061 | 3.322 | 15.67 | 16.40 |

Continuation of table 18

| Sample | Stratigraphic position | Pb (ppm) | Rb (ppm) | Sc (ppm) | Sr (ppm) | Th (ppm) | U (ppm) | V (ppm) | Y (ppm) | Zn (ppm) | Zr (ppm) |
|---|---|---|---|---|---|---|---|---|---|---|---|
| J35 | 270 | 7.021 | 31.03 | 3.829 | 679.6 | 2.686 | 1.633 | 37.44 | 17.29 | 25.84 | 39.29 |
| J34 | 230 | 11.55 | 53.58 | 6.080 | 579.1 | 5.015 | 3.511 | 62.07 | 24.67 | 43.29 | 65.57 |
| J33 | 200 | 2.566 | 11.47 | 10.12 | 760.6 | 0.417 | 0.000 | 21.21 | 8.828 | 9.50 | 17.34 |
| J32 | 175 | 10.04 | 49.32 | 6.104 | 617.6 | 3.740 | 1.142 | 52.55 | 18.08 | 39.04 | 61.99 |
| J31 | 170 | 4.664 | 19.34 | 5.858 | 771.5 | 3.043 | 0.000 | 24.38 | 8.773 | 14.98 | 25.03 |
| J30 | 140 | 9.784 | 48.25 | 6.010 | 538.9 | 4.462 | 1.129 | 57.57 | 15.98 | 38.87 | 58.97 |
| J29 | 125 | 5.322 | 14.44 | 4.353 | 714.0 | 1.426 | 0.423 | 19.85 | 8.241 | 10.93 | 21.97 |
| J28 | 80 | 13.97 | 60.55 | 8.038 | 496.7 | 5.970 | 3.491 | 77.28 | 23.90 | 69.06 | 77.78 |
| J27 | 65 | 4.453 | 15.64 | 6.666 | 820.5 | 1.478 | 1.121 | 21.81 | 9.220 | 16.82 | 24.20 |
| J26 | 45 | 9.911 | 45.96 | 7.299 | 597.6 | 3.672 | 3.799 | 57.64 | 24.44 | 35.94 | 60.80 |
| J25 | 35 | 23.46 | 100.7 | 13.65 | 328.2 | 8.578 | 7.470 | 183.57 | 24.64 | 94.09 | 127.3 |

| | | | | | | | | | | | |
|---|---|---|---|---|---|---|---|---|---|---|---|
| J24 | -5 | 4.820 | 17.67 | 5.724 | 772.4 | 2.247 | 0.027 | 26.27 | 12.08 | 17.93 | 25.01 |
| J23 | -30 | 5.168 | 15.44 | 7.379 | 620.0 | 1.800 | 0.919 | 48.45 | 9.174 | 16.69 | 24.57 |
| J22 | -55 | 3.227 | 0.790 | 10.38 | 639.3 | 0.200 | 0.000 | 9.88 | 5.361 | 0.183 | 3.493 |
| J21 | -85 | 5.706 | 19.48 | 5.648 | 701.3 | 1.858 | 0.499 | 26.92 | 12.12 | 19.38 | 26.32 |
| J20 | -120 | 18.99 | 91.05 | 11.93 | 452.6 | 8.912 | 5.300 | 96.21 | 24.80 | 66.82 | 113.8 |
| J19 | -135 | 5.761 | 22.26 | 6.723 | 757.2 | 1.899 | 0.889 | 30.85 | 13.05 | 18.67 | 30.92 |
| J18 | -150 | 19.25 | 90.71 | 10.97 | 383.2 | 7.840 | 3.820 | 91.19 | 25.32 | 65.52 | 114.1 |
| J17 | -160 | 5.589 | 16.11 | 7.921 | 564.3 | 1.777 | 0.307 | 24.31 | 9.500 | 11.84 | 22.57 |
| J16 | -185 | 20.56 | 92.73 | 10.31 | 363.7 | 7.982 | 8.040 | 125.0 | 23.00 | 64.49 | 114.9 |
| J15 | -190 | 4.860 | 19.47 | 5.802 | 678.0 | 1.375 | 1.631 | 41.73 | 15.49 | 21.74 | 28.90 |
| J14 | -210 | 13.54 | 65.06 | 7.449 | 374.7 | 6.096 | 4.613 | 150.0 | 21.43 | 63.55 | 86.73 |
| J13 | -215 | 5.656 | 13.69 | 9.030 | 616.6 | 1.287 | 1.686 | 44.97 | 10.04 | 11.79 | 19.78 |
| J12 | -255 | 19.05 | 90.82 | 11.07 | 285.7 | 6.700 | 6.814 | 206.1 | 24.60 | 88.62 | 115.4 |
| J11 | -270 | 3.394 | 12.56 | 6.469 | 588.6 | 1.613 | 1.859 | 41.83 | 10.32 | 13.19 | 18.45 |
| J10 | -300 | 18.33 | 79.39 | 9.067 | 389.0 | 7.023 | 7.995 | 163.9 | 23.51 | 58.88 | 104.1 |
| J9 | -315 | 7.791 | 33.01 | 5.671 | 531.5 | 3.566 | 3.687 | 109.5 | 20.03 | 40.04 | 43.19 |
| J8 | -330 | 21.63 | 111.8 | 15.06 | 226.2 | 9.900 | 6.405 | 284.2 | 27.63 | 106.4 | 136.4 |
| J7 | -345 | 6.147 | 19.45 | 5.969 | 555.0 | 1.622 | 2.243 | 49.00 | 12.80 | 17.62 | 24.63 |
| J6 | -370 | 18.97 | 74.01 | 8.720 | 351.8 | 7.570 | 8.171 | 183.3 | 26.36 | 67.71 | 103.6 |
| J5 | -395 | 6.651 | 18.63 | 8.054 | 604.0 | 1.918 | 2.678 | 44.15 | 11.40 | 15.33 | 26.23 |
| J4 | -420 | 16.10 | 56.69 | 6.938 | 415.3 | 5.658 | 7.253 | 126.2 | 23.20 | 46.30 | 75.77 |
| J3 | -435 | 6.546 | 18.26 | 6.252 | 699.4 | 1.720 | 1.884 | 51.97 | 16.01 | 20.02 | 27.60 |
| J2 | -460 | 18.04 | 81.77 | 10.30 | 227.7 | 7.331 | 4.888 | 316.6 | 22.10 | 104.4 | 108.1 |
| J1 | -485 | 6.090 | 19.84 | 10.13 | 699.4 | 2.013 | 0.067 | 83.70 | 17.61 | 26.90 | 27.17 |